THE
PHYSICAL REVIEW
A Journal of Experimental and Theoretical Physics
VOL. 44, No. 6 SEPTEMBER 15, 1933 SECOND SERIES

The Evaporation of Atoms, Ions and Electrons from Caesium Films on Tungsten

JOHN BRADSHAW TAYLOR AND IRVING LANGMUIR, *Research Laboratory, General Electric Company*
(Received January 19, 1933)

Precision methods for measuring the number of caesium atoms adsorbed on tungsten are described. With these methods for determining θ (the fraction of the tungsten surface covered with Cs), the rates of atom, ion and electron emission are measured as functions of θ and T, the filament temperature. *The rate of atom evaporation*, ν_a, increases rapidly with θ and with T. At low filament temperatures and high pressures of Cs vapor the concentration of adsorbed Cs atoms approaches a limit 3.563×10^{14} atoms cm^{-2} of true filament surface (one Cs atom for four tungsten atoms). This film ($\theta=1$) exhibits all the characteristics of a true monatomic layer. The formation of a second layer begins only at filament temperatures corresponding to nearly saturated Cs vapor. A theory of the formation of a second and of polyatomic layers is given and experiments supporting it are described. *The heat of evaporation* (given by the Clapeyron equation) for Cs atoms from clean tungsten is 2.83 volts (65,140 calories), 1.93 volts or 44,473 calories at $\theta=0.67$, and 1.77 volts or 40,757 calories at $\theta\leq1$. The adsorbing tungsten surface after proper aging is homogeneous, except that about 0.5 percent of it (active spots) can hold Cs more firmly than the rest. The procedure in obtaining *electron* (ν_e) and *ion* (ν_p) *emission* for zero field and the large changes in the effect of external field with θ are described. From both ν_e and ν_p the contact potential V_c is calculated, agreeing, except for very concentrated films, with V_c calculated entirely from data on neutral atom evaporation. At constant temperature the electron emission increases to a maximum at $\theta=0.67$ and decreases as $\theta=1$ is approached. The positive ion emission increases rapidly to a maximum at $\theta\leq0.01$ and then decreases. The work function (exponent in Dushman type equation) for electrons at $\theta=0.67$ is 1.70 volts (clean tungsten = 4.62 volts). The work function for ions is 1.91 volts at $\theta=0$, and 3.93 volts at $\theta=0.67$. It is shown by experiment that the saturated ion current from a clean hot (1200–1500°K) tungsten filament is an accurate measure (experimental error of about 0.2 percent) of the number of atoms striking the filament per second. *The condensation coefficient* (α) for atoms striking a tungsten filament is proved by experiment to be unity from $\theta=0$ to nearly 1. The important bearing of this fact and of the experimentally observed existence of *surface migration* or diffusion on the *mechanism of evaporation and condensation* in dilute and concentrated films is discussed. In addition surface migration is correlated with irregular ion evaporation rates occurring when two phases (dilute and concentrated films of Cs) exist on the tungsten surface. *Transient effects* in which θ changes with time are studied and entirely explained by the observed rates of evaporation and condensation. This and other facts are used to justify a *surface phase postulate* according to which all the properties of the adsorbed film are uniquely determined by θ and T.

I. INTRODUCTION

CAESIUM films on tungsten form an important and interesting case of adsorption. The adsorbed atoms are held on the tungsten by such large forces that remarkable changes in the thermionic properties of the tungsten can be observed. As the tungsten surface can be completely cleaned and the supply of caesium atoms can be controlled, this system is capable of furnishing quantitative information regarding adsorption and the electrical properties of surface films.

Films of alkali metal atoms on tungsten have been the subject of several investigations. Langmuir and Kingdon[1] found that caesium

[1] I. Langmuir and K. H. Kingdon, Science **57**, 58 (1923); Proc. Roy. Soc. **A107**, 61 (1925).

atoms adsorbed on tungsten greatly increased the electron emission of the tungsten and showed that caesium atoms striking a hot clean tungsten filament were converted into positive ions which could be collected by a plate at a negative potential. Both the electron and ion emissions were functions of the temperature (T) of the filament and of the fraction (θ) of the surface covered with caesium. The electron emission increased to a maximum at a certain value of θ and decreased with further increase in θ. The positive ion emission became appreciable only for low values of θ; at higher values of θ, caesium films evaporated only as neutral atoms. Only rough estimates of θ were made in this work.

Recently Langmuir[2] has treated the properties of caesium adsorbed on tungsten in a general discussion of evaporation, condensation, and adsorption, and has given a partial derivation of equations used in this paper.

Becker[3] has studied the evaporation of atoms, ions, and electrons from caesium films on tungsten and made measurements of θ. He attributed the maximum electron emission to a single complete layer of caesium atoms and the subsequent decrease in emission to the formation of a second layer of caesium atoms.

The present investigation was undertaken for the purpose of determining quantitatively the dependence of the rates of neutral atom evaporation (ν_a), ion emission (ν_p), and electron emission (ν_e) on θ, filament temperature T, and the field strength; ν_a, ν_p and ν_e represent the number of atoms, ions, or electrons evaporating per unit area, per unit time. To facilitate correlation of ν_p and ν_e with θ, the greater part of the work has consisted in establishing θ as a function of caesium pressure and filament temperature.

In the steady state,

$$\alpha\mu_a = \nu_a; \tag{1}$$

that is, the number of atoms evaporating per unit area per unit time (ν_a) is equal to the number condensing, which is equal to the number arriving per unit area per unit time (μ_a), multiplied by the condensation coefficient α. Evidence regarding the nature of α will be given (Section XI) and it will be shown that under our experimental conditions α is equal to unity. Therefore the experiments which give θ as a function of μ_a also give ν_a as a function of θ.

Let us now postulate that ν_a, ν_p and ν_e are functions of θ and T only. The distribution of atoms is assumed to be uniform and independent of the way (e.g., by evaporation or condensation) in which θ was reached. This "surface phase postulate" will be discussed and justified in Section XI. Determinations of ν_e and ν_p at various pressures then enable us to express ν_e and ν_p as functions of θ and T.

II. Apparent and True Filament Surface and Definition of θ

The apparent area S_A of the filament surface is that calculated from the dimensions of the filament (πld). Actually after heating to 2900° during aging, a tungsten filament becomes etched and develops[4] dodecahedral crystal faces (110) in which there are 1.425×10^{15} tungsten atoms per cm^2. The actual surface area S is thus greater than S_A (see Fig. 1).

Fig. 1. True (S) and apparent (S_A) filament surface.

It so happens that crystals of metallic caesium[5] have the same type of lattice (body-centered cubic) as tungsten and the lattice constant (6.17A) is almost exactly double that of tungsten (3.15A). Thus if, in a complete monatomic film of caesium on tungsten, the caesium atoms arrange themselves in a surface lattice identical with that of the tungsten surface but with double spacing, there will be one caesium atom for every four tungsten atoms, all the adatoms will be similarly placed with respect to the underlying tungsten atoms, and the adatoms will be at the same distances from one another as in metallic caesium.

Because the strong forces between the caesium

[2] I. Langmuir, J. Am. Chem. Soc. **54**, 2798 (1932).

[3] J. A. Becker, Phys. Rev. **28**, 341 (1926); J. Am. Electrochem. Soc. **55**, 153 (1929).

[4] I. Langmuir, Phys. Rev. **22**, 374 (1923).

[5] Simon and Vohsen, Zeits. f. physik. Chemie **133**, 165 (1928).

and the tungsten atoms must tend to make the adatoms occupy definite elementary spaces[6] determined by the tungsten lattice, we believe we are justified in adopting this 4 to 1 relation as a postulate in our further investigations. We may therefore put for the true surface concentration σ_1 of a complete caesium film on tungsten

$$\sigma_1 = 3.563 \times 10^{14} \text{ atoms cm}^{-2}. \quad (2)$$

Experiments which will be described in Section V and XII have shown that with the particular filament used, the apparent surface concentration σ_{A1} for a complete film of caesium on tungsten is

$$\sigma_{A1} = 4.80 \times 10^{14} \text{ atoms cm}^{-2}. \quad (3)$$

The ratio σ_{A1}/σ_1, which is 1.347, is thus equal to S/S_A, the ratio of the true to the apparent filament surface. Tonks has calculated[7] that with a random distribution of dodecahedral crystals the *minimum value* of S/S_A is 1.225, a value which supports our postulate.

We intend to test this postulate in future work by comparing values of σ_{A1} obtained with adsorbed films of caesium, rubidium and potassium on a single tungsten surface. If the value σ_1 as given above is correct, we should expect that σ_{A1} will be the same for all alkali metals.

Let σ_A be the apparent surface concentration of adatoms obtained by dividing the total number of adatoms by S_A, the apparent surface area (πld). Then the true surface concentration σ is $\sigma_A S_A/S$. It is probable that S/S_A may vary somewhat for different filaments according to the aging treatment and the fineness and orientation of the crystals. The intrinsic properties of the adsorbed film are presumably dependent on σ rather than σ_A. Since, however, our knowledge of σ depends upon our postulated value of σ_1, as given by Eq. (2), it is preferable to express these properties as functions of the covering fraction θ defined by

$$\theta = \sigma_A/\sigma_{A1}. \quad (4)$$

All the values of θ in this paper have been calculated in this way from σ_A by using the value of σ_{A1} given by Eq. (3). It should be noted that θ is also equal to σ/σ_1.

We must also have clearly in mind the relation of S and S_A to our definitions of μ and ν. We shall define μ_a as the number of incident atoms per unit time per unit area of *apparent surface* S_A. Thus from the kinetic theory

$$\mu_a = p(2\pi mkT)^{-\frac{1}{2}} = 3.796pT^{-\frac{1}{2}} \text{ atoms cm}^{-2} \text{ sec.}^{-1} \quad (5)$$

where p is the pressure in baryes and T is the temperature of the caesium vapor.

In a similar way we define ν_a as the number of atoms which escape from the filament by evaporation per unit time per unit area of *apparent surface* (S_A).

We wish, however, to know the rate of evaporation per unit area of true surface S for this alone should be an intrinsic property of the adsorbed film.

In the steady state to which Eq. (1) applies, the condensation on and evaporation from each element of area must balance. The atomic flux density in the neighborhood of the filament must therefore be isotropic just as is the heat radiation within an enclosure at uniform temperature. The values of μ and ν over the surface of S, in Fig. 1, must thus be the same as over the surface S_A.

Consider now the irreversible evaporation of adatoms from a filament in a space in which $\mu = 0$. We see from S in Fig. 1 that a large fraction of the atoms that evaporate from the valleys (and a smaller fraction from the peaks) are intercepted by the surface of the opposing peaks before they can escape. The concentration of adatoms thus decreases near the peaks faster than in the valleys unless surface mobility equalizes their concentration.

If mobility does maintain a uniform θ and if $\alpha = 1$ so that all incident atoms condense, it follows from the reversibility principle (see Section XII) that the emission occurs in accord with Lambert's cosine law. The situation is exactly analogous to that in optics where the brightness of an incandescent black body is independent of its contour.

During irreversible condensation from a vapor with a given μ, the concentration at the peaks

[6] I. Langmuir, J. Am. Chem. Soc. **38**, 2287 (1916); **40**, 1366 (1918).

[7] L. Tonks, Phys. Rev. **38**, 1030 (1931).

should increase faster than in the valleys, assuming no mobility. Since the experiments (see Section XI) have shown no difference in properties of a film with a given average value of θ whether it was obtained by irreversible condensation or evaporation, we must conclude that surface mobility equalized θ over the surface. Because of this mobility and the fact that $\alpha=1$, we may therefore conclude that the values of ν defined in terms of apparent surface are identical with the evaporation rates per unit area of true surface.

III. Methods for Determining θ

There are four methods available for determining θ. Common to all methods is the measurement of the caesium vapor pressure (controlled by bulb temperature) in terms of μ_a, by observing the positive ion current to a collector at a negative potential with respect to a hot ($>1200°$K) tungsten filament. As will be demonstrated later, every atom striking the filament leaves as a positive ion so that I_p/e, the saturation positive ion current density divided by the electronic charge, gives μ_a.

Becker's method

Becker observed the time (t_m) required for the electron emission from a filament (initially cleaned by flashing) to reach a maximum value while the filament at temperature T_1 was being coated by a constant supply of Cs vapor. At the maximum, θ was assumed to be unity, that is, the film was taken to be a complete monatomic layer. It was then possible to raise the temperature of the filament to various temperatures (T_2), where the equilibrium θ was less than unity. If the temperature was now lowered to T_1, the electron emission again passed through a maximum as θ increased through unity. The time (t_3) needed for this completion of the film served to measure the θ at T_2 since $\theta=1-t_3/t_m$.

Direct flashing method

If a tungsten filament having a film for which θ is less than 0.08 is suddenly flashed in an accelerating field at a high temperature, all the caesium evaporates as ions giving a ballistic kick on a galvanometer. The filament area together with the ballistic calibration of the galvanometer allow calculation of σ_A and hence of θ.

Two filament method

As shown diagrammatically in Fig. 2, two parallel straight tungsten filaments, A and B, were mounted near the axis of three coaxial

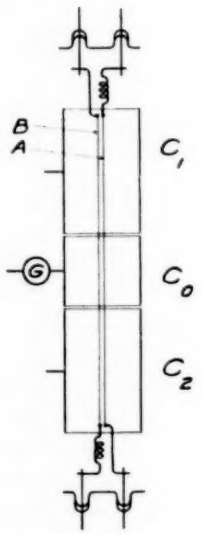

Fig. 2. Filament and collector arrangement in two filament method (diagrammatic).

cylindrical electrodes c_1, c_0 and c_2, placed end to end so that by the guard-ring principle the electron or ion emissions from a known length of the central part of either filament could be measured. The tube is highly evacuated but contains saturated caesium vapor whose pressure is controlled by the tube temperature. The rate of arrival of atoms, μ_a, is measured with B at a temperature of $\sim1200°$K. This steady current is then balanced out so that only changes in current are indicated by the galvanometer (G) connected to c_0; c_1, c_2 and c_0 were usually maintained at 45 volts negative to filament B. The potential of filament A is made 41 ± 2 volts negative to B (4 ± 2 volts positive to c_1, c_2 and c_0). Filament A is then cleaned by flashing at 2400°K. After a steady state (θ) is reached on its surface at any of a series of lower temperatures (300–1200°K), the temperature of A is suddenly raised to about 1800° so that at these voltages all the adsorbed atoms evaporate instantly as neutral atoms, which travel in straight

lines towards the cylinders c. A definite fraction f of these, however, are intercepted by the hot filament B and are converted into ions which pass to the cylinder c_0. The resulting ballistic kick indicated by the galvanometer, together with the known diameters of A and B and the distance of A from B give data for the calculation of σ_A and θ.

The use of the second filament B as a means of measuring concentrations on filament A too high to be flashed directly from A as ions was suggested by Dr. Tonks of this laboratory.

The potential chosen for filament A insures that neither ions nor electrons shall pass to c_0 as the adsorbed atoms are suddenly evaporated. The correct potential for A is most easily found by flashing A when nearly fully coated, with B cold. If A has been made too negative with respect to c_0, a ballistic kick due to electrons is observed; if not sufficiently negative a kick due to ions is noted. With the correct adjustment (critical only to about ± 2 volts) there is no detectable galvanometer deflection when A is flashed even if the initial values of θ on A are varied from 0 to above 1. This fact that the potential of A can be varied as much as 4 volts without detectable galvanometer deflections when B is cold proves that the zero value of current is not due to a balance between electron and ion currents from A, but that each of these currents is zero. This is undoubtedly caused by space charge limitation of the currents during the excessively short time that they can flow while the filament is being flashed. We therefore believe that no source of error is introduced into these measurements by currents from A. Although the sudden evaporation of atoms was usually accomplished by heating the filament by a condenser discharge, increasing the filament current to a value giving a temperature of about 1800° by closing a switch in a battery circuit also gives sufficiently rapid evaporation.

The accumulation method

If μ_a is small, changes in the properties of the film with time can be measured as θ increases slowly from zero. In this method ν_a must remain equal to zero since σ_A and θ are found from the product $\mu_a \times t$. This is accomplished either by working in the lower ranges of θ or at low filament temperatures.

Comparison of the methods for determining θ

(a) Becker's method may be used to determine θ's from about 0.01 to the optimum value θ_{opt} which gives the maximum in the electron emission; it will be shown later that $\theta_{opt} = 0.67$. The method requires not only that θ_{opt} shall be attained and that the electron emission at the optimum be measurable, but also that re-evaporation of atoms is negligible until the maximum is passed. Thus with the sensitive galvanometer used in the present experiments (7×10^{-11} amp./mm) the allowable μ_a was limited to the range between approximately 6×10^{11} and 2×10^{13}, using a testing temperature (T_1) of ~ 550°K. At lower testing temperatures the electron emission cannot be measured. A higher testing temperature raises the lower limit for μ_a. Even though θ_{opt} may be passed through, unless the testing temperature is low enough, atom evaporation may begin near θ_{opt} causing an increase in the time (t_2) required to reach θ_{opt} and a consequent error in the determination of θ. At higher values of μ_a the coating time becomes too short in comparison with the times required to bring the filament from a high temperature to a steady state at the lower testing temperature. For example, a 2 mil filament requires ~ 15 seconds to cool from 1220°K to 600°K. A filament in a bulb containing caesium at room temperature is completely coated in less than one second. The method also fails at high pressures because the θ's to be measured may already be above the optimum.

We have often found another serious difficulty in the application of Becker's method. Fig. 3 shows emission *vs.* time curves taken as in Becker's method. The curve a with a single maximum is obtained for caesium on a clean homogeneous tungsten surface. With extremely minute traces of gaseous impurities which are sometimes hard to avoid but which do not interfere with the application of the other methods of determining θ, we have often obtained two maxima as shown in curve b. With slight modification of the conditions the two maxima may merge into one. In such cases

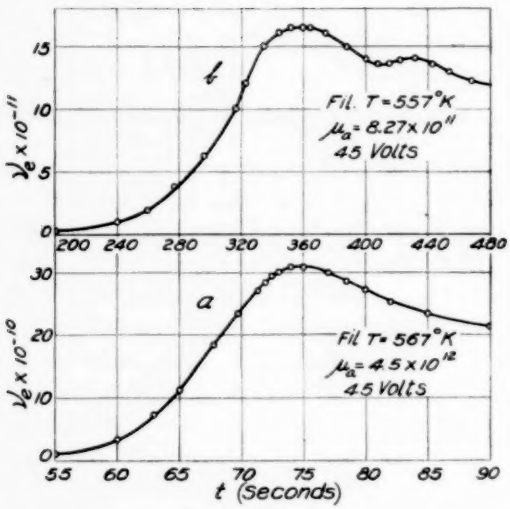

FIG. 3. Electron emission *vs.* time curves as obtained in Becker's method for measuring θ. (a) Clean filament, (b) partly gas covered.

difficulties of interpreting the curves may lead to considerable error in the determination of θ.

(b) The direct flashing method is applied only below $\theta \sim 0.08$ but is so extremely sensitive that θ as low as 10^{-4} can be measured easily.

(c) The accumulation method may be used to produce any value of θ provided μ_a is kept below $\sim 10^{13}$ to give sufficient time for observations. It should find a useful application in the study of contact potentials. Known changes in the surface condition of an electrode receiving electrons can be produced. The resultant changes in contact potential could then be measured up to $\theta = 1$. If the filament or electrode can be cooled sufficiently below the temperature of the tube, the properties of polyatomic films may be studied.

(d) The two filament method was used in the present investigation to study θ from 0.05 to unity. It may be used to study even polyatomic films which may be formed by maintaining the filament for a short time in saturated Cs vapor or by producing supersaturated vapor by rapidly heating the bulb after the filament has cooled.

Calibrations

The validity and accuracy of the various methods for determining θ were tested chiefly by observation of transient effects, i.e., phenomena involving changes in θ with time. In these tests it was assumed first that α is unity under all experimental conditions and second that the positive ion current from a clean hot tungsten filament is an exact measure of μ_a. Experimental proof of both assumptions will be given in Section XI.

If a clean tungsten filament is allowed to coat with caesium for the time t in a retarding field for ions ($\nu_p = 0$), the direct flashing method, if valid, should give measurements from which the number of atoms accumulating per cm^2 in the time t can be calculated. This number should be $\mu_a \times t$.

Fig. 4 shows data obtained by the direct flashing method with the filament at room

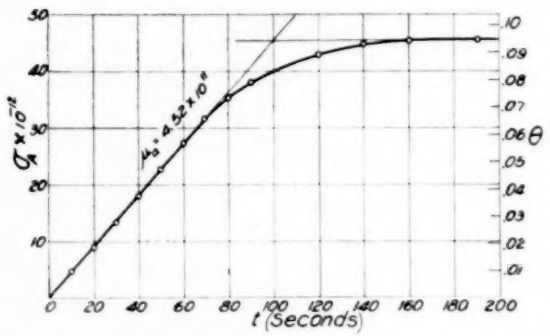

FIG. 4. Accumulation of caesium (concentration σ_A) with time as obtained by the direct flashing method. Filament at room temperature.

temperature during the accumulation period. The ordinates are σ_A (atoms cm^{-2}) as calculated from the ballistic galvanometer kicks. If Q is the quantity of electricity corresponding to the observed kick, $\sigma_A = Q/S_A e$ atoms cm^{-2}, where e is the electron charge. The galvanometer was calibrated ballistically by discharge of a standard condenser charged to a known voltage. The sensitivity was 3.3×10^{-10} coulombs mm^{-1}. The right-hand ordinates are the values of θ. Each point shown corresponds to a separate run in which Cs was allowed to accumulate for the time t after cleaning the filament by flashing.

The straight line in the figure has been drawn with the slope μ_a as given by the steady ion current. The points lie on this line within the experimental error of <1 percent for θ below about 0.07. The deviation above $\theta = 0.07$ is due to evaporation of Cs partly as atoms during the flash to obtain the ballistic kick. These curves remained unchanged if the coating temperature

was varied from 300° to 800°. At still higher temperatures, deviations set in due to the re-evaporation of arriving Cs atoms. These will be described in Section XI.

In the same way the 2-filament method was tested by measuring accumulated amounts of caesium corresponding to θ from ~ 0.05 to nearly 1.0. In this case the ballistic kick Q should equal $S_A \mu_a t f e$, where f is the fraction of the atoms intercepted by filament B. As found from the distance (2.85 mm) between filaments A and B, measured by a microscope with eyepiece scale, f was 0.0071. On plotting the observed values of σ_A, calculated from the ballistic kicks, ($\sigma_A = Q/S_A e f$), it is seen, Fig. 5, that these values

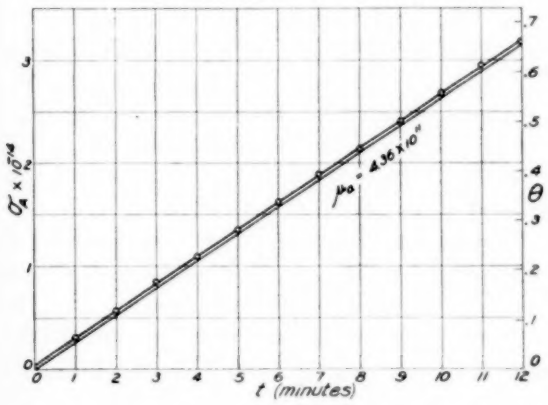

FIG. 5. Calibration of two filament method.

have accurately the calculated slope, μ_a, but are displaced slightly with respect to the calculated line. Thus the kicks extrapolated to zero time were not zero. This displacement was shown to be independent of θ and caesium pressure. A brief investigation did not reveal the cause of the displacement; it is probably connected with the pressure lags mentioned in the next section. This small empirical correction (-0.0086) was applied to all values of θ obtained by the 2-filament method.

In addition to these preliminary comparisons, later measurements of equilibrium values of θ by both the direct flashing and 2-filament methods in the range of θ from 0.05 to 0.08 were in good agreement.

Becker's method was tried out extensively and the limitations already given as to testing temperature and Cs pressure found.

IV. Description of the Experimental Tube

To obtain accurate results by the foregoing methods many precautions are necessary in the construction of the apparatus and in its use.

The caesium pressure must be exactly controlled. The ordinary construction with metal cylindrical electrodes inside a glass bulb does not allow this. These cylinders become heavily coated in the presence of caesium vapor and since their temperature is indefinite and affected by radiation from the filaments, the rate of supply of Cs is non-uniform. The use of metal electrodes deposited directly on the walls of the tube avoids this, by giving more direct thermal contact with the bath liquid.

The guard ring principle must be employed to allow measurement of currents from a known length of filament and to prevent measurement of currents from the ends or any portion of the filament which is not at the temperature of the central part of the filament. This is far more important in studies of caesium on tungsten than for clean tungsten. For example, if the central part of the filament is hot enough to be practically free from caesium, the end portions may be cooled sufficiently by the leads to have high values of θ from which the electron emission is thousands of times greater than from the cleaner central part.

The filaments should be so long that the cooling effect of the leads does not cause a non-uniform temperature over the central part even at low filament temperature.

(1) Preparation of the tube

Fig. 6a shows the glass mantle. The two annular folds (E) were made by pressing together while hot two enlarged sections of the tube. These folds divide the tube into three sections, c_1, c_0 and c_2, spaced $\sim \frac{1}{2}$ mm apart, which later are to serve as electrodes. The connections to each electrode consist of tungsten seals from which 5 mil platinum wires are led to and are partially imbedded in the glass wall.

In Fig. 6a, P is the 10 mil platinum filament in place ready for the coating of the walls by evaporation. The tube at this stage was evacuated and baked at 400°C for 2 hours, after which the oven temperature was lowered to

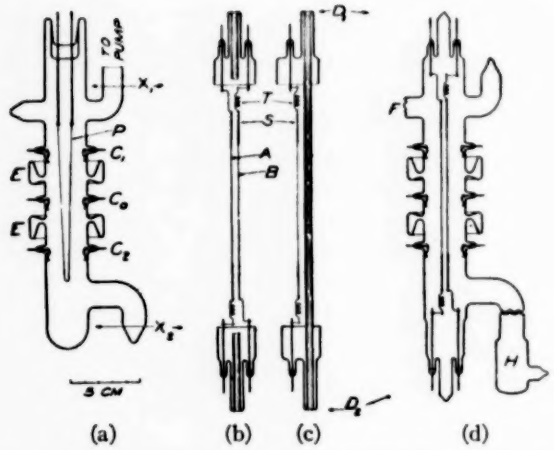

FIG. 6. Preparation of the experimental tube. (a) Outer glass mantle with platinum filament for coating walls. (b) Frame on which the filament structure is mounted and inserted in outer tube. (c) Frame turned through 90°. (d) The completed tube.

about 300°C. The filament was now heated to a temperature where the evaporation of platinum in a period of about two hours was sufficient to coat the glass walls with a film whose resistance as measured between the pairs of leads to each section was less than 50 ohms. Since the greater part of each annular fold received no platinum in this evaporation process, these folds now acted as insulation between the three electrodes, c_1, c_0 and c_2. In addition these folds could later be conveniently heated by a few turns of resistance wire to prevent electrical leaks which otherwise often occurred at the higher caesium pressures.

(2) Preparation of the filament structure

Since the filaments A (2 mil) and B (5 mil) must be accurately and uniformly spaced, they were first mounted on a frame as shown in Fig. 6b. This frame consisted of two pairs of glass seals (with tungsten leads) separated by a rigid glass rod. Fig. 6c shows the frame turned through 90°. The filament structure was adjusted and aligned entirely on this frame. The total length of each filament was 30 cm while the length of the central part in cylinder c_0, was 3 cm. To obtain this length of 30 cm more conveniently, the ends of each filament were wound into tight spirals, (S), the 2 mil filament being wound on a 3 mil mandrel and the 5 mil on a 5 mil mandrel, leaving a straight length of 10 cm between the spirals. By trial the tension springs (T) were selected and stretched so that when heated the filaments remained taut and did not shift laterally.

(3) Complete assembly

Now the platinum coating filament was removed at X_1 and the tube also opened at X_2. The frame carrying the filaments was next inserted, lower end (of smaller diameter than the inside of the main tube) first. It was sealed at X_1 and X_2 after which the glass rod having fulfilled its purpose was removed and its supporting tubes sealed off at D_1 and D_2. The filaments remained as previously adjusted. Fig. 6d shows the completed tube. The tube, with charcoal tube and ionization gauge attached at F, was then evacuated, rebaked and tested with the gauge for leaks and slow evolution of gas. The charcoal tube was separately outgassed at a higher temperature. Just before sealing off, a thin walled glass capsule of caesium was broken in a side tube and about one cc of caesium distilled into the large appendix H. The usual gas evolution in this process was avoided by using capsules filled with caesium which had already been well freed from gas.

The filaments A and B were 2.85 mm apart as determined by examination with a microscope through the clear glass annular folds. From this spacing and the known diameters of A and B, the fraction (f) of the atoms leaving A which are intercepted by B was calculated. $f=0.0071$.

Aging of tungsten filaments

In previous work on the electron emission from clean tungsten it has been found necessary to age the filaments to obtain reproducible results. With Cs on W an aging process is perhaps even more important. All filaments used were aged at 2400°K for at least 10 hours followed by an hour at 2600° and finally several short flashes at 2900°. It was further shown that the rate of evaporation of Cs ions from the filament was a most sensitive guide in this process. The cold filament was allowed to coat with Cs, the tube being at room temperature. The tube was then immersed in liquid air to freeze out all Cs vapor. Next the filament was heated to a temperature (about 850°K) where the rate of ion evaporation was slow enough to be followed

on a sensitive galvanometer. If the filament were not sufficiently aged, the plot of evaporation rate against time or against the amount of Cs, θ, left on the surface at any time, showed a number of maxima or peaks as in Fig. 7. These

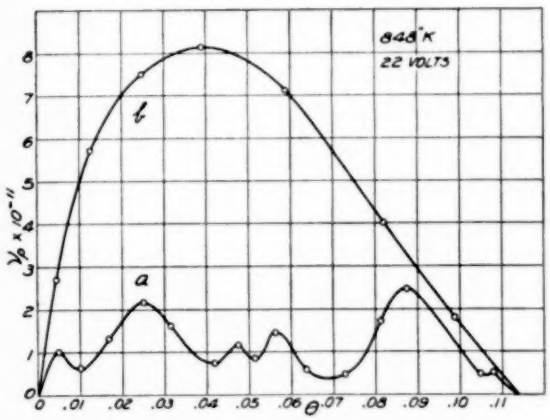

FIG. 7. (a) Irregular evaporation rate for ions from an unaged filament. (b) Uniform variation of evaporation rate from a sufficiently aged filament.

peaks were also observed by Kingdon in earlier unpublished work. Such irregular evaporation is probably caused by non-uniformities of the tungsten surface and would make it difficult to obtain rates and heats of evaporation characteristic of the whole surface. After sufficient aging, the rates of evaporation increased to maximum values and the peaks merge into a smooth curve as also shown in Fig. 7. Further aging produces no change. It was found that a fine grained filament was most easily brought into this final condition and such filaments were used in this work. The average grain size in these filaments was about one-fifth the diameter of the wire.

Control of μ_a

In these experiments μ_a was varied about one thousand-fold from $\sim 10^{11}$ to 10^{14} atoms cm^{-2} $sec.^{-1}$. To maintain any particular pressure a large Dewar flask containing kerosene vigorously stirred surrounded the tube. The bath was heated electrically or cooled below room temperature by use of a coil containing liquid air. In preliminary experiments only the appendix *H* was immersed in the bath, the rest of the tube being at room temperature. It was then observed that the galvanometer readings following ballistic kicks, especially at high θ's, did not return immediately to zero, but showed a lag of several seconds. This lag was found to be due to the burst of atoms suddenly liberated from filament *A*. These apparently did not come instantly to equilibrium with the walls of the tube and there resulted a pressure increase of short duration which was registered on filament *B*. This effect was eliminated by freshly coating the walls of the tube with caesium before any daily series of experiments and by immersing the whole tube in the bath liquid. This served to cover and keep covered any spots on the walls of the tube which were not acting as true caesium surfaces.

Filament temperatures

The filament temperatures were found from the known diameter and the measured value of filament current. The temperature scale for tungsten and the tables given by Jones and Langmuir[8] were used.

Below $\sim 550°$, even with the long filament used, cooling of the central part of the filament *A* became appreciable, because of conduction from the leads at bath temperature. Below, $\sim 750°$K, an increase in filament temperature due to radiation received from filament *B* (1200°) sets in.

The lead cooling correction was calculated[9] and it was shown that though the temperature of the 3 cm long central part of the filament was reduced, the distribution remained uniform to $<1°$. The lead loss correction was $-3°$ at 550°K and $-20°$ at 430°K, the lowest temperature used in measurements of atom evaporation.

The radiation correction was determined in two ways. First the change in resistance of the filament *A* was observed with *B* hot and cold, at various temperatures of *A*. Second, the current required to produce a given electron emission (μ_a constant) when filament *B* was hot and cold was observed. By comparison the true temperature of *A* with *B* hot was obtained. The radiation correction amounted to $+3°$ at 750°K and $+50°$ at 430°K.

[8] H. A. Jones and I. Langmuir, G. E. Rev. **30**, 310, 354 (1927).

[9] I. Langmuir, S. MacLane and K. B. Blodgett, Phys. Rev. **35**, 478 (1930).

V. Determination of σ_{A1}

Various low pressures ($\mu_a = 10^{11}$ to 10^{13}) of caesium were established and then filament A was maintained at a low temperature T_1 until trial showed that σ_A had reached its limiting steady value fixed by the balance between evaporation and condensation. In successive experiments, as T_1 was progressively lowered, it was found that σ_A, as given by the 2-filament method, increased at first rather rapidly and then very slowly until finally when T_1 was reduced below about 325°K no further increase in σ_A occurred. This quite definite limiting value which was observed in numerous experiments was presumed to be the value σ_{A1} corresponding to a complete monatomic film. These experiments gave $\sigma_{A1} = (4.80 \pm 0.05) \times 10^{14}$ atoms cm^{-2}.

Intervals at higher temperatures ($\sim$400°K) to allow possible favorable rearrangements by migration did not change σ_{A1}. Only by cooling the filament (by immersion of leads in liquid air) below the temperature (bath temperature) corresponding to saturated caesium vapor were other values of σ observed. These were greater than 4.8×10^{-14} and increased very rapidly as the filament was cooled below bath temperature. If the filament was now heated only slightly above bath temperature, $\sigma_{A1} = 4.8 \times 10^{-14}$ was again obtained.

In these experiments no detailed study was made of the conditions which give values of σ_A slightly lower than σ_{A1}. In later experiments, Section XII, the actual slow variation of σ with T and μ_a in this region was recorded and further justification is given for regarding this limiting value as that corresponding to a complete monatomic film.

VI. Analysis of Experimental Data on Atom Evaporation

Fig. 8 gives the experimental data on atom evaporation. The apparent (observed) concentration of adsorbed caesium, σ_A, is plotted as a function of $1/T$. For each curve μ_a is constant and has the value indicated. The values of σ_A above 0.25×10^{14} were determined by the 2-filament method. Below 0.30×10^{14}, σ_A was determined by the direct flashing method. An enlarged plot of the lower σ_A data is also given.

The equation chosen for analysis of the data is

$$\ln \nu_a = A_a - B_a/T, \tag{6}$$

where A_a and B_a were functions of θ only. It has been shown theoretically[2] that A_a consists of two parts such that

$$A_a = A + S, \tag{7}$$

where

$$S = \ln \theta + 1/(1-\theta) - \ln (1-\theta). \tag{8}$$

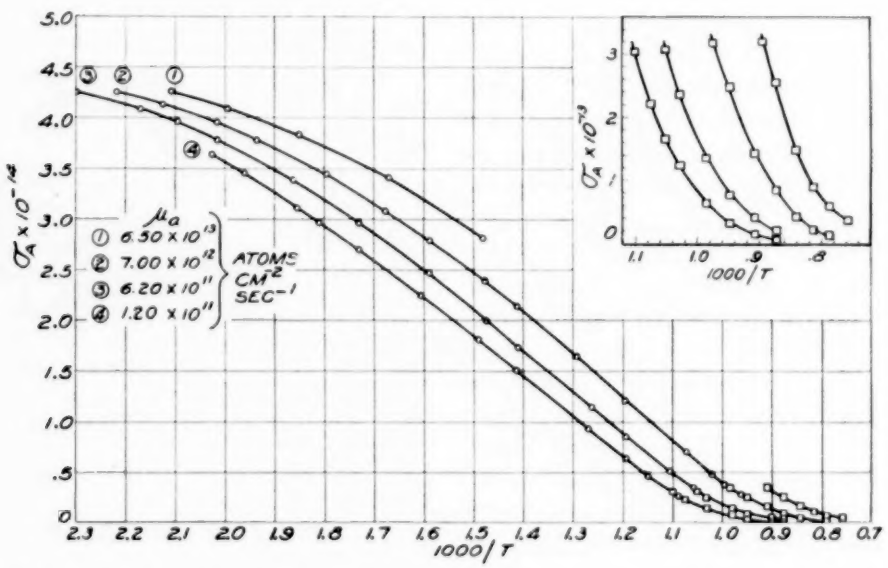

Fig. 8. Experimental data on atom evaporation. Observed concentration of caesium (σ_A) as a function of $1/T$.

The dependence of A and B_a on θ remained to be determined by the experiments.

If this form of equation is applicable to the observed data, then $(\ln \nu_a - S)$ plotted as a function of $1/T$, at any value of θ, should give straight lines of slope B_a and intercept A. With the values of $\nu_a (=\mu_a)$ and $1/T$ at various constant values of σ, read from the smooth curves (Fig. 8) drawn through the experimental points, such straight lines were obtained. The intercepts, A, showed a small variation with θ expressed empirically by

$$A = 61 + 4.8(\theta - \tfrac{1}{2}\theta^2). \qquad (9)$$

With values of A and S from Eqs. (9) and (8) A_a was calculated as a function of θ. From these values of A_a and the observed values of ν_a and T from the data shown in Fig. 8, B_a was calculated by Eq. (6). For values of θ up to about 0.6, it was found empirically that B_a for all values of μ_a could be represented by

$$B_a = 32{,}380/(1 + 0.714\theta) \qquad (10)$$

within the experimental error of about 0.3 percent. For larger θ's, B_a deviated from this expression slightly; however, the deviation was about 2 percent at $\theta = 0.8$ and 4 percent at $\theta = 0.9$.

The extent of the agreement of the values of B_a obtained from the experimental data with the empirical equation, Eq. (10), is shown in Fig. 9 which is a plot of $1/B_a$ against θ. If the data are to agree with Eq. (10), the points should lie on a straight line.

In the first analysis of the data by this method, values of $1/B_a$ were obtained which fitted Eq. (10) down to $\theta = 0.05$. Below this $1/B_a$ deviated as shown at X in Fig. 9. Such a deviation means that the observed values of ν_a were less than those calculated by Eq. (6) when using values of B_a from Eq. (10). At such low surface concentrations, repulsive forces between adatoms should begin to be inappreciable so that the equation of state of the adsorbed film on a *homogeneous* tungsten surface should approach that of an ideal 2-dimensional gas, *viz.*, $F = \sigma kT$. This would mean that the heat of evaporation measured by B_a should change very little with θ for these small values of θ. It seems possible to account for the increasingly rapid

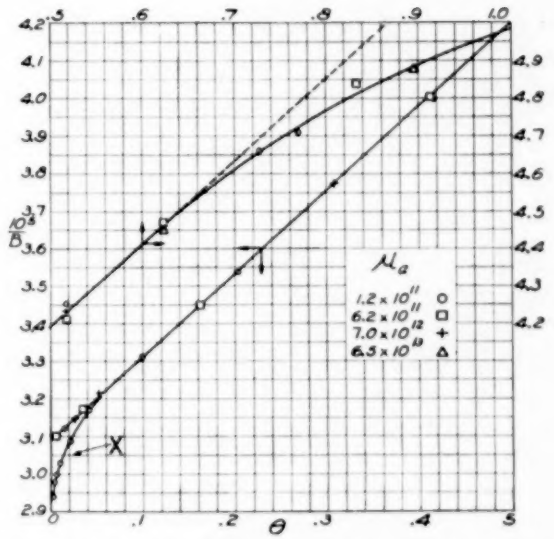

FIG. 9. Experimental variation of $1/B_a$ with θ. B_a is proportional to the heat of evaporation for atoms. X is the deviation caused by the active areas.

change in B_a at low θ as shown by curve X, only if the tungsten surface is not completely homogeneous. By trial it was found that this difficulty disappeared if it was assumed that 0.5 percent of the tungsten surface holds caesium so much more firmly than the rest that this *active surface* becomes saturated before more than 0.5 percent of the remaining surface is occupied. Thus the total concentration could be expressed as

$$\sigma_{obs} = \sigma_a + \sigma_n = \sigma_{A1}(\theta_a + \theta_n), \qquad (11)$$

where the subscripts refer to the active and normal parts of the surface. When the active surface becomes saturated, so that $\theta_a = 0.005$,

$$\theta_n = \theta_{obs} - 0.005. \qquad (12)$$

Calculating ν_a or $1/B_a$ from Eqs. (6) and (10) with θ_n instead of θ_{obs} gave agreement with experiment down to values of θ_n as low as 0.01, as shown by the points that lie along the straight line in Fig. 9. Any deviations which existed below this concentration were to be attributed to lack of saturation of the active surface, i.e., when $\theta_a < 0.005$.

The validity of Eqs. (6), (9) and (10) and likewise the precision of the experimental determinations of θ, is shown by the fact that the experimental points in Fig. 8 have an average deviation from the calculated curve of about 1°

in T with no deviation greater than 3° up to $\theta \backsimeq 0.6$; at higher θ's the deviations vary from 2 to 15°.

For convenience in calculation, Eq. (6) may be written with common logs as

$$\log_{10} \nu_a = \mathbf{A}_a - \mathbf{B}_a/T \qquad (13)$$

where $\mathbf{A}_a$ and $\mathbf{B}_a$ in heavy faced type represent the values of A_a and B_a (from Eqs. (7) and (10)) divided by 2.303. Table I in the first two columns contains values of $\mathbf{A}_a$ and $\mathbf{B}_a$. Up to $\theta = 0.6$ the tabulated values of $\mathbf{B}_a$ were calculated from Eq. (10). At higher θ's the experimental variation of $\mathbf{B}_a$ with θ was used as determined from Fig. 9. Complete explanation of the use of Table I will be given in Section X after electron and ion emission have also been discussed.

Fig. 10 shows θ_n as a function of $1/T$ (calculated through Table I) for a large range of values of μ_a.

TABLE I. *Data for calculation of evaporation rates.*
$\text{Log}_{10}\, \nu = \mathbf{A} - \mathbf{B}/T$

(Note that here common logs are used. To obtain values of A_a and B_a for use in Eqs. (6) to (10) multiply the tabulated values by 2.303.)

	Atoms (ν_a)		Ions (ν_p)		Electrons (ν_e) $\mathbf{A}_e = 27.55$	
θ_n	$\mathbf{A}_a$	$\mathbf{B}_a$	$\mathbf{A}_p$	$\mathbf{B}_p$	$\mathbf{B}_e$	V_e
0		14061.2		10293.6	23990	0.000
0.002	24.2328	14043.2	23.9318	10409	23853	.0268
.005	24.6401	14013.3	24.3391	10515.6	23716	.0540
.01	24.9558	13963.8	24.6549	10730.1	23452	.1064
.02	25.2859	13866	24.9849	11141.8	22941	.2079
.03	25.4913	13769	25.1904	11530	22457	.3038
.04	25.6459	13673	25.3450	11898	21992	.3960
.05	25.7719	13579	25.4709	12248	21549	.4840
.06	25.8804	13486	25.5795	12582	21122	.5686
.07	25.9764	13394	25.6755	12894	20719	.6487
.08	26.0633	13304	25.7623	13196	20325	.7267
.10	26.2179	13127	25.9169	13761	19584	.8738
.12	26.3556	12954	26.0546	14284	18888	1.012
.15	26.5388	12703	26.2379	15029	17893	1.2094
.20	26.8081	12306	26.507	16095	16429	1.500
.25	27.050	11934	26.749	17061	15089	1.7658
.30	27.276	11583	26.975	17907	13891	2.0034
.40	27.707	10939	27.406	19365	11792	2.420
.50	28.142	10364	27.841	20350	10230	2.73
.55	28.375	10098	28.069	20588	9726	2.83
.60	28.629	9849	28.328	20638	9424	2.89
.65	28.916	9623	28.612	20563	9272	2.92
.70	29.256	9425	28.955	20368	9272	2.92
.75	29.683	9256	29.377	20103	9373	2.90
.80	30.266	9110	29.965	19800	9524	2.87
.85	31.159	8985				
.90	32.821	8881				
.95	37.495	8798				
1.00		8733				

Theory of adsorption by isolated active spots

If the isolated active areas are all alike and each is capable of holding only one adatom, the average life τ_a of an adatom on the active area is independent of σ_a. Since the probability per second for the evaporation of any adatom is

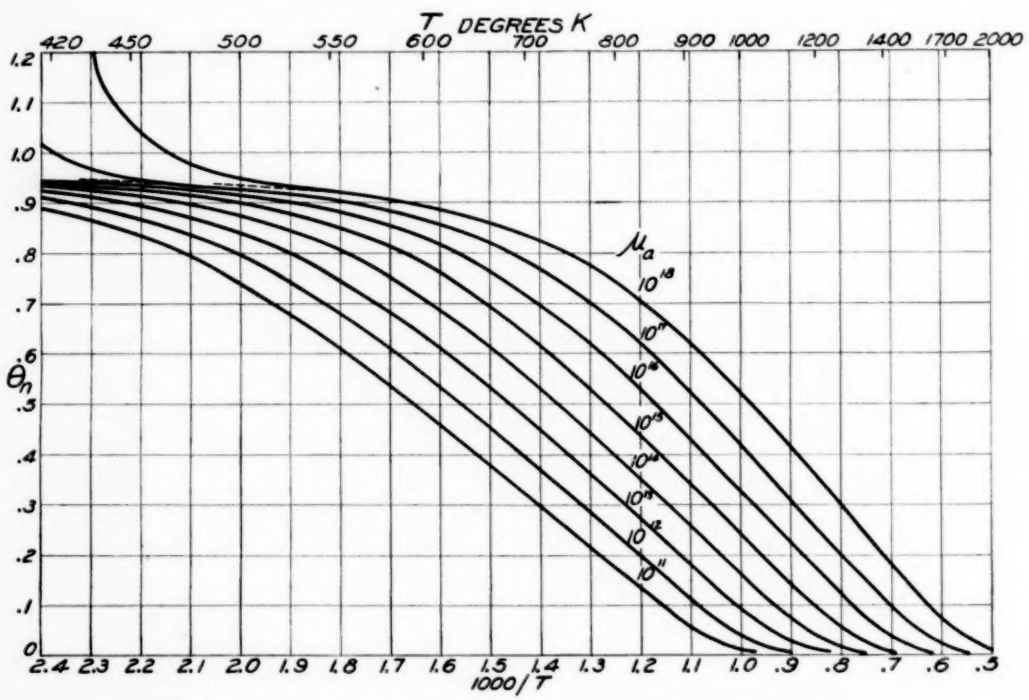

FIG. 10. Fraction (θ_n) of the tungsten surface covered with caesium at the temperature T; calculated (Eq. (6) or Table I) for different μ_a's. μ_a is proportional to caesium pressure.

$1/\tau_a$, the total rate of evaporation from the active areas is σ_a/τ_a.

In a steady state this must be balanced by the rate of arrival of adatoms from the vapor phase. Since α for the surface as a whole is unity, we must assume that an incident atom whose path is directed towards an elementary space of the active area which is already occupied by an adatom, condenses in an adjacent vacant normal space. The total rate of arrival into the active areas from the vapor phase is thus $\mu(\theta_{a1}-\theta_a)$, where θ_{a1} is the maximum value of θ_a. Equating the rates of evaporation and condensation we have

$$\mu(\theta_{a1}-\theta_a)/\theta_a=\sigma_{a1}/\tau_a. \qquad (14)$$

Langmuir has derived a general equation for the life of adatoms which may readily be put in the form[10]

$$\tau/\sigma_{a1}=1.73\times10^{-27}M^{\frac{1}{2}}T_M^{-1}\epsilon^{b/T} \qquad (15)$$

where T_M is the mean temperature over the range of validity of the equation. Taking $T_M=800°$ and $M=133$ (the atomic weight of Cs) and eliminating σ_{a1}/τ_a between this equation and Eq. (14) we obtain

$$\ln[\mu(\theta_{a1}-\theta_a)/\theta_a]=65.8-b/T.$$

With common logarithms this becomes

$$\log_{10}[\mu(\theta_{a1}-\theta_a)/\theta_a]=28.58-\mathbf{B}'/T. \qquad (16)$$

In these equations θ_{a1} and $\mathbf{B}'$ should be constants whose values we now wish to determine from our experimental data on θ_{obs} as a function of μ and T for very dilute caesium films. These data are given in the first three columns of Table II.

TABLE II. *Relation of adsorption on active and on normal areas for dilute caesium films.*

1 μ_a	2 θ_{obs}	3 $10^3/T$	4 $\mathbf{A}_a$	5 $\mathbf{B}_a$	6 θ_n	7 θ_a	8 θ'	9 $\mathbf{B}'$
1.2×10^{11}	.00209	.891	23607	14059	.00048	.00161	.322	19306
	.00419	.925	24076	14050	.00141	.00278	.555	19020
	.00628	.945	24345	14037	.00257	.00371	.742	19000
7.0×10^{12}	.00209	.775	23739	14058	.00065	.00144	.288	19797
	.00419	.810	24219	14043	.00195	.00224	.448	19328
	.00628	.828	24461	14030	.00337	.00291	.582	19188
	.01047	.850	24744	14000	.00630	.00417	.835	19388

[10] See reference 2. The above Eq. (15) is obtained by combining Eqs. (5), (6), (7) and (37) on pages 2799 and 2806.

A series of trials has shown that the best agreement of these data with Eq. (16) is obtained if we take $\theta_{a1}=0.005$ as found in the preliminary analysis which led to Eq. (12).

Since μ can be expressed as a function of θ_n and T by Eqs. (6) to (10) or by Table I, we can by a series of approximations (or graphically) determine θ_n for each set of experimental values of μ and T. The values calculated in this way are given in the 6th column of Table II. Columns 4 and 5 contain values of $\mathbf{A}_a$ and $\mathbf{B}_a$ used in these calculations.

Subtracting θ_n from θ_{obs} in accordance with Eq. (12) we obtain the values of θ_a given in the 7th column. The 8th column contains θ', the fraction of the active surface occupied by adatoms:

$$\theta'=\theta_a/\theta_{a1}=200\theta_a.$$

The 9th column contains values of $\mathbf{B}'$ calculated from Eq. (16) from the values of μ, θ_a, and T in the table. These results fully justify our assumption that $\mathbf{B}'$ is independent of θ_a and indicate that the adatoms in the active areas are so far apart that they do not influence one another and therefore are to be regarded as isolated active spots. Eq. (16) becomes

$$\log_{10}[\mu(1-\theta')/\theta']=28.58-19{,}300/T. \qquad (17)$$

These "active" spots may be located at any reentrant angle between crystal planes or at irregularities in the lattice which may cause a Cs atom to be held more tightly than at other points. Thus the active area θ_{a1} will probably vary in extent depending on the grain size of the filament and on the heat treatment given. However, the properties of the normal surface will be unaffected. It is to be noted that Eq. (17) is in such a form as to be valid even if θ_{a1} should change.

VII. Equation of State and Evaporation Equation for the Adsorbed Cs Film

The equation of state of the two dimensional gas making up the adsorbed film was found theoretically[2] for molecules which repel as dipoles, by means of the Clausius virial. The forces are repulsive forces varying as the inverse 4th power of the distance (r) between adatoms. This equation gave the spreading force F in

terms of θ, T, and the dipole moment M. By use of Gibbs' equation for the adsorption isotherm, the rate of evaporation of atoms ν_a could be expressed in terms of θ, T, and the spreading force F. These equations were of the form required by the experimental data. Therefore F and hence M could be calculated as functions of θ entirely from data on the evaporation of atoms.

The contact potential of the surface against that for pure tungsten could also be calculated from the relation.

$$V_c = 2\pi M\sigma(\text{c.g.s.}) = 1885 M\sigma_1\theta \text{ volts.} \quad (18)$$

After obtaining V_c, the electron emission ν_e was calculated for any value of θ from the Boltzmann equation,

$$\nu_e/\nu_w = \exp(V_c e/kT) \quad (19)$$

and Dushman's equation for ν_w, the electron emission from clean tungsten.

Likewise the rate of ion evaporation, ν_p, was calculable[11] with the aid of the Saha equation and was given by

$$\ln(2\nu_p) = \ln \nu_a + (e/kT)(V_w - V_i - V_c) \quad (20)$$

where V_w is the electron affinity of pure tungsten 4.62 volts, V_i is the ionizing potential of the caesium atoms 3.874 volts, and V_c is the contact potential as defined above. Thus from data on neutral atom evaporation (ν_a, θ, T) it was possible to calculate M, V_c, ν_e, and ν_p for comparison with the experimental values of these quantities. Further details and a tabulation of the calculated values of F, M, V_c, and other quantities included in the theoretical equations are given in reference 2.

VIII. Contact Potential and Electron Emission (Experimental)

The electron emission, ν_e, was measured from filament A at various filament temperatures and pressures of Cs. The relation between θ and pressure being known, the θ corresponding to each emission was also known. As a check in part of the runs, θ was determined immediately following the measurement of ν_e, by flashing to filament B (2-filament method).

The values of ν_e involved in the calculation of contact potentials from the Boltzmann Eq. (19) and for use in equations relating ν_e to ν_a and ν_p, must correspond to thermodynamic equilibrium and hence were measured at zero field. The effect of the external field on the electron emission from Cs coated tungsten is in general larger than for pure tungsten and varies with θ. Current-voltage data were taken for a series of constant temperatures and constant values of Cs pressure, corresponding to values of θ from 0.16 to 0.80. As shown in Fig. 11 there were sharp breaks in the plotted data and the value of ν_e at the break was taken to represent ν_e at zero field. The great variation of the effect with θ is readily seen. Fig. 12 shows that at high and low values of θ the variation of ν_e with voltage approaches that for clean tungsten. The largest departure is near $\theta = 0.55$ and decreases rapidly beyond a θ of about 0.65. The slopes below θ's of 0.30 were not measured accurately enough to

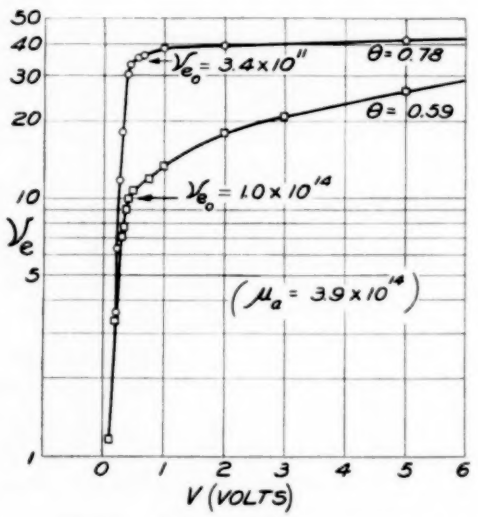

FIG. 11. Electron emission (ν_e) *vs.* voltage for Cs on W. Example of curves used to determine ν_e at zero field.

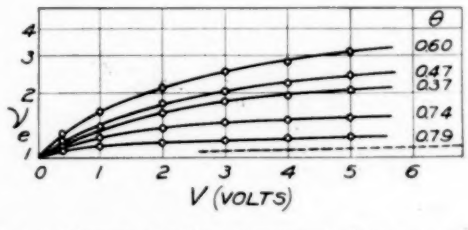

FIG. 12. Change of effect of external field on ν_e with θ. Dotted line indicates slope of curve for pure tungsten, $\theta = 0$.

[11] See reference 2, pages 2825–2826.

show how rapidly the behavior of clean tungsten was approached at low θ. It should also be noted (Fig. 13) that the zero-field emission as obtained in this way may be far lower than that value obtained by extrapolating the normal higher voltage range Schottky slope to zero field as Dushman has done.[12]

To compare these electron emission data with the values calculated from experiments on atom evaporation as described in Section VII, the corresponding values of the contact potentials against a pure tungsten surface are plotted in Fig. 14 as functions of θ. The heavy line curve

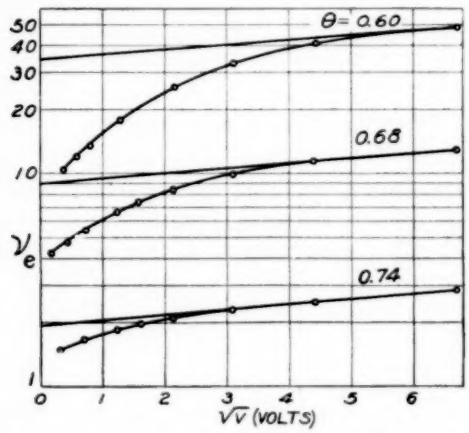

FIG. 13. Theoretical Schottky slope (straight lines) compared to actual course of current-voltage curves as zero field is approached.

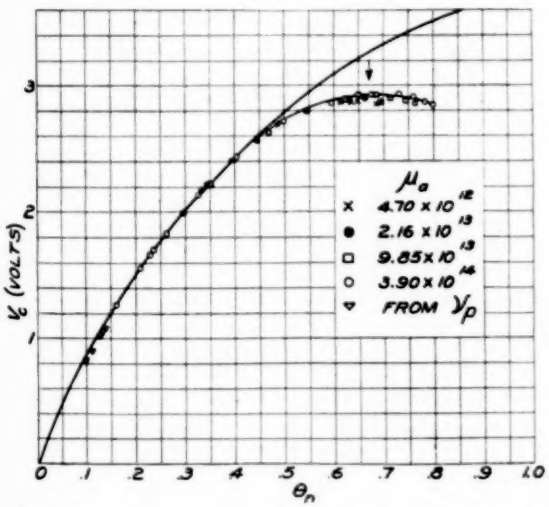

FIG. 14. Contact potential V_c. Variation with θ as determined from measurements of ν_e given by circles, etc. V_c from measurements of ν_p given by triangles. Values calculated from atom evaporation data given by heavier solid curve.

[12] S. Dushman, G. E. Rev. **26**, 157 (1923).

is calculated from data on ν_a by the methods described in Section VII, by using a temperature of 800°K. The values obtained with $T=600°$ or $T=1000°$ are practically identical with those at 800° (within about 0.02 volt for V_c). The points indicated by circles, etc., are the contact potentials calculated by Eq. (19), from the ratio of the observed electron emission to that from pure tungsten. The agreement is excellent up to θ of about 0.50. At this point the values obtained from ν_a deviate and show no maximum as do the points calculated from the observed electron emission. The deviation in this region is probably to be explained by a change in the law of force between adatoms as the atoms become crowded. The force varying as r^{-4}, as used in the theory, is evidently no longer adequate.

Table III contains the data on ν_e for a series of values of θ and T at four different Cs pressures, together with the contact potentials calculated from Eq. (19). Over the entire range of θ, T changed about 500°. At constant θ, ν_a varied about 100-fold and T changed 20 to 30° in going from the lowest to the highest Cs pressure. This small range of T prevents any conclusions as to the effect of temperature on the contact potentials. However, the value 2.8 volts, obtained by Langmuir and Kingdon,[13] for a heavily Cs coated filament, by direct measurement at ~300°K, suggests there is no large dependence on temperature.

It is to be noted that the maximum V_c or ν_e occurs at $\theta=0.67$ and decreases as θ approaches 1.0. As θ's of 0.5 to 0.6 are approached, the adsorbed Cs atoms begin to form a fairly continuous layer. The outer surface of the layer begins to have the properties of Cs and not those of a composite surface of Cs and bare tungsten as is the case at lower θ's. At still higher values of θ the already crowded layer tends to be compressed and the adsorbed atoms are given in effect smaller atomic volumes. In general, smaller atomic volume is accompanied by lower electron emission. This may explain the decrease in ν_e at values of $\theta>0.7$.

Since the values of contact potential from ν_a and ν_e agree so well below $\theta=0.50$, the values from ν_a have been used with Eq. (19) to construct

[13] I. Langmuir and K. H. Kingdon, Phys. Rev. **34**, 129 (1929).

TABLE III. *Data on electron emission and calculated contact potential.*

$\mu_a = 4.70\times10^{12}$				2.16×10^{13}				9.85×10^{13}				3.90×10^{14}			
T	θ	ν_e	V_c	T	θ	ν_e	V_c	T	θ	ν_e	V_c	T	θ	ν_e	V_c
774	.333	5×10^{10}	2.17	836	.298	7×10^{10}	1.99	928	.238	9×10^{10}	1.70	1050	.167	1.0×10^{11}	1.31
736	.392	3×10^{11}	2.41	801	.345	3.6×10^{11}	2.22	906	.264	2.4×10^{11}	1.85	1001	.211	2.5×10^{11}	1.56
677	.492	1.7×10^{12}	2.70	736	.443	3.7×10^{12}	2.57	836	.349	2.4×10^{12}	2.24	980	.231	4.5×10^{11}	1.66
613	.613	1.0×10^{12}	2.86	677	.545	9×10^{12}	2.80	736	.499	3.3×10^{13}	2.71	950	.263	1.0×10^{12}	1.82
604	.632	6×10^{11}	2.87	630	.631	3.8×10^{12}	2.89	677	.598	3.2×10^{13}	2.87	895	.327	6.2×10^{12}	2.14
596	.648	3.2×10^{11}	2.86	613	.663	1.5×10^{12}	2.89	661	.625	2.1×10^{13}	2.89	836	.402	3.1×10^{13}	2.43
586	.668	1.6×10^{11}	2.85	596	.696	4×10^{11}	2.87	646	.652	1.3×10^{13}	2.91	789	.467	7.6×10^{13}	2.62
578	.685	6.5×10^{10}	2.84					630	.682	5.6×10^{12}	2.91	707	.595	1.0×10^{14}	2.86
								613	.713	1.9×10^{12}	2.90	661	.673	4.2×10^{13}	2.93
								596	.745	3.7×10^{11}	2.87	630	.729	8.8×10^{12}	2.93
								586	.763	1.4×10^{11}	2.84	613	.755	2.3×10^{12}	2.93
												596	.783	3.4×10^{11}	2.86
												586	.797	1.6×10^{11}	2.85

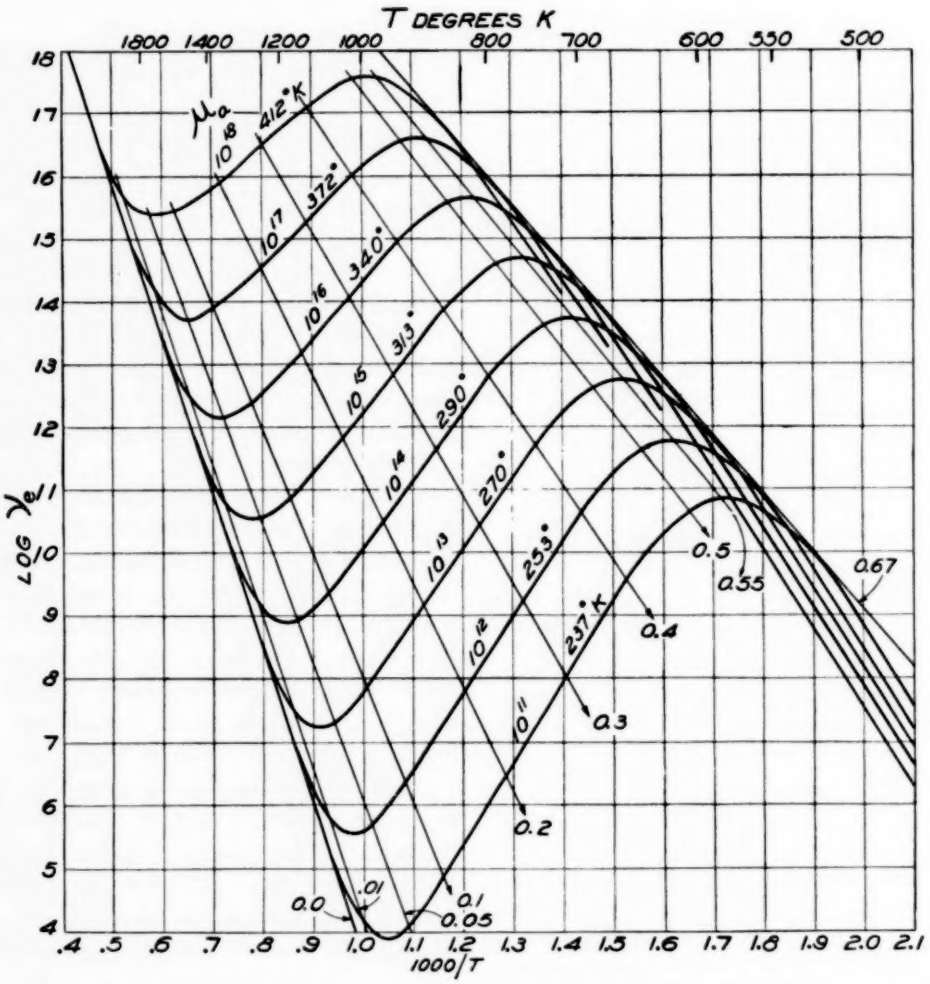

FIG. 15. Field-free electron emission (calculated) from a tungsten filament in equilibrium with Cs vapor at the filament temperature T. Rate of arrival (μ_a) of Cs and bath temperatures given on each curve. Pressure at 237°K is 6.7×10^{-7} baryes; at 412°K it is 8.8 baryes. Diagonal straight lines intersecting the curves give corresponding values of θ_n.

plots of ν_e *vs.* $1/T$ down to low values of θ. Fig. 15 shows a family of curves calculated for a series of values of μ_a. The curves were found for $\theta > 0.5$ by using the values of V_c taken from the smooth curve (Fig. 14) through the points calculated from ν_e. The highest (412°K) corresponds to a pressure of 8.8 baryes; the lowest (237°K) to 6.7×10^{-7} baryes. The curves at higher pressures may be compared with older unpublished data of Kingdon taken in the region of very low θ (0–3 percent), where the caesium emission approaches that of pure tungsten (ν_w). This is of particular interest because it may show whether the equations and constants obtained at the pressures of the present experiments can be used to calculate electron emissions at pressures many thousand times greater.

The comparison showed a difference of about 20 percent in the ratio ν_e/ν_w, the calculated values of ν_e/ν_w being lower. This is a satisfactory agreement considering the difficulty of making experiments at high pressures.

In connection with this comparison with the data of Kingdon, it is desired to correct certain equations and statements in the first paper by Langmuir and Kingdon[1] on the *Thermionic Effects Caused by Vapors of Alkali Metals*. In this work no scale of θ was available and an equation (Eq. (10), page (71)) from which θ had been eliminated was derived. This equation was to be applied in the region of very low θ. This equation in corrected form should be,

$$(\nu_e/\nu_w)^{a_1/c} \quad \ln(\nu_e/\nu_w) = (c/d)\nu_a \qquad (21)$$

derived from the two approximate equations, valid for low values of θ,

$$\ln(\nu_a/\theta) = a + a_1\theta; \quad \ln(\nu_e/\theta) = c\theta.$$

The equations representing ν_a and ν_e in the present experiments have been put in this form and the constants determined.

$$a_1 = 23{,}100/T + 6.8; \quad \ln d = 62 - 32{,}380/T$$

$$a = 62 - 32380/T; \quad a_1/c = 0.188 + 5.53 \times 10^{-5} T.$$

$$c = 123{,}000/T.$$

Calculations of ν_e or ν_e/ν_w from Eq. (21) give good agreement with the exact Eq. (19) up to θ of about 0.04. This treatment is probably applicable to dilute films in general.

In developing an equation of state, Gibbs' equation was given in a wrong form. Correctly it should be $dF/d \ln \nu_a = nkT$ as given in the present paper.

Fig. 1 in the paper by Langmuir and Kingdon shows electron emission curves plotted as in Fig. 15 of the present paper. The data of Langmuir and Kingdon were not corrected for the cooling effects of the filament leads and were not determined for zero field. Comparison of corresponding points shows emissions in Fig. 15 to be 1/3 to 1/8 of those found by Langmuir and Kingdon.

IX. Positive Ion Evaporation (Experimental)

The rate of ion evaporation was also studied as a function of filament temperature and θ at various pressures of caesium. The emission varies with field about as much as for electron emission; ν_p at zero field was obtained in the same manner as for ν_e, although (Fig. 16), the break in the log ν_p *vs.* voltage curve was not as readily determined. For this reason a slightly different method was also employed. The voltage required to keep ν_p constant as the filament temperature was varied was found to change rapidly as the

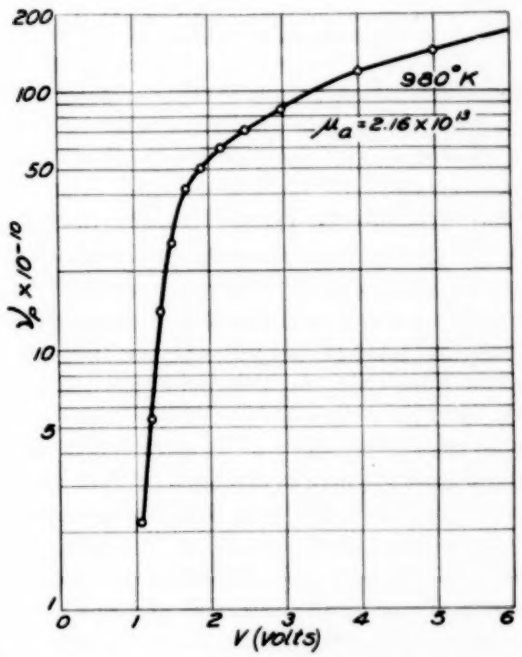

Fig. 16. Current voltage data for positive ion evaporation.

zero of potential was approached, thus allowing a closer estimate of ν_p at zero field, by choosing the point of greatest curvature. Fig. 17. Since $\mu_a = \nu_a + \nu_p$, θ could be found for any value of ν_p from the known relation between ν_a and θ. To compare with the theoretical value of ν_p, Eq. (20) was used together with ln $\nu_{p(\text{obs})}$ to calculate the contact potential V_c. The points in Fig. 14 in the region $\theta = 0.10$ to 0.14 were so calculated. The disagreement is not greater than might correspond to errors in obtaining ν_p at zero field.

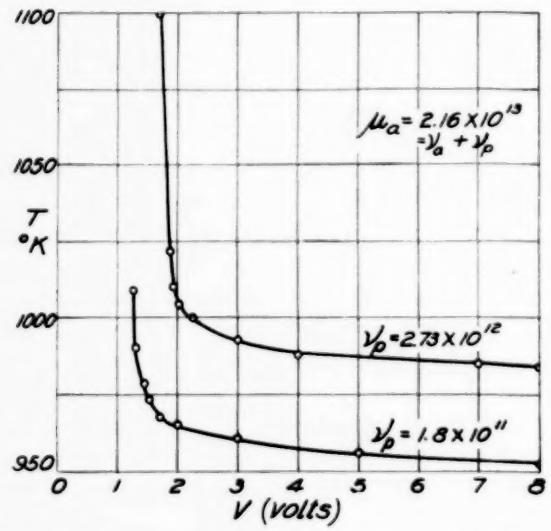

FIG. 17. Temperature voltage data for constant ν_p. Curves used to determine ν_p at zero field.

In connection with the study of positive ion evaporation rates as a function of θ, the following general characteristics of positive ion evaporation may be given.

Fig. 18 shows the exponential increase of ν_p with temperature at constant values of $\mu_a (= \nu_a + \nu_p)$. Depending on the pressure, a discontinuity sets in at a fairly definite critical temperature (which increases with μ_a) and ν_p rises at a constant rate until the value characteristic of a clean tungsten filament is reached. The variation of this maximum value of ν_p with temperature and the external field is discussed in Section XI. The discontinuity has been observed previously by Langmuir and Kingdon,[1] Killian[14] and Becker.[3] Langmuir and Kingdon[1] have shown that this discontinuity indicates the existence of caesium in two surface phases.

[14] T. J. Killian, Phys. Rev. **27**, 578 (1926).

Becker[3] was the first to point out that the existence of the two stable phases was a consequence of the relation between $\nu_a + \nu_p$ and θ.

Fig. 19 shows both atom and ion evaporation rates (calculated) in the region where ν_a and ν_p are of comparable magnitude. The full line ABC gives the sum of atom and ion rates from a tungsten filament at 848°K in caesium vapor and exposed to an accelerating field for ions.

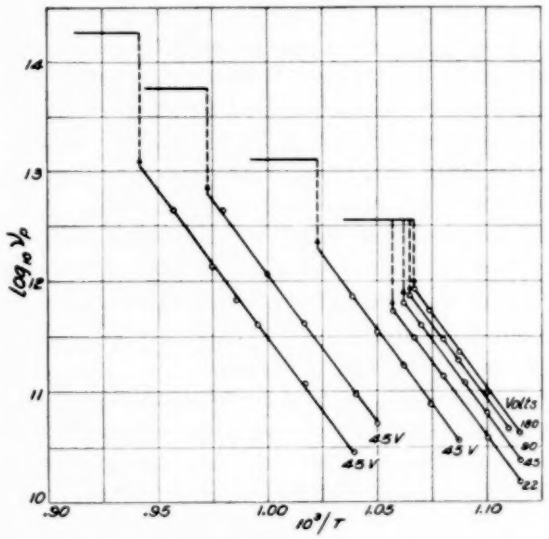

FIG. 18. Exponential increase of positive ion evaporation rate followed by discontinuous rise to maximum value of ν_p, $(\nu_p = \mu_a)$.

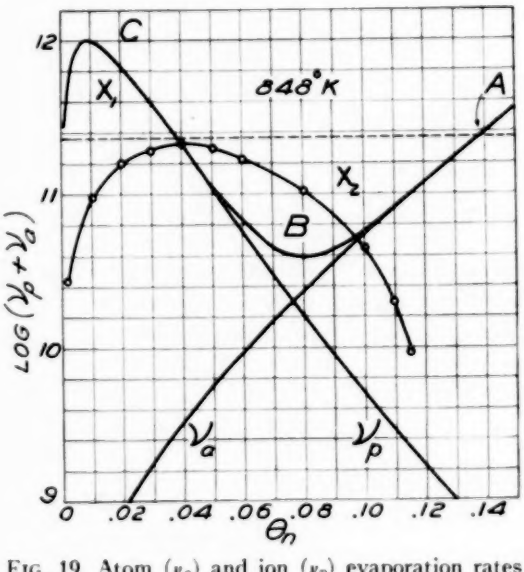

FIG. 19. Atom (ν_a) and ion (ν_p) evaporation rates for zero field at the lower values of θ. (Calculated at 848°K.) Circles give observed data under conditions as described in text.

It is seen that for constant values of $\mu_a(=\nu_a+\nu_p)$ there are three values of θ, as indicated, for example, by the intersections of the dotted line with the curve. Thus at a given pressure two values of θ may exist corresponding to two phases, a dilute (β) and a concentrated (α) phase. The intermediate θ is unstable. These phases are separated by a distinct boundary whose movement gives the observed rate of change of ν_p at the discontinuity. Migration has been shown to exist at the boundary between the phases and the velocity of propagation has been used to measure D, the coefficient of surface diffusion in a recent note[15] by the authors.

The dotted line in Fig. 19 and ABC enclose the two areas X_1 and X_2. Mathematical analysis[16] shows that the condition for a stationary boundary (when D, the surface diffusion coefficient, can be taken to be independent of θ) is that $X_1=X_2$ when $(\nu_a+\nu_p)$ is plotted as a function of θ. The dotted line in Fig. 19 has been so drawn. If μ_a is raised, the concentrated α phase will appear. The velocity of motion depends on the displacement of μ_a.

Boundaries are established by the formation and growth of nuclei at slight inhomogeneities of the surface on which θ may increase or decrease more rapidly than on neighboring areas. Nucleus growth is not possible above point A in Fig. 19 since the dilute β phase is unstable. It may and does occur for any value of μ_a producing a θ between points A and B. The μ_a or θ at which formation and growth begin depends on the surface conditions and on how rapidly μ_a (or θ) is varied.

In particular, in Fig. 18 the points where a discontinuity sets in depend entirely on this accidental nucleus formation and have no other significance. A detailed comparison of these points in Fig. 18 with the curves of Fig. 19 is difficult since ν_p in the former is affected by the field, whereas the latter curves represent field free emission of ions.

As previously discussed (Section IV), a series of ion evaporation experiments were carried out with the bulb in liquid air so that μ_a was negligible. The rate was changed by aging from an irregular to a uniform variation with θ (Fig. 7). These experiments may now be explained more fully. Since μ_a is negligible, there is no mechanism for stopping the growth of newly formed nuclei after θ's lower than those corresponding to the level of point C are reached ($\sim$0.18 percent for Fig. 19). The rate of evaporation will increase rapidly as the perimeter (boundary) of the nucleus increases, and fall off when two advancing boundaries meet. Each peak in Fig. 7 may be formed by this process. A new peak is formed as other nuclei increase their perimeters. Diffusion at the boundaries from the concentrated to the dilute phases speeds the process.

These conclusions were verified by experiments in which, after one or more peaks in the evaporation rate had been passed, the field was reversed so that only atoms could evaporate (very slowly in the region B–C). After waiting several minutes the field was again reversed and ions allowed to evaporate. The ion evaporation, however, did not proceed at the previous rate but at a rate two or three times as great. This was because θ had been made uniform, by migration from areas of high θ to those already cleared by the first peaks. A uniform low θ could also be produced by coating the clean filament in a retarding field for ions. Here again, on reversing the field, the values of ν_p were larger than when the same total θ was reached by ion evaporation.

It is emphasized that the inhomogeneities needed to serve as nuclei for these discontinuous boundary effects do not compose any appreciable part of the tungsten surface. They are probably crystal boundaries or irregularities in these boundaries and need occupy no more than the one-half percent of surface discovered in the analysis of the atom evaporation data. That the effects are not accidental, such as might be caused by gas covered areas, is shown by the exact repetition of the peaks in numbers of experiments made at any stage in the aging process. Aging probably removed certain of the inhomogeneities and caused the rest to become sufficiently uniformly distributed to produce a regular evaporation rate.

As further evidence that the smooth curve finally obtained is still disturbed by the formation and growth of nuclei and does not represent

[15] I. Langmuir and J. B. Taylor, Phys. Rev. **40**, 463 (1932).

[16] I. Langmuir, J. Chem. Phys. **1**, 3 (1933).

the true variation of ν_p with θ, the observed values of ν_p have also been plotted (circles) in Fig. 19. At higher values of θ, $\nu_{p(\text{obs})} > \nu_{p(\text{calc})}$. This is due to the formation of nuclei and boundaries as just explained. At lower values of θ, $\nu_{p(\text{obs})} < \nu_{p(\text{calc})}$. This is because the high rate of evaporation from the few remaining concentrated patches is finally overbalanced by the practically zero rate from the large areas of nearly bare tungsten. Thus the observed maximum at $\theta \sim 0.04$ and the whole behavior of $\nu_{p(\text{obs})}$ depends on the average of the rates from these two (concentrated and dilute) phases and on the displacement of the phase boundary. The surface at $\theta_{\text{obs}} = 0.04$ is made up of patches whose concentration is greater than that corresponding to $\theta = 0.04$ and areas of nearly bare tungsten.

Although the above types of experiments may give us a more detailed picture of the tungsten surface, it must be concluded that they are not suited for studies of ν_p from the main homogeneous part of the tungsten surface. As already shown, experiments made under steady conditions ($\nu_p + \nu_a = \mu_a$) do give values of ν_p in accord with theory.

The films obtained in the manner described above by evaporation of ions in accelerating fields illustrate the existence under these conditions of films which do not conform to the surface phase postulate.[17]

Killian[14] has obtained current-voltage characteristics for potassium and rubidium ions in the region of space charge limitation. He showed that the theoretical equation was followed and also gave curves exhibiting a remarkably sharp break at the saturation voltage. Figs. 20 and 21 were obtained for caesium ions and electrons in the present investigation. To avoid question as to the correct zero of potential the 2/3 power of the current has been plotted against the voltage. The break at saturation for ions is so sharp that it can be almost entirely accounted for by the small voltage drop along the central part of the filament. For electrons the transition occurs much more gradually and must have another explanation. With the masses of the

[17] A more detailed analysis of this postulate and its implications in connection with a phase rule for adsorption has been presented by I. Langmuir, in reference 16.

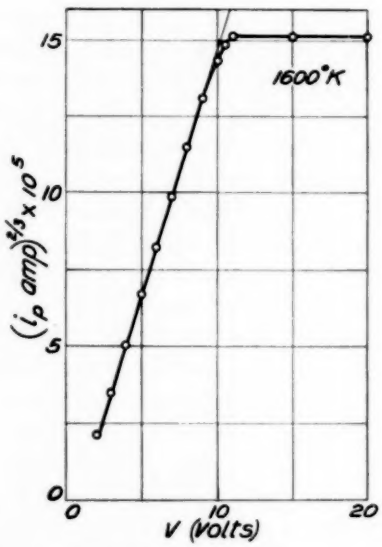

FIG. 20. Positive ion currents limited by space charge for Cs ions.

electron and of the single Cs atom, the theoretical slopes were calculated. For electrons the calculated slope was 1.14×16^{-3} and the observed 1.05×10^{-3}. For ions the calculated slope was 1.82×10^{-5} and the observed value was 1.65×10^{-5}. The agreement is satisfactory since no attempt was made to correct for the influence of the second filament held at the potential of the first in these experiments. The second fila-

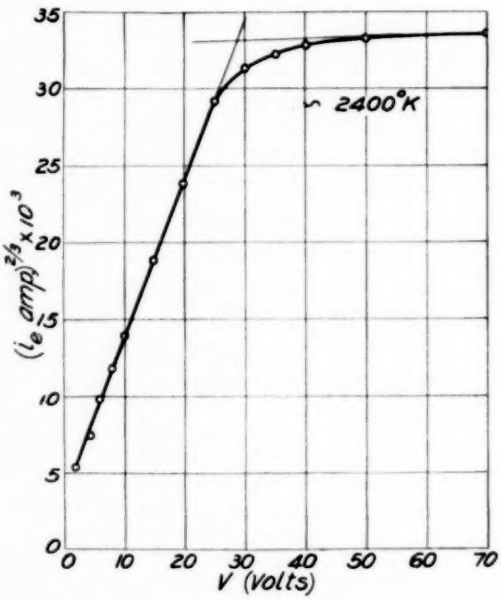

FIG. 21. Electron currents limited by space charge from clean tungsten.

ment, acting as a grid, would decrease the observed emissions and hence the slopes as found. The theoretical ratio of ion to electron slopes is 62.6 and the observed value was 63.6.

An equation, similar to Eq. (21), for the rate of positive ion evaporation at very low θ's may be developed

$$\ln(\nu_p/\theta) = b + b_1\theta,$$
$$b = 61.31 - 23{,}699/T, \qquad (22)$$
$$b_1 = 6.80 - 99{,}900/T.$$

This equation gives ν_p within one percent up to approximately $\theta = 0.02$. The limit of application is near $\theta = 0.03$ where the error is about 15 percent. By differentiation an expression giving the position of the maximum in the ν_p *vs.* θ curve is obtained

$$\theta_{max} = T/(99{,}900 - 6.8T) \qquad (23)$$

at 500°K, 1000°K, and 2000°K, θ_{max} is 0.00513, 0.01075 and 0.0232.

X. General Methods for Calculation of ν, θ and T

Table I has been given to simplify calculations of ν, θ and T. In the construction of this table the type of equation

$$\log_{10}\nu = \mathbf{A} - \mathbf{B}/T \qquad (24)$$

was used, where for use in the equation with common logs

$$\mathbf{A} = A/2.303 \quad \text{and} \quad \mathbf{B} = B/2.303. \qquad (25)$$

For example, A_a and B_a (for atom evaporation) refer to Eq. (1) as previously given with natural logs, $\ln\nu = A - (B/T)$. A_a and B_a have been calculated from Eqs. (7), (8), (9) and (10), which give their dependence on θ. In addition, the corresponding quantities have been calculated for positive ion emission. For ion emission,

$$A_p = A_a - \ln 2,$$
$$B_p = B_a + 11{,}606(V_c + V_i - V_w)$$
$$= B_a - 8681 + 11{,}606\,V_c,$$

as given by Eq. (20). For electron emission the Boltzmann equation gives $\ln\nu_e = \ln\nu_w + V_c e/kT$.

In the range 600°–1000°K the electron emission from tungsten is very closely given by

$$\ln\nu_w = 63.44 - 4.76e/kT.^* \qquad (26)$$

Therefore

$$\ln\nu_e = 63.44 - (e/kT)(4.76 - V_c)$$

or

$$A_e = 63.44, \quad B_e = 11{,}606(4.76 - V_c).$$

The contact potential (V_c) was calculated from atom evaporation data for $\theta < 0.5$ and from emission data for $\theta > 0.5$.

Here also the above values of A and B are for the equations with natural logarithms of ν, ($\ln\nu$). The **A**'s and **B**'s in Table I have been converted (by Eq. (25)) for use in the equation with logarithm to the base ten.

As an example of the use of the table, in Fig. 22, ν_a, ν_p, and ν_e have been calculated and

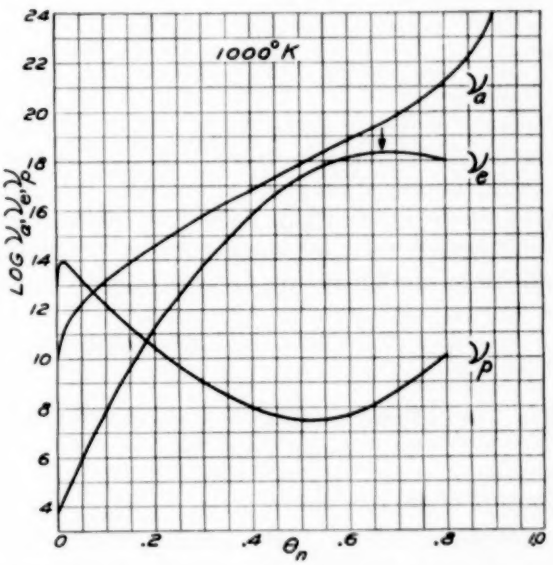

Fig. 22. Atom (ν_a), ion (ν_p), and electron (ν_e) evaporation rates at 1000°K, with zero field.

plotted as functions of θ at the constant temperature 1000°K. Fig. 19 is a similar example. Fig. 22 gives the relations between ν_e, ν_p, and ν_a as θ changes. The curves are calculated for 1000°K but their general course is similar at other temperatures.

Heats of evaporation, according to the Clapeyron equation, are given by $b_0 = -k[d\ln p/d(1/T)]$ and are obtained for atoms, ions and

* See reference 2, Eqs. (7) and (98).

electrons at any value of θ as follows:

$$b_0 = 1.987[2.303\mathbf{B} + T/2] \text{ calories}$$
$$= \frac{2.303\mathbf{B} + T/2}{11{,}606} \text{ volts},$$

where $\mathbf{B}$ is $\mathbf{B}_a$ for atoms $\mathbf{B}_p$ for ions, and $\mathbf{B}_e$ for electrons. The term $T/2$ is introduced when Eq. (24) is changed to a form containing the pressure (p) instead of the rate (ν) in accord with Eq. (5), in order to calculate b_0 as given by the Clapeyron equation. T may be taken as $T_m = 800°$, the average filament temperature in the range (600–1200°K) ordinarily used. $T/2$ corresponds at most to only a few hundredths of a volt.

The work function for electrons, i.e., the exponent (V_e) in an equation of the Dushman type

$$\nu_e = KT^2 \exp(-V_e e/kT)$$

is

$$V_e = (2.303\mathbf{B}_e - 2T_m)/11{,}606 \text{ volts}.$$

A similar equation containing $\mathbf{B}_p$ gives the work function (V_p) for ions. The term $2T_m$ corrects for the simplification made in adopting Eq. (26). Also $V_e = V_w - V_c$, where V_w is the work function (4.622 volts) for pure tungsten and V_c is the contact potential. It is to be noted that

$$V_e = (b_{0e} - (5/2)T)/11{,}606 \text{ volts}.$$

XI. The Condensation Coefficient α and Transient Phenomena

Concept of surface phase

Each phase in a heterogeneous equilibrium has properties which are uniquely determined by a definite number of parameters such as composition, temperature, pressure, etc.

If similar factors determine the properties of adsorbed films of caesium on tungsten, we may expect that all the properties of such a film would be uniquely determined by θ and T. On the other hand, one may well conceive of conditions under which the properties would depend on many other factors. For example, it is possible that the surface of the underlying tungsten may vary according to its method of preparation so that the rate of evaporation of caesium atoms from different tungsten surfaces would differ even if θ and T were the same. Or again, if a caesium film with given θ is formed in two different ways, as, for example, by condensation on to a bare surface or by evaporation from a more concentrated film, the distribution of Cs atoms over the surface might be different and thus cause variations in the properties. The properties could thus depend upon whether or not the film is in equilibrium with the surrounding Cs vapor.

It will be very useful, however, to look upon the unique dependence of the properties on θ and T as an ideal case which may be approached under favorable conditions. Let us, therefore, consider the properties of adsorbed films which conform to the following postulate.

Surface phase postulate: All the properties of an adsorbed film on an underlying surface of given composition are uniquely determined by θ and T

If this condition is fulfilled, ν_a, ν_p and ν_e are functions of θ and T only, *even if the film is not in equilibrium with the vapor phase.* The adsorbed film in equilibrium with caesium vapor is thus a system possessing two degrees of freedom in the sense of the phase rule.[16]

Under non-equilibrium conditions we then have

$$d\sigma/dt = \alpha_a\mu_a + \alpha_p\mu_p - \nu_a - \nu_p. \quad (27)$$

Case I. Retarding field for ions. Under these conditions the ions which evaporate must all be brought back to the filament surface by the field so that if there is no external source of ions,

$$\alpha_p\mu_p = \nu_p \quad (28)$$

and therefore Eq. (27) becomes

$$d\sigma/dt = \alpha_a\mu_a - \nu_a. \quad (29)$$

Under steady conditions we then have

$$\alpha_a\mu_a = \nu_a. \quad (30)$$

Case II. Accelerating field for ions. In this case $\mu_p = 0$ so that

$$d\sigma/dt = \alpha_a\mu_a - \nu_a - \nu_p. \quad (31)$$

In a steady state we have

$$\nu_p = \alpha_a\mu_a - \nu_a. \quad (32)$$

Determination of $\alpha_a\mu_a$ from the ion current

According to Eq. (32), the value $\alpha_a\mu_a$ can be calculated from the positive ion saturation current density I_p by the relation

$$\alpha_a\mu_a=(I_p/e)(1+\nu_a/\nu_p). \tag{33}$$

At high filament temperatures θ becomes very small and ν_a/ν_p approaches a limiting value which may readily be obtained from Eq. (20) by putting $V_e=0$. Inserting numerical values of V_w and V_i we thus find

$$\log_{10}(\nu_a/2\nu_p)=-3770/T. \tag{34}$$

The value of ν_p in this equation is that corresponding to zero field. In experimental determinations of I_p to measure $\alpha_a\mu_a$ we usually employed a potential of -45 volts on the cylinders. Such fields (about 3000 volts per cm at the cathode) have been shown (at constant θ) to increase ν_p about 7-fold without having any effect on ν_a. Thus the ratio ν_a/ν_p corresponding to experimental conditions should be 1/7 of that given by Eq. (34). We thus calculate that ν_a/ν_p in Eq. (33) should have values that range from 2.1×10^{-4} at $T=1200°$ to 5.8×10^{-4} at 1400°. The errors involved in neglecting ν_a/ν_p in Eq. (33) are therefore negligible.

The experimental data given in Table IV were obtained to test this conclusion. The 2nd column gives the galvanometer deflection (300 = 0.027 microampere) produced by the ion current obtained with 45 volts on the cylinder, with the filament temperatures given in the first column.

TABLE IV. *Experimental test of constancy of the ion current at high filament temperatures.*

Voltage = 45; E = 3000 volts cm^{-1}; caesium pressure 2.4×10^{-5} baryes; $\alpha_a\mu_a=3.4\times10^{12}$.

T °K	i_p galv. defl.	i_{photo}	$i_{\text{photo}}+300.3$	θ_n
1143	300	0.02	300.3	1.2×10^{-6}
1307	300	0.50	300.8	8.6×10^{-8}
1380	302	1.5	301.8	3.3×10^{-8}
1457	305	4.6	304.9	1.3×10^{-8}
1591	325	23.1	323.4	3.4×10^{-9}
1717	381	87	387	1.1×10^{-9}
1839	560	255	555	4.6×10^{-10}

It is seen that from 1143° to nearly 1400° the current remains remarkably constant, but rises increasingly rapidly at higher temperatures. This rise has been found to be due to photoelectric emission from the adsorbed caesium film on the cylinder under the influence of the light radiated from the filament. Such photoelectric emission is also observed when light is allowed to fall on the tube.

Since the light intensity of each wave-length varies in accord with Wien's law, the logarithm of the intensity is a linear function of the reciprocal of the filament temperature, the slope of the line, for natural logarithms, being C_2/λ, where the radiation constant C_2 is 1.433 cm deg. Analyzing the data for i_p in Table IV it is found, in fact, that the observed current i_p can be resolved into two parts, one having the constant value 300.3, and the other, the photoelectric current, being given by

$$\log_{10}(i_{\text{photo}})=9.08-12{,}270/T. \tag{35}$$

The 3rd column contains values of i_{photo} calculated by this equation. The 4th column shows that the sum of these two currents, $300.3+i_{\text{photo}}$ agrees well with the observed value of i_p.

By immersing the bulb in liquid air the ion current became zero, but the photocurrents remained and were found to be 15 percent lower than those given by Eq. (35), so that the constant 9.08 in this equation needed merely to be changed to 9.01.

Repeating the experiments of Table IV, with -310 volts on the collector instead of -45, gave currents which, analyzed in the same way, gave a constant ion current having the same value (300.3) as before, but gave photocurrents 2.2 times as great as with the weaker field, the coefficient of $1/T$ in Eq. (35) being unchanged. By placing the bulb in liquid air these photocurrents were reduced as before by 15 percent.

The effective wave-length of the radiation producing these photocurrents (a kind of Crova wave-length) can be determined by equating the coefficient of $1/T$ in Eq. (35) to $2.303\times C_2/\lambda$; it is found to be 5070A, which is reasonable for caesium photoelectric cells.

We may estimate the magnitude of θ under the conditions of the experiments of Table IV by the limiting form (as θ approaches zero) of Eq. (22),

$$\log_{10}(\nu_p/\theta_n)=26.625-10{,}294/T. \tag{36}$$

Here ν_p is the ion evaporation rate without accelerating field. Since in these experiments ν_p, which was equal to μ_a, was increased 7-fold by the field, we may put $\nu_p = 4.9 \times 10^{11}$ in Eq. (36). The values of θ_n, calculated in this way, are given in the last column of Table IV. For such low values of θ, ν_e cannot differ appreciably from that for a pure tungsten surface, so that the assumptions made in deriving Eq. (34) are justified.

The experiments thus indicate that within the experimental error of about 0.2 percent the saturation ion current is independent of temperature and of field strength for ranges of temperature from 1200 to 1500° and for fields from 3000 to 20,000 volts cm^{-1}.

We must conclude from both theory and experiment that the ion saturation current method provides an extremely accurate measurement of $\alpha_o\mu_a$; where α_o is the value of α_a for very small values of θ.

Methods for the experimental determination of α_a and α_p

If, now, we had some independent means of determining the vapor pressure of caesium, from which we can calculate μ_a, we could determine α_o from our knowledge of $\alpha_o\mu_a$. However, as none of the available vapor pressure methods appears to be comparable in accuracy or sensitivity with that of the measurement of ν_p, we need to investigate other ways of finding α_a.

Experimental data, such as that of Table IV, which were also obtained for a wide range of other values of μ_a, *prove that* α_o *is strictly independent of temperature* in the range from about 1000 to 1500°, and *is independent of E, the accelerating field.* This suggests strongly that α_o is unity since any smaller value would probably vary with temperature. There are, however, other methods open to us for measuring α_a.

(1) *Direct flashing method.* Caesium is allowed to accumulate on the filament at a temperature T_1 at which ν_a is negligibly small, at the rate $\alpha_a\mu_a$. After a time t, σ_A is measured by the D.F. method (see Section III and Fig. 4). $\sigma_A = \bar{\alpha}_{av}\mu_a t$ where α_{av} is an average value of α_a over the range in θ from 0 up to the final value at time t.

Fig. 23 gives some typical data with the filament during accumulation at 300°, at 970 and 1001°.

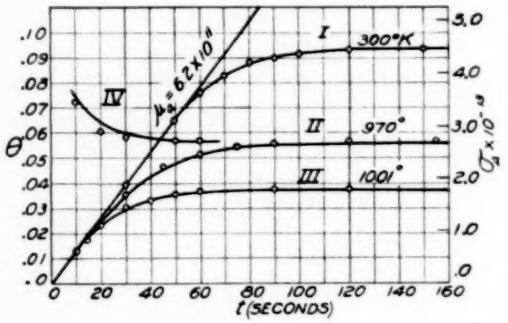

FIG. 23. σ_A *vs.* time at 300°, 970° and 1001°K, for $\mu_a = 6.20 \times 10^{11}$. Data obtained by direct flashing method for use in measuring α_a.

Each experimental point shown for curves I, II and III corresponds to a separate run in which the caesium was allowed to accumulate for the time t after cleaning the filament by flashing. The straight line drawn through the origin has been drawn with a slope equal to $\alpha_o\mu_a$ as determined by this steady ion current method. The experimentally determined points are seen to lie quite accurately on these lines at sufficiently low values of θ. We shall see that at 970 and 1001° the deviations from the straight line at the higher θ's in curves II and III agree with those calculated from the known evaporation rates of these films at those high temperatures.

The data obtained with the filament at 300°K during the accumulation time, curve I, show that the observed points lie quite accurately on the straight line through the origin up to values of θ of about 0.07. The deviations at higher θ are due to evaporation of Cs as atoms during the flashing. This is shown by the fact that the curve remains entirely unchanged if T_1 is varied from 300 to 800°K, but the deviations do depend slightly on the flashing temperature and on the rapidity with which the temperature is raised. The direct flashing method is thus only applicable for values of θ up to about 0.08.

The fact that the experimental points lie on the straight lines of slope $\alpha_o\mu_a$ for sufficiently small θ proves that $\alpha_{av}\mu_a t$ equals $\alpha_o\mu_a t$. We conclude that for temperatures up to about 800° and for values of θ up to 0.07, α_a is constant and equal to α_o within the experimental error

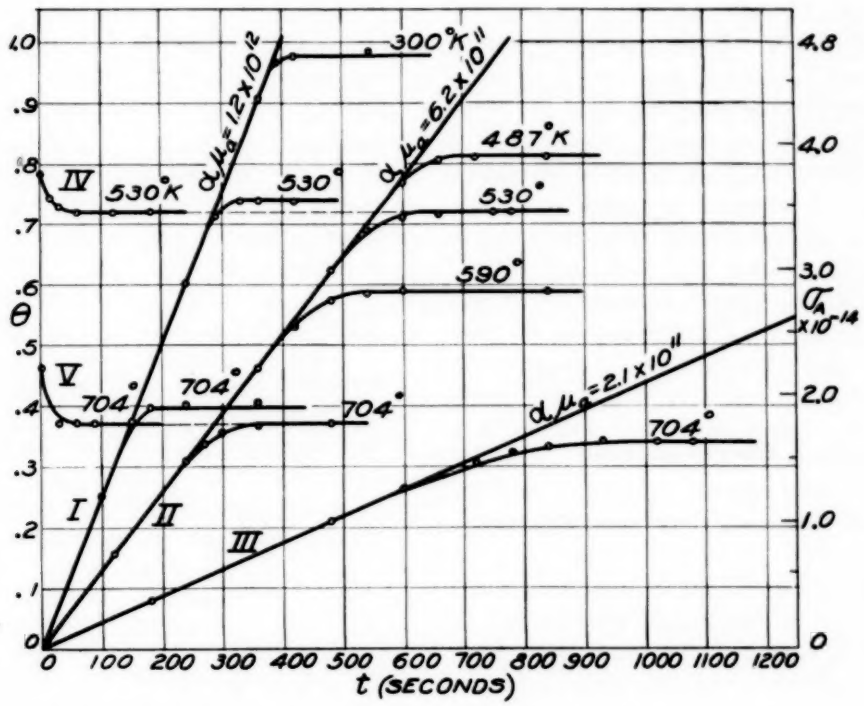

FIG. 24. σ_A *vs.* time at various filament temperatures and Cs pressures (μ_a) as indicated. Data obtained by two filament method for use in measuring α_a.

of less than 1 percent. At 970° the same conclusion may be drawn up to $\theta = 0.02$.

(2) *Two filament method.* After allowing caesium to accumulate on filament A at temperature T_1 up to a definite value of $\sigma_A = \alpha_{av}\mu_a t$, σ_A is measured by the two filament method. If Q represents the quantity of electricity corresponding to the observed ballistic kick produced when A is flashed, we have

$$Q = \alpha_{av}\mu_a t S_A f \alpha_o e, \tag{37}$$

where S_A is the apparent surface area of the filament A within the cylinder C_o, and e is the electron charge. By dividing Q by $S_A fe$, we thus obtain values of $\alpha_{av}\alpha_o\mu_a t$.

The experimental points shown in Fig. 24 represent data obtained by this method for a series of relatively low filament temperatures, *viz.*, 300, 487, 530, 590 and 704°K and with three different caesium pressures which gave, by the steady ion current method, values of $\alpha_o\mu_a$ of 1.20×10^{12}, 2.1×10^{11} and 6.2×10^{11} atoms cm^{-2} sec.$^{-1}$.

The straight lines marked I, II and III which pass through the origin have been drawn with slopes $\alpha_o\mu_a$ as determined by the steady ion current method. It is seen that the observed points, for sufficiently low θ, lie within the experimental error on the straight lines. Since the ordinates of the experimental points are $\alpha_{av}\alpha_o\mu_a t$, while those of the straight lines are $\alpha_o\mu_a t$, this agreement proves that $\alpha_{av} = 1$ and therefore $\alpha_a = 1$ for values of θ up to 0.98. We shall see that the deviations of the observed points from these straight lines as θ approaches a limiting value, are due to evaporation and do not indicate values of α_a less than unity.

In the next section we shall discuss the theoretical significance of the experimental fact that $\alpha_a = 1$ up to nearly $\theta = 1$.

Value of α_p

Moon[18] has shown that when a beam of Cs ions (without Cs atoms) is directed against a tungsten filament heated to high temperatures, no net current flows to the filament if there is a field near the filament which draws away ions. Without this field, or at a lower filament temper-

[18] P. B. Moon, Proc. Camb. Phil. Soc. **27**, 570 (1931).

ature, a current is observed which presumably measures the number of ions which strike the filament. Moon concludes that *all* of the ions which condense on the very hot filament leave it again as ions (none as atoms). This is a proof that ν_a/ν_p is very small, but does not necessarily prove that $\alpha_p=1$, although it makes this probable. In view of the strong attractive forces between the ions and the tungsten surface (image force) it is, however, almost certain that there cannot be any appreciable reflection of low velocity ions, and we may safely conclude that $\alpha_p=1$.

Transient effects in atom evaporation

We use the term *transient effects* to describe the phenomena involving changes in θ as distinguished from *steady* states in which θ stays constant. The accumulation periods which we have discussed correspond to transient states in which ν_a and ν_p are negligible compared to μ_a. Let us now consider the theory of the changes in θ which occur when ν_a and μ_a are comparable in magnitude, and when a retarding field for ions makes $\nu_p=\mu_p$.

The data of Figs. 23 and 24 show that if a clean filament is held at constant temperature in Cs vapor of a definite pressure, θ increases at first at the steady rate μ_a/σ_{A1} but thereafter the rate decreases until finally θ approaches a steady limiting value which we shall call θ_∞. Eq. (29), which applies to this case, may be written in the following form, since $\alpha_a=1$

$$\sigma_{A1}d\theta/dt=\mu-\nu. \tag{38}$$

In this discussion we shall omit the subscripts of μ_a and ν_a except where necessary to prevent confusion.

Values of θ_∞

When $\theta=\theta_\infty$ we should have $\nu=\mu$. Thus, since by Eqs. (6) to (10) and the data of Table I, ν is given as a function of θ_n and T, we can calculate θ_n from μ and T. For each of the temperatures used in the experiments of Figs. 23 and 24 we have constructed, by the data of Table I, a curve giving ν as a function of θ_n in the range near θ_∞ and from this curve have read off the value of θ_n by taking $\nu=\alpha_a\mu_a$ as given by the steady ion current method. θ_∞ (by Eq. (12)) is then equal to $\theta_n+0.005$. The horizontal portions of the full line curves in Figs. 23 and 24 have been drawn by using these calculated values of θ_∞. The close agreement of these horizontal lines with the limiting values of θ given by the experimental points is an illustration of the accuracy of our general equations for ν_a in terms of θ and T, and serves to justify our use of the surface phase postulate.

Calculation of transient curves

By expressing ν as a function of θ and T, we can, by integration of Eq. (38), theoretically obtain θ as a function of t. The experimental determinations of ν_a have shown that ν_a at constant T increases very rapidly with θ, so that within any narrow range of values of θ, say between θ_1 and θ_2, we may put

$$\nu=K\exp(H\theta), \tag{39}$$

where K and H are constants within the range θ_1 to θ_2, but depend on the values of θ_1 and θ_2. More strictly, we may define H by differentiation of Eq. (39)

$$H=d\ln\nu/d\theta. \tag{40}$$

In Fig. 25 the ordinates are values of H calculated in this way by differentiation of the expression we have derived for $\ln\nu_a$ as functions of θ and T. It is seen that except for very small and very large values of θ, H changes relatively slowly with θ, so that the use of Eq. (39) is justified if the range θ_1 to θ_2 is not very great.

Inspection of the experimental data of Fig. 24 shows that the transition between the sloping straight line ($\sigma=\mu t$) and the horizontal straight lines ($\theta=\theta_\infty$) is very rapid. Because of the large magnitude of H, a very small decrease in θ below θ_∞ lowers ν_a to a value which is negligible compared to μ, so that $d\theta/dt$ becomes constant. Thus, to calculate the whole curve, we need only to have an expression for ν which applies to a narrow range of θ.

Introducing the value of ν from Eq. (39) into Eq. (38), we find that the final steady value θ_∞ is given by

$$\nu=K\exp(H\theta_\infty)=\mu. \tag{41}$$

Case I. If we start with a completely coated

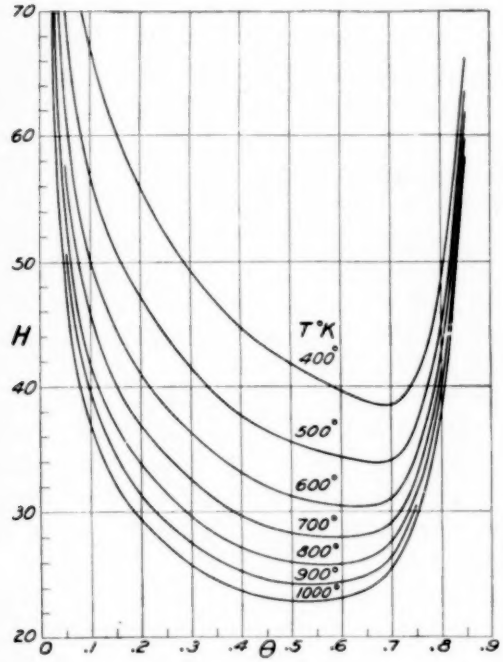

FIG. 25. Values of H, the relative rate of increase of ν_a with θ, defined by Eq. (40).

filament at $t=0$ we obtain by integration

$$\exp(-\mu I I t/\sigma_{A1}) = 1-\exp[-I(\theta-\theta_\infty)]. \quad (42)$$

Curves IV and V in Fig. 24 and curve IV in Fig. 23 are examples of Case I. For each point the completely coated filament was suddenly raised to the indicated temperatures by a condenser discharge and held there by the proper current.

The full line curves IV and V in Fig. 24 were calculated accurately by Eq. (42), by using $\mu=6.2\times10^{11}$, $\sigma_{A1}=4.8\times10^{14}$, and for curve IV, $\theta_\infty=0.72$, $H=33.9$ at 530°, while for curve V, $\theta_\infty=0.372$, $H=30.4$ at 704°. For Fig. 23 (curve IV), $\theta_\infty=0.056$ at 970°. As these values of θ_∞ were calculated from the values of μ, no adjustable parameters have been used in the construction of these curves.

Case II. Starting with $\theta=0$ at $t=0$ integration gives (if we neglect $\exp(-I\theta_\infty)$ compared to unity):

$$\exp(-\mu I I t/\sigma_{A1}) = \exp(-I\theta)-\exp(-I\theta_\infty). \quad (43)$$

The curve $OPNP'C$ in Fig. 26 is the curve given by this equation. Except for a short

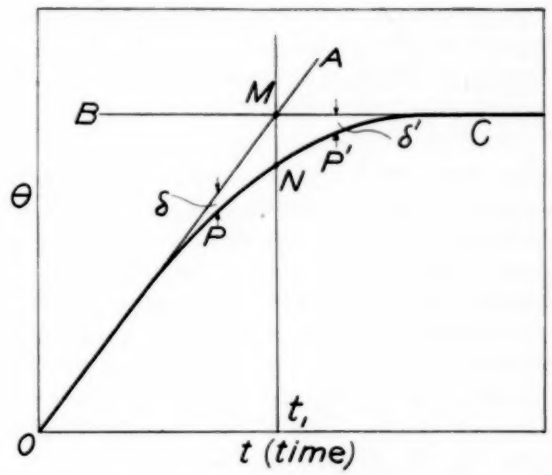

FIG. 26. Curve and construction describing Eqs. (43) to (45) used in calculation of transient curves.

transition region the curve nearly coincides with its two asymptotes OA and BC. It is therefore more convenient to express it in terms of the vertical displacement δ of a point P from the line OA or the displacement δ' from the horizontal line BC. If we let t_1 be the abscissa corresponding to the intersection M of OA and BC, our equations become

$$\exp(I\delta) = 1+\exp I\mu(t_1-t)/\sigma_{A1} \quad (44)$$

and

$$\exp(I\delta') = 1+\exp I\mu(t-t_1)/\sigma_{A1}. \quad (45)$$

Thus at points P and P', which are displaced from MN by equal horizontal distances, but in opposite directions, δ and δ' are equal. The slope of the tangent to the curve at N is one-half the slope of the line OA.

The full line curves which branch off from the lines I, II and III in Fig. 24 have been accurately calculated by these equations without the use of adjustable parameters.

The nearly perfect agreement of the points with the curves proves that the transient states during the condensation and evaporation of caesium atoms from these concentrated films are determined by the balance between the rates of condensation and evaporation as given by Eq. (38).

These experiments also prove that the surface phase postulate (S.P.P.) is applicable to these films. The agreement between the calculated curves and the experimental points show that

ν_a is determined by θ and T in accordance with Eqs. (6 to 10) and does not depend on the manner in which θ has been reached; i.e., by condensation or by evaporation.

In the transient experiments at low θ (Fig. 23) departures from the S.P.P. might be expected to occur. It has been shown that one-half percent of the surface of the filament consisted of "active spots." The final value of θ_n for 970° and $\mu_a = 6.2 \times 10^{11}$ (curve II) is calculated to be 0.051, but the plotted data show that in about 2 minutes a final value of 0.056 was reached, indicating that the active areas ($\theta = 0.005$) had been completely filled. Now in the transient state, as the filament is slowly coated, the concentrations in the normal and active areas would remain equal if there were no surface mobility by which the active areas could be filled. In 2 minutes the maximum value of θ (no reevaporation) which could be produced by the arriving atoms is ~ 0.16. However, the active areas contribute only 1/200 of this or a θ of ~ 0.0008 and without migration can be filled only after more than 12 minutes. It was particularly observed that the value of θ (0.056) reached in 2 minutes showed no increase after periods as long as 60 minutes. Also a cold filament nearly completely coated ($\theta \sim 1.0$) when heated to 970° (curve IV) quickly attained the same final value of θ leaving no doubt as to the absence of any delay in reaching a steady value of θ. The full line branching curves in Fig. 23 calculated with the assumption of complete occupation of the active spots by migration early in the coating process, agree excellently with the observed points. The existence of an *interphase surface mobility* is thus well demonstrated. It is only by virtue of such mobility[15] that the S.P.P. applies to these experiments with dilute films.

Since the surface diffusion coefficient for these films is known[15] from other experiments, it has been possible[19] to calculate the distance which the adatoms may move in reaching active spots without disturbing the surface phase equilibrium. This distance (~ 0.03 cm) was found to be large compared to the distance (~ 0.001 cm) between active spots assuming these are located along crystal boundaries.

[19] See reference 16, discussion of Eq. (12).

XII. Mechanism of Condensation and Evaporation for Concentrated Films

The fact that $\alpha_a = 1$ up to values of θ as high as $\theta = 0.98$ is of profound significance in its bearing on possible mechanisms of condensation and evaporation.

According to the reversibility principle[20] "every element in the mechanism of a reversible process must itself be reversible," so that "the mechanism of evaporation must be the exact reverse of that of condensation even down to the smallest detail."

Let us postulate several different possible mechanisms for evaporation and see whether or not, when they are reversed, they yield reasonable mechanisms for condensation and whether these are consistent with the experimental fact that $\alpha = 1$.

We first need to define some terms which will help to make our concepts more precise. In a state of equilibrium the atoms near a plane surface may be divided in general into four groups:

(1) *Adsorbed atoms or adatoms.* These are the atoms on the surface which contribute to θ.

(2) *Incident atoms*, or atoms which are moving towards the surface from remote regions. The paths described *by the nuclei* of such atoms are called *incident paths.*

(3) *Emergent atoms*, or atoms which are receding from the surface along paths (emergent paths) that will carry them to remote regions.

(4) *Hopping atoms*, or atoms whose nuclei describe paths (hopping paths) that originate and terminate on the surface.

We may define the *remote region* as that region which lies outside of the range of the surface forces, where the paths of the atoms are straight lines. The region closer to the surface where the paths are curved we shall call the *force sheath.*

When the nucleus of an incident, or a hopping atom, approaches to a definite point close to the original surface, the atom either becomes an adatom or it starts to describe a new path (emergent, or hopping). Let us call this definite point the *terminus of the path.* Similarly, each

[20] I. Langmuir, J. Am. Chem. Soc. **38**, 2221–2295 (1916). See particularly page 2253 and footnote on page 2262.

emergent and hopping path has an *origin*. The straight paths of the incident and emergent atoms in the remote region, if extended as straight lines to their intersections with an ideal plane at the adsorbing surface, give points which we shall call the *flight termini* and *flight origins*.

When equilibrium prevails, the concentration of atoms, their directions of motion, and their velocities are governed by the laws of the Maxwell-Boltzmann distribution (M.B.D.) throughout the force sheath as well as the remote region. Thus, all the paths (incident, emergent and hopping) that pass through any point have a spherically symmetrical distribution of directions at that point. The concentrations of atoms must vary in accord with the Boltzmann equation:

$$n = n_0 \exp(-Ve/kT), \tag{46}$$

where Ve is the increase in potential energy of an atom when it passes from a region where the concentration is n_0 to one at which it is n.

We see, then, that the flight termini and flight origins must be uniformly distributed over the ideal surface plane (i.e., distributed with uniform probability per unit area).

Since the adatoms are held by strong forces originating from the underlying tungsten atoms which are arranged in a definite surface lattice, there must be a strong tendency for the adatoms to occupy definite positions (elementary spaces) on the surface. Experiments on the mobility of caesium adatoms on tungsten[15] have shown that the activation energy needed to cause an adatom to hop from one elementary space to an adjacent one is about 0.6 electron-volts. Introducing this value into the exponent of Eq. (46) we find that at $T = 1000°$ the probability per unit volume for the occurrence of an atom (i.e., its nucleus) in the potential depression near the center of an elementary space is 1050 times as great as the corresponding probability for a position at the potential barrier which separates the elementary spaces.

Thus the adatoms are normally oscillating about equilibrium positions corresponding to the elementary spaces, with amplitudes which are rather small compared to the distance between elementary spaces, and only rarely hop from one position to another.

Evaporation of adatoms from dilute films

With the foregoing concept of elementary spaces, it might seem reasonable to postulate that most of the evaporating adatoms pass from their normal positions directly into the vapor phase as emergent atoms. If we think of the reverse process, however, we recognize that since the flight termini must be uniformly distributed over the surface, the incident atoms cannot in general have paths which lead them directly to the normal equilibrium positions. A large portion of the incident atoms must make their first contact with the surface in positions close to the potential barriers, and if $\alpha = 1$ all of these must then move to their final normal positions by a series of hops. Conversely, we must reason, by the reversibility principle, that a large fraction of the emergent atoms have flight origins near the potential barriers in spite of the low concentration of adatoms in these regions.

A little closer consideration shows that although at the barrier the concentration is only 1/1000th of that at the normal positions, this difference is counterbalanced by the fact that the probability of evaporation of any atom at the barrier is 1000 times as great as for an atom in a normal position. Thus the evaporation is essentially uniform over the surface, although the distribution of adatoms is nearly discontinuous.

It is thus evident, if $\alpha = 1$, that hopping paths must be enormously more numerous than emergent paths. Surface mobility is an essential part of the mechanism of evaporation.

Emergent atoms from nearly saturated films

Let us imagine a nearly saturated adsorbed film ($\theta \sim 1$) from which adatoms pass as emergent atoms into the gas phase. If this is the only mechanism of evaporation, then condensation can occur only when incident atoms make their first contact with the surface in a vacant elementary space. All other incident atoms must be reflected; that is, they must escape again by emergent paths. Hopping paths would have to be excluded, for they would provide other opportunities for condensation, and therefore there would be other mechanisms for evaporation than those which we postulated as the only possible ones.

The probability that a flight terminus shall lie in a vacant space is $1-\theta$. The probability that an incident atom should fly into a vacant space without colliding with adjacent atoms is very much less than $1-\theta$. Thus, on the basis of our assumed mechanism, α would have to be less than $1-\theta$.

An apparent reflection coefficient approaching unity for incident atoms striking a covered part of the surface may readily be accounted for by an extremely high evaporation rate from the 2nd layer of atoms as compared to that from the 1st layer.[21] It is reasonable to assume, however, that an atom cannot exist, even momentarily, in a 2nd layer unless it can be supported by four underlying adatoms in the 1st layer. The chance that a given space is occupied is θ and the chance that 4 given spaces are occupied is θ^4. Thus the probability that an incident atom will evaporate from the 2nd layer is θ^4 so that the apparent value of α would be $1-\theta^4$. Experiments with steel balls thrown at random onto a surface partly covered (to the fraction θ) with similar balls, in random arrangement in spaces which form a square lattice, show that the fraction of incident balls which go into a second layer is, in fact, very close to θ^4, for values of θ from 0.2 to 1.0. Thus for $\theta=0.85$, α would be 0.48 and for $\theta=0.98$, $\alpha=0.078$.

With this mechanism for condensation, most of the atoms which evaporate would have to make one or more collisions with the adjacent adatoms before they escape.

Although this postulated mechanism is probably suitable for the explanation of many cases of adsorption of gases on solids, it obviously is inapplicable to the case of caesium films on tungsten and all other cases in which $\alpha=1$ up to high values of θ.

With high values of θ and α the emergent atoms must come from a second adsorbed layer

Since the paths of incident atoms cannot in general be directed towards regions in which the surface concentration is below the average, it must follow, if $\alpha=1$, that just after condensation the concentration is locally raised at the point of condensation. Conversely, an atom can emerge only from regions having locally abnormally high surface concentrations and the act of emergence must bring the local surface concentration back to normal. It thus seems impossible to reconcile the observed simultaneous occurrence of high values of α and of θ with any mechanism by which an appreciable fraction of the emergent atoms have path origins in the first adsorbed layer, even if we assume a high mobility among the adatoms.

These difficulties disappear, however, if we postulate that the origins of a large fraction of the emergent paths lie in a second adsorbed layer. We must assume that adatoms in the first layer hop, from time to time, up into a second layer which, however, covers only a very small fraction of the surface. The atoms in this second layer migrate over the surface and may evaporate or may hop back into vacant spaces in the first layer. Since an atom which evaporates from the dilute film of the second layer does not leave a "hole," no difficulty occurs in assuming that all incident atoms condense by the reverse process.

Covering fraction θ_2 in second layer

We have seen that the heat of evaporation (at constant pressure) of caesium adatoms from tungsten, for values of θ approaching unity, is about 41,000 calories per gram atom, which is equivalent to 1.78 electron-volts. This, of course, represents the energy that must be expended in taking an adatom from the first layer of adatoms out to a remote region.

An atom in a second layer is not in direct contact with the tungsten surface, but is in approximately the same condition as an atom on the surface of metallic caesium. The vapor pressure p of caesium is given (in baryes) by[1]

$$\log_{10} p = 10.65 - 3992/T. \qquad (47)$$

The heat of evaporation corresponding to this equation is 18,240 calories or 0.79 volt, or only 44 percent of that of adatoms in the first layer.

The average "evaporation life" of an atom[22] in the surface of a solid or liquid is given by

$$\tau = (2\pi mkT)^{\frac{1}{2}}\sigma_1/p, \qquad (48)$$

where τ may be defined by the statement that

[21] I. Langmuir, Proc. Nat. Acad. Sci. 3, 141 (1917).

[22] See Eq. (15), reference 2.

dt/τ is the probability that any surface atom will evaporate in the time dt. Placing $\sigma_1 = 3.56 \times 10^{14}$ we thus find that for Cs atoms in the temperature range from $T = 300$ to 1100°, τ is given in seconds by

$$\log_{10} \tau = -12.82 + 3840/T. \quad (49)$$

Let us now assume provisionally that τ is the same for all exposed adsorbed atoms in the 2nd (or 3rd) layer on tungsten as for atoms in a surface of metallic caesium at the same temperature. We thus take τ to be independent of the surface concentration of atoms although for the 1st adsorbed layer on tungsten the strong repulsive dipole forces between adatoms cause τ to decrease as θ_1 increases. Since Cs atoms on a layer already covered by caesium probably have very small dipole moments, and any small moment that does exist may be compensated for by attractive forces, it seems reasonable to make this simplifying assumption.

We may then put

$$\tau = \sigma_1 \theta_2 / \nu \quad (50)$$

and under steady conditions in which $\nu = \mu$ we then have from Eq. (49)

$$\log_{10} (\mu/\theta_2) = 27.37 - 3840/T. \quad (51)$$

Here θ_2 represents the fraction of the available part (θ_1^4) of the first layer which is covered by the adatoms in the second layer. The total number of atoms in the second layer per unit area of true tungsten surface is thus $\sigma_1 \theta_1^4 \theta_2$.

When μ increases to the value μ_2 corresponding to saturated vapor at the temperature of the filament, θ_2 must rise to unity. Thus by Eq. (51) we have as an equivalent definition of θ_2

$$\theta_2 = \mu/\mu_2. \quad (52)$$

In experiments on transients μ or ν must have values which give reasonable time intervals for coating or depleting the surface. With $\mu = 10^{11}$ the coating time to $\theta = 1$ is one hour and with 10^{15} it is 0.4 second. Let us therefore choose these values of μ and calculate by Eq. (6) for various values of θ_n the corresponding temperatures. These data are given under T in Table V.

With these values of T, putting $\nu = \mu$ we calculate by Eq. (51) the values of θ_2 given in Table V. The values of T in the lowest line are those obtained from Eq. (51) by putting $\theta_2 = 1$; these are the temperatures at which liquid caesium (polyatomic layers) would condense on the filament.

Examination of these data shows that $\theta_1^4 \theta_2$, the number of caesium atoms per unit area in the second layer needed to give an evaporation rate equal to μ is extremely small until θ_1 reaches values of about 0.96. For still higher values of θ_1, θ_2 increases rapidly. When θ_2 becomes comparable with unity, we must take into account the adsorption in the third and higher layers.

Polyatomic layers with nearly saturated vapor

A mathematical theory of the building up of polyatomic adsorbed layers as the vapor approaches saturation has already been given.[23] This theory should now be modified by assuming that adsorption of an atom in the nth layer can occur only on an underlying group of at least 4 atoms in the $(n-1)$st layer. A rough estimate of the number of atoms in each layer may be made by assuming that the number of atoms in the successive layers decreases in the ratio $1 : \theta_2^4$. Thus σ, the total number of atoms adsorbed (in all layers) per unit area of the

[23] I. Langmuir, J. Am. Chem. Soc. **60**, 1374 (1918).

TABLE V. *Covering fractions θ_1 and θ_2 for the first and second layers and rates of interchange ρ of atoms between these layers.*

θ_n	θ_1	θ_1^4	$\mu = 10^{11}$ T°K	θ_2	ρ	$\mu = 10^{15}$ T°K	θ_2	ρ
0.5	0.505	0.065	605	9.5×10^{-11}	1.3×10^{17}	789	3.2×10^{-8}	5.6×10^{19}
0.7	.705	.24	516	1.2×10^{-9}	8.4×10^{17}	661	2.8×10^{-7}	2.5×10^{20}
0.9	.905	.67	407	1.2×10^{-7}	1.6×10^{19}	498	2.2×10^{-6}	4.6×10^{21}
0.95	.955	.83	332	1.5×10^{-5}	4.1×10^{20}	391	3.0×10^{-3}	1.7×10^{22}
0.96	.965	.89	306	1.6×10^{-4}	2.1×10^{21}	355	2.8×10^{-2}	8.4×10^{23}
0.97	.975	.91	270	6.9×10^{-3}	2.8×10^{22}	308	—	—
			234	1		310	1	—

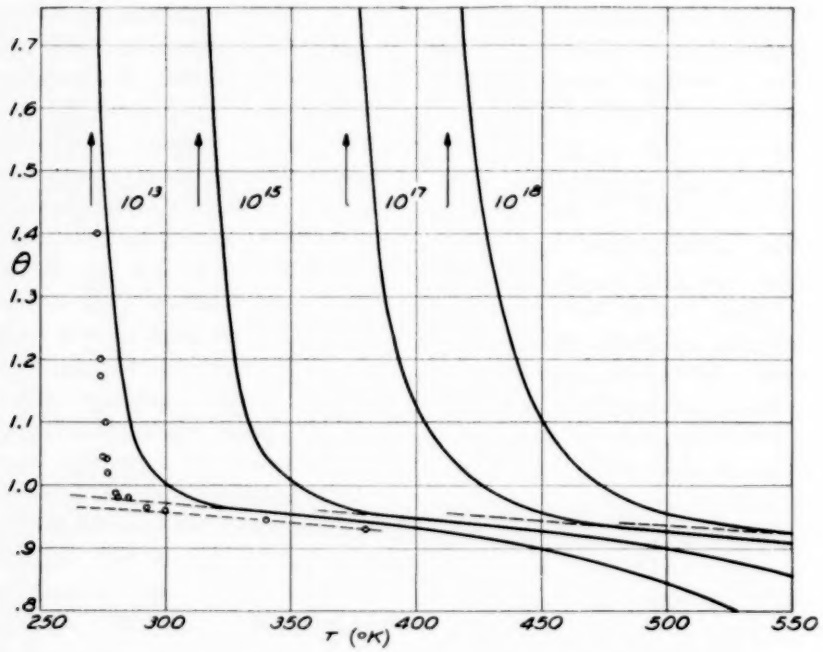

FIG. 27. Formation of a second layer of Cs atoms (calculated by Eqs. (6) and (53)) for different values of μ_a. Arrows give temperature corresponding to saturated Cs vapor. Circles give experimental data obtained at $\mu_a = 10^{13}$.

filament surface, is

$$\theta = \sigma/\sigma_1 = [\theta^1 + \theta_1{}^4\theta_2(1 + \theta_2{}^4 + \theta_2{}^8 + \cdots)]$$

or (53)

$$\theta = [\theta_1 + \theta_1{}^4\theta_2/(1 - \theta_2{}^4)].$$

The rapidly rising portions of the curves in Fig. 10 near $\theta = 0.95$ have been calculated by this equation with values of θ_1 and θ_2 obtained from Eqs. (6) to (10) and (51).

With the bulb containing saturated caesium vapor at a temperature T_s, θ does not exceed unity until the filament temperature T is lowered to within 25° of T_s for $\mu = 10^{11}$ (or 80° for $\mu = 10^{18}$). When $T - T_s$ is 8° (or 24°), θ_2 is 0.3 so that 30 percent of the surface is covered by a second layer of atoms although 2 percent (or 5 percent) of the tungsten surface is still bare (due to repulsive forces in this layer). There are then only enough atoms in the 3rd layer to cover 0.007 of the surface. When $T - T_s$ is 0.6° for $\mu = 10^{11}$ (or 1.9° for $\mu = 10^{18}$) θ_2 is 0.9 so that the covering fractions for the successive layers are roughly 0.98, 0.77, 0.33, 0.14, 0.06, 0.026, etc., the total value of σ/σ_1 being about 2.3.

Experimental test of the formation of polyatomic layers

Fig. 27 shows the building up of a second layer of caesium atoms according to Eq. (53), for various values of μ. The vertical arrows represent the temperatures corresponding to saturated caesium vapor.

It was thought desirable to test for this formation of a second layer. At $\mu_a = 10^{13}$ filament A was maintained, either by passage of small currents or by radiation from filament B, at various temperatures slightly above $T_{sat.}$ (270°). The temperatures were computed from the measured resistance of the filament.

The adsorbed atom concentration at each temperature was measured by the two filament method. The circles in Fig. 27 give the experimental results. It was found that as indicated by the theory θ increased only slowly until a temperature within 20° of $T_{sat.}$ was reached. The increase up to this point was closely that given by Eq. (6) for atom evaporation in the first layer.[24] At ~293° a much more rapid rise

[24] This behavior of θ near 1.0 makes it likely that σ_{A1} is more closely 4.9×10^{14} than 4.8×10^{14} as given by the

set in until at 273° a total θ of 1.4 was reached. The direction of the deviation from the theoretical curve shows that atoms evaporate more easily from the 2nd layer of Cs on tungsten than from metallic caesium. Since θ depends on the probability of evaporation of the adsorbed atoms in the 2nd layer, application of the Boltzmann equation serves to indicate the amount by which the heat of evaporation differs from that of liquid Cs.

$$n/n' = \exp(\Delta Ve/kT),$$

where n and n' are the theoretical and observed concentrations. Since n/n' is approximately 6 between 275° and 295°, $\Delta V \backsimeq 0.045$ volt. Thus the theory is extraordinarily well confirmed. There is no tendency to form a second layer until near $T_{\text{sat.}}$. Atoms adsorbed in the second layer are not held by forces at all approaching in magnitude those holding Cs directly to tungsten; since ΔV for metallic caesium and Cs adsorbed on tungsten in the first layer is almost 1 volt. The heat of evaporation from the second layer is even less than that from metallic caesium. All this is striking evidence of the true monatomic nature of the first layer of Cs on tungsten.

Mobility and surface diffusion coefficient of adatoms

Let us consider σ adatoms per unit area distributed at random among elementary spaces which are arranged in a square surface lattice, each elementary space being a square of side a so that $a^2 = 1/\sigma_1$. Let τ be the average life of an adatom in a particular space when the 4 adjacent spaces are vacant. The probability per second that an atom in a given space will hop into a given adjacent vacant space is $1/4\tau$. We may take the probability of hopping into an occupied space to be zero. If we may assume that the atoms exert no appreciable forces on one another (except that needed to keep 2 out of a single space), τ may be taken to be independent of σ.

The flux φ of atoms per cm of length across a line midway between two adjacent rows (A and B) of elementary spaces (perpendicular to X axis) is

$$\varphi_{AB} = (a\sigma_A/4\tau)(1-\sigma_B/\sigma_1) \quad \text{from } A \text{ to } B$$

and (54)

$$\varphi_{BA} = (a\sigma_B/4\tau)(1-\sigma_A/\sigma_1) \quad \text{from } B \text{ to } A.$$

The net flux or drift flux φ_D is thus

$$\varphi_D = (a/4\tau)(\sigma_A - \sigma_B) = (a^2/4\tau)d\sigma/dx. \quad (55)$$

The surface diffusion coefficient D may be defined by equating φ_D to $D\, d\sigma/dx$ and thus we find for all values of θ from 0 to 1

$$D = a^2/4\tau = 1/4\sigma_1\tau. \quad (56)$$

In case we have to deal with a hexagonal surface lattice in which atoms may hop to any one of six adjacent spaces, this equation needs to be modified merely by replacing the 4 in the denominator by 3. For tungsten surfaces which have been highly heated, the atoms are arranged in a surface lattice in which the elementary rectangle of dimensions 3.15×4.46A has one atom at each corner and one atom in the center. Each surface atom has thus 4 near neighbors and therefore Eq. (56) should be applicable.

This equation has been derived on the assumption that the time τ during which an atom remains in an elementary space is large compared to a/v, the time required for the passage of an atom from one space to the next.

When the time of transit a/v is not negligible, Eq. (56) needs to be modified merely by adding a/v to τ so that

$$D = a^2/4(\tau + a/v_2), \quad (57)$$

where v_2 the average velocity parallel to the plane of the surface (2-dimensional velocity) is given in cm sec.$^{-1}$ by

$$v_2 = (\pi kT/2m)^{\frac{1}{2}} = 11{,}428(T/M)^{\frac{1}{2}}, \quad (58)$$

M being the molecular or atomic weight.

If τ is negligible compared to a/v_2, this reduces to

$$D = (1/4)av_2. \quad (59)$$

In the elementary kinetic theory of gases it is shown[25] that the coefficient of self-diffusion of a gas is $D = (1/3)\lambda_3 v_3$ where v_3 is the average

previous less detailed experiments of Section V, introducing a possible error of about 2 percent in the calculations of θ.

[25] See for example *Dynamical Theory of Gases*, J. H. Jeans, p. 326, Cambridge, 2nd Edition.

(3-dimensional) molecular velocity and λ_3 is the 3-dimensional free path. A similar calculation for the 2-dimensional case of surface diffusion leads to

$$D=(1/2)\lambda_2 v_2, \tag{60}$$

where λ_2 is now the length of the projection of the free path on the plane of the surface. If we identify λ_2 with a, this equation is the same as Eq. (59) except for the numerical factor. This difference is due to the fact that in deriving Eq. (60) it was assumed that all directions of motion in the plane are equally probable, while for Eq. (59) the motions were taken to be parallel to the two axes of the square lattice.

Measurements of the surface diffusion coefficient D_1 for Cs adatoms on tungsten for an average value of θ of about 0.03 have given,[15] for the temperature range from 650 to 812°K,

$$\log_{10} D_1=-0.70-3060/T. \tag{61}$$

Since the number of tungsten atoms per cm² on a tungsten surface is 1.425×10^{15} we must take this to be the number of elementary spaces and thus get

$$a_1=2.64\times10^{-8}\text{ cm}. \tag{62}$$

Using this value of a_1 and the value of v_2 from Eq. (58) we calculate τ_1 at various temperatures in the range from 650 to 812° and find that they are represented by

$$\log_{10}\tau_1=-15.09+3082/T. \tag{63}$$

Values of τ_1 and D_1 (for Cs atoms in the 1st layer) are given for several temperatures in the 3rd and 2nd columns of Table VI.

TABLE VI. *Surface diffusion coefficients for Cs adatoms in 1st and 2nd layers.* τ_1 and τ_2 are the "lives" in elementary spaces in 1st and 2nd layers as given by Eqs. (63) and (64); τ is the "evaporation life" in 2nd layer given by Eq. (49).

T	D_1(cm² sec.$^{-1}$)	τ_1(sec.)	τ_2	a_2/v_2	D_2	τ
			$\times10^{-14}$	$\times10^{-14}$		
300	1.2×10^{-11}	1.5×10^{-5}	175.	31.	0.00034	0.95
400	4.3×10^{-9}	4.1×10^{-6}	26.	27.	.00134	5.9×10^{-4}
500	1.5×10^{-7}	1.2×10^{-6}	8.1	24.	.0022	7.2×10^{-6}
600	1.6×10^{-6}	1.1×10^{-10}	3.8	22.	.0027	3.8×10^{-7}
700	$8.\times10^{-6}$	2.1×10^{-11}	2.2	20.	.0032	4.6×10^{-8}

The mobility of adatoms in the 2nd layer must be much greater than that in the 1st layer since the atoms in the 2nd layer are held by much weaker forces. For low values of θ_1 at which D_1 was measured, the heat of evaporation of atoms from the 1st layer is 2.83 volts. The potential barrier corresponding to the coefficient of $1/T$ in Eq. (63), 3082, is, as we have seen, 0.61 volt which is 21.5 percent of the heat of evaporation. The potential barrier separating the elementary spaces for the 2nd layer must be much less than 0.61 volt which is 78 percent of the heat of evaporation (0.79 volt) from the 2nd layer. It seems reasonable to assume that the barrier in this case also is approximately 21.5 percent of the heat of evaporation. This would give 0.17 volt. The Cs atoms in the 1st layer, however, because of their larger size compared to W atoms, constitute a rougher support for the atoms in the 2nd layer than is provided for the 1st layer of atoms by the underlying tungsten surface. Thus we may adopt the rough value 0.2 volt as most probable value for the barrier in the 2nd layer. This corresponds to a coefficient 1000 for $1/T$. This gives for the life τ_2 of an adatom in an elementary space of the 2nd layer

$$\log_{10}\tau_2=-15.09+1000/T. \tag{64}$$

We have taken the term -15.09 to be the same as in Eq. (63), since for evaporation[26] and for diffusion[27] this term remains nearly constant even for different substances.

Thus a general equation for the evaporation life τ was found[26] to be

$$\tau=4.7\times10^{-27}M^{\frac{1}{2}}\sigma_1 T^{-1}\epsilon^{b/T}. \tag{65}$$

Because of the similarity of the processes of evaporation and of mobility, by which atoms hop from one position to another, we may expect this equation to be at least roughly applicable to surface diffusion. Putting $M=133$, $\sigma_1=3.56\times10^{14}$ and $T=500$ (the mean temperature) we find from Eq. (65)

$$\log_{10}\tau=-13.4+0.43b/T. \tag{66}$$

The values of τ_2 calculated from this equation by putting $0.43b=1000$ are of roughly the same

[26] Reference 2. See particularly Eq. (37) on page 2806.

[27] S. Dushman and I. Langmuir, Phys. Rev. **20**, 113 (1922).

magnitude as those by Eq. (64). A change of about 10 percent in the assumed value of the coefficient of $1/T$ would bring the two equations into agreement at a given temperature.

The values of τ_2 calculated from Eq. (64) are given in the 4th column of Table VI, and D_2 calculated from these by Eq. (57) taking

$$a_2 = 5.3 \times 10^{-8} \tag{67}$$

is given in the 6th column while the time of transit a_2/v_2 is given in the 5th column.

The last column of Table VI gives the evaporation life of adatoms in the 2nd layer as calculated from Eq. (49). Comparing τ with τ_2 and a_2/v_2 we see that at $T=300$ each adatom in the 2nd layer moves through about 10^{12} elementary spaces before evaporating and even at 700° it moves through 10^5 spaces during its life. This fact affords a simple explanation of the high values of α.

Surface random flux

A very useful concept[28] in the study of electric discharges in gases is that of random current density I_e. If n is the number of electrons per unit volume in a uniform plasma and v is their average velocity, then across any imaginary plane there is a current density $I_e = (1/4)nve$ of electrons which pass across the plane from one side to the other and an equal current of electrons passing back in the opposite direction.

Similarly for the motions of adatoms on any surface in a steady state we may define the *random flux density* φ as the number of atoms per unit length which cross any imaginary line in the surface from one side to the other (while an equal flux passes in the opposite direction).

If the adatoms move in random directions parallel to the plane of the surface with the average velocity v, then one-half the atoms on one side of the line are approaching the line with an average velocity $(2/\pi)v$. Thus we find

$$\varphi = (1/\pi)\sigma v = (\sigma_1/\pi)\theta v. \tag{68}$$

If the adatoms, instead of moving with uniform velocity, hop from space to space as postulated in the derivation of Eqs. (54), (55) and (57), we obtain

$$\varphi = a\sigma_1\theta(1-\theta)/4(\tau + a/v_2) = (\sigma_1 D/a)\theta(1-\theta). \tag{69}$$

Rate of interchange of atoms between the first and second adsorbed layers

Consider that the first layer in a square surface lattice is nearly completely filled by adatoms as indicated in Fig. 28, so that the $\sigma_1(1-\theta_1)$ vacant

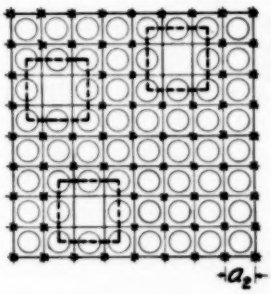

FIG. 28. First layer in a square surface lattice nearly completely filled by adatoms, denoted by circles. Available spaces in the second layer are indicated by crosses.

spaces per unit area are separated from one another. The available elementary spaces in the second layer are indicated in the figure by crosses. Each vacant space in the first layer causes a decrease of four in the number of available spaces in the second layer; this number per unit of filament surface is therefore $\sigma_1[1-4(1-\theta_1)]$, which for values of θ_1 close to unity agrees with $\sigma_1\theta_1^4$ as deduced previously.

Any adatom in the second layer which migrates across the dotted line in Fig. 28, which has a perimeter $8a_2$, evidently falls into the vacant space in the first layer. Thus the rate ρ at which atoms pass from the second to the first layer, expressed in atoms cm^{-2} $sec.^{-1}$, is

$$\rho = 8a_2\varphi_2\sigma_1(1-\theta_1). \tag{70}$$

Under equilibrium conditions this must be balanced by the passage of an equal number of atoms from the 1st to the 2nd layers. Thus ρ may be termed the *rate* of *interchange* between the 2 layers. If this rate is very high compared to the rates of evaporation ν or condensation μ from or to the surface, the relative numbers of adatoms in the two layers $\sigma_1\theta_1$ and $\sigma_1\theta_2\theta_1^4$ will be the same whether or not the adsorbed films are in equilibrium with the vapor phase. There-

[28] I. Langmuir and H. Mott-Smith, G. E. Rev. **27**, 449 (1924); I. Langmuir and K. T. Compton, Rev. Mod. Phys. **3**, 221 (1931).

fore the conditions for which the surface phase postulate will be fulfilled are $\rho/\nu \gg 1$, and $\rho/\mu \gg 1$.

In deriving Eq. (70) we considered the rate at which atoms in the 2nd layer move to and drop into holes in the 1st layer. It is, however, possible, because of the mobility in the 1st layer, for holes in the 1st layer to move to atoms in the 2nd layer. Considerations like those used in deriving Eq. (69) lead to the conclusion that the diffusion coefficient for *holes* is the same as for *atoms* and that the surface flux of holes as well as that of atoms is given by the last member of Eq. (69). Taking Eq. (70), after eliminating φ_2 by Eq. (69),

$$\rho = 8\sigma_1^2(D_2+\theta_1 D_1)(1-\theta_1)\theta_2(1-\theta_2). \quad (71)$$

The values of ρ given in Table V were obtained by this equation, with the data for D_2 given by Table VI. They are large compared with μ or ν and therefore the surface phase postulate applies.

The Nature of Gas Ions

OVERTON LUHR, *Eastman Laboratory, Massachusetts Institute of Technology*

(Received May 11, 1933)

The mass of gas ions formed in a glow discharge and aged up to 10^5 impacts was determined by a Dempster type of mass-spectrograph. In hydrogen it is found that the primary ion, H_2^+, changes within a few thousand collisions to H_3^+, together with small quantities of H^+. The nitrogen primary ions, N^+ and N_2^+, attach to neutral molecules in about 10^5 impacts to form N_3^+ and N_4^+. In pure oxygen the ions consist almost entirely of O_2^+ with small quantities of O^+. Air ions include all possible nitrogen and oxygen ions, the aged air ions consisting principally of N_3^+, N_4^+ and O_2^+ together with the oxides of nitrogen. Charges are transferred from O_2^+ to NO, NO_2 and N_2O. Water vapor is particularly active in acquiring a charge by transfer and H_2O^+ ions may be most numerous in apparatus not baked out. No heavier clusters than N_4^+ were observed. No negative ions were observed. Some conclusions published in earlier work must be revised.

INTRODUCTION

IN an earlier paper[1] the writer reported some work in determining the mass of the "normal" gas ion. The method consists essentially in production of the ions in a glow discharge, aging by allowing them to drift at low velocity through some cm of gas, then formation of a molecular beam by passage of ions and gas molecules through a fine slit into a highly evacuated space where the ratio of charge to mass is determined in a Dempster type of mass-spectrograph. The rate of formation of secondary ions by attachment of neutral molecules or transfer of charge in the drift space may be studied qualitatively by varying the pressure or the drift field and distance.

With a new and improved apparatus results have been obtained which require revision of some of the former conclusions, and indicate certain definite trends in the aging process for relatively new ions.

APPARATUS

The form of apparatus employed during most of the experiment is shown in Fig. 1. A discharge was maintained between the water-cooled aluminum electrodes *A*. A few ions passed through the grid *G* where they drifted under the action of a field, usually of the order of a volt per cm, to the slit S_1 which was made very narrow (about 0.01 mm) in order that the pressure in the analyzing chamber could be kept down to 10^{-4} mm for pressures above the slit varying from 0.1 to 0.5 mm. The drift space could be varied from 2.5 to 5.0 cm. Except for minor improvements the analyzing chamber was similar to the one previously described.

Wax was eliminated by the use of ground joints throughout, together with an annular ring *C* of pressed amber for insulation of the slit S_1 from the remainder of the apparatus. The present apparatus also has narrower slits S_2 and S_3 than the older apparatus, and is connected to an electrometer of higher sensitivity. Water cooling of the electrodes allowing a more intense discharge,

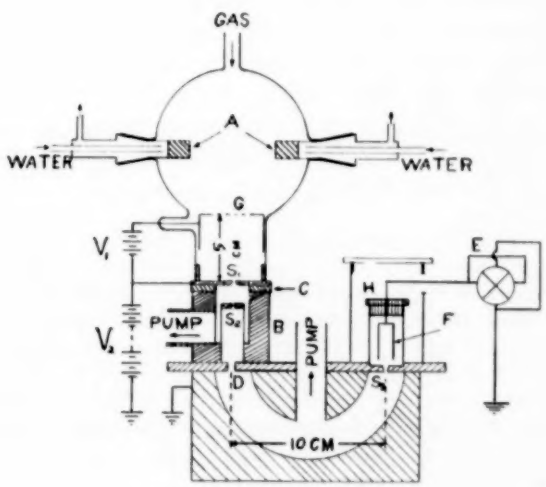

FIG. 1. Diagram of apparatus.

[1] O. Luhr, Phys. Rev. **38**, 1730 (1931).

together with faster pumping, and increase of the drift space to 5.0 cm made it possible to more than double the age of the ions.

Results

1. Hydrogen

In hydrogen H^+, H_2^+ and H_3^+ were found. The H_2^+ and H_3^+ did not appear to break up into simpler ions in the analyzing chamber. At a pressure of 0.3 mm, and with a field of 0.8 volt per cm in the 2.5 cm drift space, 80 percent of the ions were H_3^+ and the remainder about equally divided between H_2^+ and H^+. At lower pressures the percentage of H_2^+ increased relative to the other two, indicating H_2^+ is the primary ion.

2. Nitrogen

Results for nitrogen are shown in Figs. 2 and 3.[2] When the higher pressures and longer drift space were used, N_3^+ and N_4^+ ions appeared. These are apparently formed by the attachment of N^+ and N_2^+ to neutral molecules after a large number of collisions. The curve of Fig. 3 was taken with a discharge between a hot filament and a grid of the type used by Smyth[3] instead of a glow discharge. The tube had been operated too short a time to remove all the water vapor. It appears that the N_{3-2}^+ ions (mass 18.6) previously reported were water vapor ions.

3. Oxygen

The curves obtained with tank oxygen and that prepared from potassium permanganate and potassium chlorate were puzzling at first. The interpretations given in the Figs. 4, 5 and 6 were finally adopted. A nitrogen discharge was passed through the tube before the oxygen was admitted. It seems that nitrogen occluded in the surfaces of the apparatus was sufficient to yield the NO^+ and NO_2^+ for many hours operation of the tube. When a new tube was used with oxygen, the NO^+ and NO_2^+ ions disappeared very soon. After air was used in this tube the ions having masses of 30 and 46 reappeared as shown in Fig. 5, dotted curve. No quantitative correlation between the relative numbers of the various oxides of nitrogen was obtained. There was a tendency for NO^+ to predominate with the larger quantities of nitrogen.

4. Air

All possible oxygen and nitrogen ions occur in air, with the addition of the nitric oxides, water vapor if the tube is not thoroughly dried, and Hg^+ if mercury is not carefully removed by liquid air traps. Typical results are shown in Fig. 7 for relatively new ions. As expected the quantity of N_3^+ and N_4^+ becomes greater with increasing age. Traces of an ion of molecular weight 68 have been found but it disappears after the discharge has been operating a short time. Contrary to results previously reported other heavier ions, probably due to wax vapors, are absent in the present apparatus.

5. Water vapor

Water ions appear to be largely secondary in nature, being readily formed by transfer of charge from other ions, as their number is relatively increased when the aging is greater. Since a small amount of water vapor gives a large H_2O^+ ion current, the probability of transfer of charge to the water molecule is evidently large. In Fig. 3 two peaks appear. One is attributed to HO^+. Sometimes the H_2O^+ peak is displaced toward the heavier ions. It is suggested that this may be caused by the kinetic energy given to the ion when it acquired its charge. This effect may have been responsible for the consistent appearance of 18.6 ions in the earlier experiment which were attributed to N_{3-2}^+.

6. Negative ions

No negative ions were found in any gas. The arrangement of the apparatus is such that the probability of attachment of electrons to molecules in the drift space is small even in oxygen and the few negative ions formed in the discharge could not be observed with the extremely narrow slit S_1, necessary in this experiment.

[2] It should be noted here that the ordinate scale of the curves is arbitrary, and the actual electrometer deflections in the case of the dotted curve have been divided by ten to show the relative numbers of light and heavy ions. The total intensity of ionization depends on the width of the slit S_1 (Fig. 1) and decreases rapidly with increasing pressure, becoming practically zero above 0.5 mm. The scale of electrometer deflections in Figs. 3, 4 and 5 have likewise been adjusted to show approximately equal quantities of the primary ions.

[3] H. D. Smyth, Phys. Rev. **25**, 452 (1925).

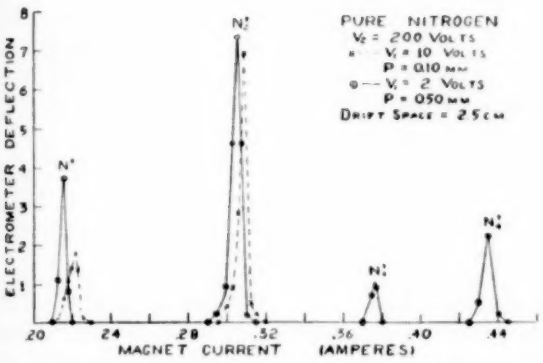

FIG. 2. Ions in nitrogen showing relative intensities with variation of age in a drift space of 2.5 cm.

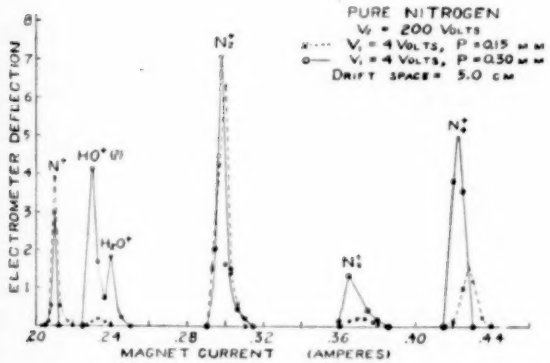
PURE NITROGEN
V_2 = 200 VOLTS
V_1 = 4 VOLTS, P = 0.15 MM
V_1 = 4 VOLTS, P = 0.30 MM
DRIFT SPACE = 5.0 CM
ELECTROMETER DEFLECTION
MAGNET CURRENT (AMPERES)

FIG. 3. Ions produced by a filament and grid in nitrogen, showing effect of varying the pressure in the drift space.

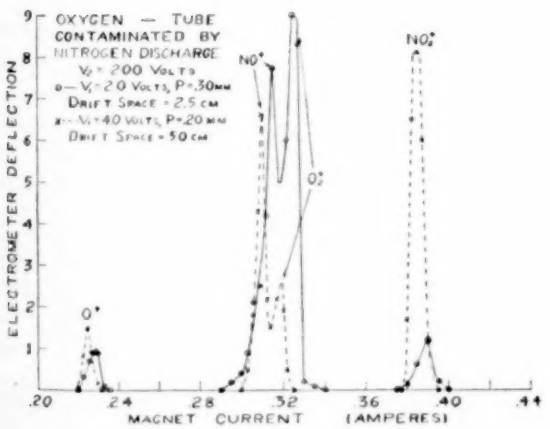
OXYGEN — TUBE CONTAMINATED BY NITROGEN DISCHARGE
V_2 = 200 VOLTS
V_1 = 2.0 VOLTS, P = .30 MM
DRIFT SPACE = 2.5 CM
V_1 = 4.0 VOLTS, P = .20 MM
DRIFT SPACE = 5.0 CM
ELECTROMETER DEFLECTION
MAGNET CURRENT (AMPERES)

FIG. 4. Ions in oxygen showing the effect of varying the age when nitrogen contamination is present.

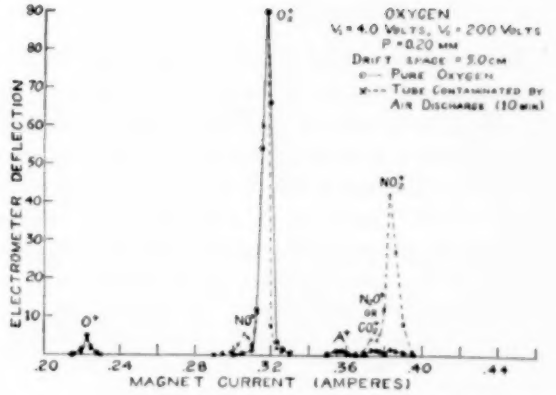
OXYGEN
V_1 = 4.0 VOLTS, V_2 = 200 VOLTS
P = 0.20 MM
DRIFT SPACE = 5.0 CM
PURE OXYGEN
TUBE CONTAMINATED BY AIR DISCHARGE (10 MIN)
ELECTROMETER DEFLECTION
MAGNET CURRENT (AMPERES)

FIG. 5. Ions in pure oxygen and in the same tube after contamination by nitrogen resulting from nitrogen discharge.

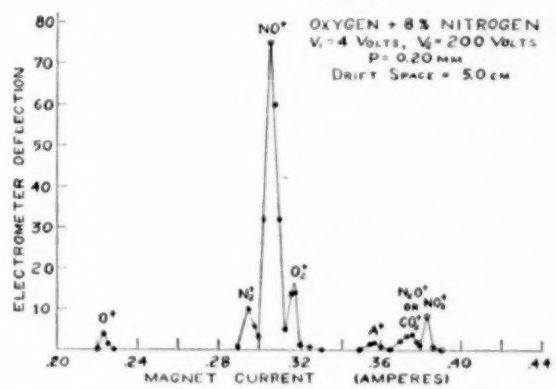

FIG. 6. Nitric oxide ions produced by transfer of charge in the drift space predominate where a small percentage of nitrogen is added to oxygen.

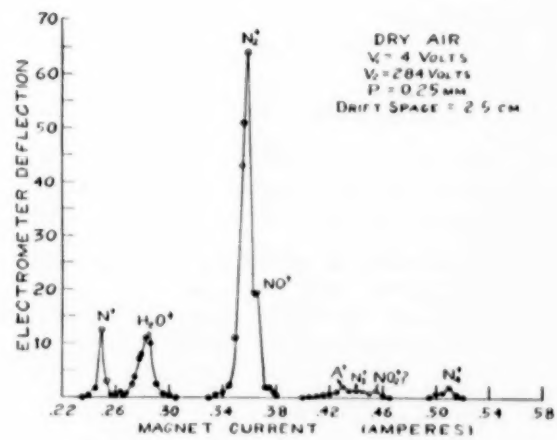

FIG. 7. Relatively new ions in air.

Discussion of Results

Assuming the usual relations between mobility of ions, pressure, and field strength the number of collisions for an ion in crossing the 5 cm drift space under a drift field of 0.8 volt per cm at a pressure of 0.5 mm is 10^5. This corresponds to an age of 4×10^{-6} seconds at atmospheric pressure. The age of ions usually measured in mobility experiments is 0.001 to 1.0 second. Hence the results here are of value only in determining the phenomena occurring in the earlier stages of the aging process.

In hydrogen, the normal positive ion under some conditions may be H_3^+ as that ion appears to form from H_2^+ after a few thousand collisions.

In nitrogen N^+ and N_2^+ appear to be primary products of ionization. The complexes N_3^+ and H_4^+ form after 10^5 collisions or a time of 4×10^{-6} seconds at atmospheric pressure. This result was calculated by a procedure similar to that used by Loeb[4] in determining the attachment coefficient of electrons.

The only ions observed in pure oxygen were O_2^+ with traces of O^+. When the oxygen is contaminated with nitrogen, the oxides NO, NO_2 and N_2O are formed and receive charges by transfer from the O_2^+ ions.

In air all possible nitrogen and oxygen ions were found. After the maximum aging possible in this experiment the ions in air chiefly O_2^+, N_3^+, and N_4^+.

Finally it has been established that up to 10^{-5} seconds at atmospheric pressure no complex ions except H_3^+, N_3^+ and N_4^+ are formed and that the ions H_2O^+, NO^+ and NO_2^+ are formed by transfer of charge. Transfer processes are probably more important under the usual conditions of purity than are the formations of complexes, and it is certain that such phenomena play an important rôle in any aging process.

The writer wishes to express his thanks to Mr. Edwin Kass, who assisted in taking some of the measurements, and to Professor L. B. Loeb, of the University of California, who has read the manuscript critically.

[4] L. B. Loeb, *Kinetic Theory of Gases*, p. 507, New York (1927). The available data must be extrapolated somewhat for these low pressures but should be correct at least in order of magnitude.

The Collisions of Neutrons with Protons

FRANZ N. D. KURIE,† *Sloane Physics Laboratory, Yale University*

(Received July 17, 1933)

A linear polonium source of about 2 millicuries strength is surrounded by beryllium contained in a brass cylinder coated with a layer of paraffin. This assembly is mounted on the piston in the center of a large automatic Wilson cloud chamber, in which the tracks due to protons projected from the paraffin layer by the neutrons are photographed. The angle between the proton track and its associated radius is measured. Corrections for scattering volume and effective solid angle of the cloud chamber are applied. On plotting the corrected number of proton tracks against the angle of projection a sharp maximum is found at 0°. The bearing of this distribution on the structure of the neutron is discussed.

THE field of the neutron may be studied by examining the interaction of that field with some particle. It is of course desirable that the particle chosen be as simple as possible in order that the results may be easily interpreted. For that reason we have chosen the proton, since the possibility is still open that in close encounters with other more complex nuclei the neutron may penetrate the potential barrier and be scattered by the internal field of the nucleus. Collisions between neutrons and protons may be brought about by bombarding a hydrogen-rich substance such as paraffin with neutrons. Protons will be knocked out of the paraffin by the impacts and will be distributed at angles to the neutron paths in numbers directly dependent upon the form of the neutron's potential field.

Several authors[1] have developed models of the neutron which account for such characteristics as its great penetrating power and its failure to interact with electrons. The models proposed may be summarized as follows: (1) an elastic sphere, (2) a dipole, (3) a proton imbedded in an electron. On classical theory the impact of elastic spheres of equal mass is such that the number projected at an angle θ to the direction of motion of the incident sphere is proportional to $\cos\theta$. H. S. W. Massey[1] has calculated the distribution of projected protons for the case of the dipole neutron and has shown that the number tends to infinity as θ tends to 90°. The third case cannot be treated by quantum mechanics in its present condition since the large binding energy necessary calls for relativity methods. In the same paper Massey has made an approximation to the third case, however, by considering a neutron in which the electron is bound very tightly to the proton by a fictitious high nuclear charge Z. To account for the penetrating power of the neutrons Massey is obliged to choose $Z \geq 2500$. The distribution-in-angle of projected protons exhibits a maximum which moves from 65° to 0° as Z increases from 2500 to infinity. In the latter limit the distribution is proportional to $\cos\theta$.

It was hoped at the outset of this work that experimental evidence in favor of one or the other of these models might be advanced, and so give insight into the nature of the neutron. It became apparent however that the data would conform to none of the prophecies.[2]

EXPERIMENTAL ARRANGEMENT

For this study a Wilson cloud chamber was used, which together with the camera has been described previously.[3] Since it was not necessary

† Sterling Fellow.

[1] H. S. W. Massey, Proc. Roy. Soc. **A138**, 460 (1932). J. L. Destouches, *État Actuel de la Théorie du Neutron*, Paris, 1932. J. Solomon, J. de Physique **4**, 210 (1933). I. I. Rabi, Phys. Rev. **43**, 838 (1933).

[2] The distribution reported by the author in a Letter to the Editor, Phys. Rev. **43**, 672 (1933), should be corrected by deleting the sentence "The present data seem best to fit the cosine curve which describes the scattering of elastic spheres." This statement arose through a numerical error in computing the solid angle subtended by the cloud chamber. This calculation will be given in the section headed "Corrections."

[3] F. N. D. Kurie, Rev. Sci. Inst. **3**, 655 (1932).

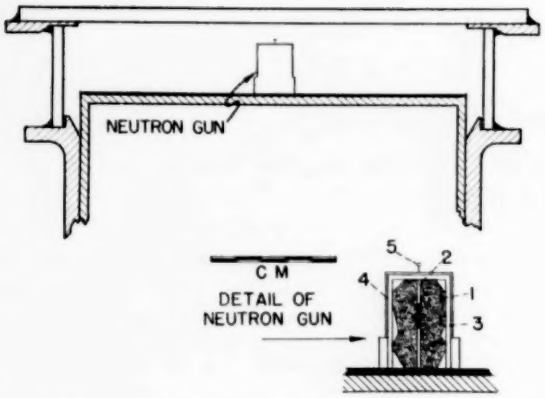

FIG. 1. Arrangement of the neutron source in the cloud chamber. In the inset is shown a cross section of the gun.

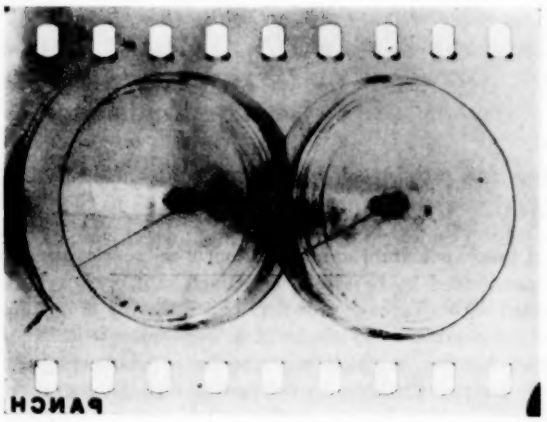

FIG. 2. A simultaneous pair of photographs of a proton track ejected by a neutron from the neutron gun in the center of the chamber.

to know the stopping power of the gas in the chamber to any high degree of precision the chamber was operated with a shorter interval between expansions than is permissible for more exact work. Actually the chamber made three expansions per minute.

The source of neutrons is shown in Fig. 1. Two pieces of beryllium had flat surfaces with a 1 mm step in them cut by a surface grinder. By not quite meshing these steps together a square hole *2* about 1 mm on a side was formed in the composite piece of beryllium *1*. In this hole a 2 millicurie polonium source was deposited by evaporating a polonium solution drop by drop. The source is indicated by the black portion of the hole *2* in the figure. The pieces of beryllium with the polonium were placed in a small brass cylinder *3* and centered by two pins one at either end (not shown in the figure). The box was blackened chemically and then dipped in paraffin saturated with lampblack, forming a thin layer *4* on the surface. The purpose of the blackening was to cut down the reflected light from the brass box which would otherwise spoil the pictures. The cylinder was waxed on the roof of the piston as shown. A small platinum bead *5* on the top of the cylinder served as a fiducial mark in the measurements of the tracks.

The direction of motion of the neutron is thus fairly well known, since it originates in a small volume and proceeds with negligible scattering to the point at which the proton is projected. There are some disadvantages to this arrangement as we shall see later but it has the desirable features that the paraffin subtends a large solid angle at the neutron source and allows the camera good vision of the chamber.

The tracks of the protons were photographed from two directions at right angles by a single lens camera.[3] (See Fig. 2.) The measurement of the tracks was accomplished by reprojecting the photographed images through the same optical system and recombining them on a screen equipped with divided circles so that the complete orientation of the track could be read directly. In Fig. 3 are shown the two angles, φ and δ, measured directly. The vertical distance y between the fiducial bead and the origin of the proton track was also measured.

The neutrons were assumed to move along the X axis, Fig. 3, this being merely a horizontal radius vector. Of the neutrons striking any point on the paraffin layer, the majority will come from that portion of the source which is nearest it so that the most probable direction of motion of the neutrons is in a horizontal plane. Corroborative evidence is furnished by the data shown in Fig. 4 where the number of protons is plotted as a function of y, the distance of their origin below the fiducial bead. This clearly shows a flat topped maximum over the length of the source, and so points to the reasonableness of the assumption that most protons are due to neutrons which arise from the part of the neutron source nearest the origin of the proton track. This assumption is an admitted compromise, since the true direction of the neutron's path cannot be precisely known.

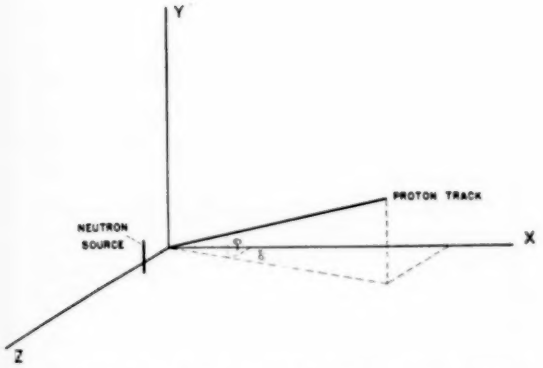

FIG. 3. The two angles φ and δ, which are measured for each proton track shown in their relation to the source of neutrons.

but it is believed to be the best that can be made.

The angle θ between the direction of motion of the neutron and the direction of motion of the proton is then simply $\cos^{-1}(\cos\delta\cos\varphi)$. This angle was computed from the measured angle for 160 tracks and a curve was plotted showing the number of tracks found between $\theta-5°$ and $\theta+5°$. Before this curve has any significance a number of corrections must be applied.

CORRECTIONS

In order to avoid the chance of mistaking α-particles due to contamination for protons only those tracks were considered which extended completely to the cylindrical periphery of the chamber. This restriction gives rise to a correction for the volume of paraffin effective in scattering. Referring to Fig. 5, let ON be the direction of motion of the neutron and AP that of the proton. Now let R be the mean range of the proton and R' the least emergent range (roughly 8 cm); then $\rho=R-R'$ is the greatest range in paraffin permissible. The effective scattering volume per unit length of the cylinder is then $\pi(a^2-r^2)$, where $OB=a$ and $OA=r$. Since $\rho\leqq 20$ cm air $=0.009$ cm paraffin ρ^2 may be neglected. We are here using 26 cm as the range of the protons;[4] using the longer ranges that are now being found by others will not affect this point. The effective scattering volume is finally

$$\pi(a^2-r^2)=2\pi a\rho\cos\theta. \qquad (1)$$

The observed distribution must then be multiplied point by point by $1/\cos\theta$.

The solid angle subtended by the chamber varies greatly with θ so that an approximate calculation must be made of this quantity in order that the observed data may be expressed as the number of protons projected per unit solid angle in the direction θ. We may simplify the problem by considering all the protons to start at the center of the neutron source, namely, at a point on the axis of the cloud chamber 7.5 mm from the bottom and 29.5 mm from the top. Taking the origin of a system of spherical polar coordinates

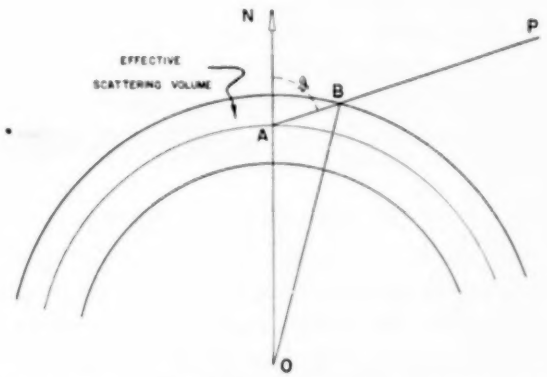

FIG. 5. Diagram indicating the dependence of the effective scattering volume in the paraffin layer on the angle θ.

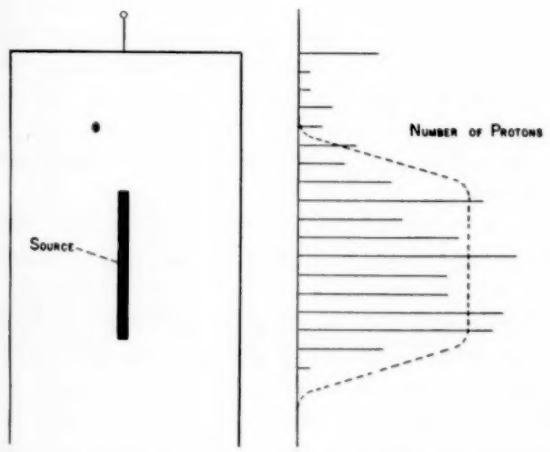

FIG. 4. Vertical distribution of the origins of the proton tracks, indicating that on the average the protons are projected by neutrons which start from the nearest portion of the neutron source.

[4] I. Curie and F. Joliot, Comptes Rendus **194**, 273 (1932).

at this center we require the area on a sphere of radius equal to that of the chamber and with center at the origin between the cones $\theta=\theta_1$ and $\theta=\theta_2$ and the planes $x=h_1$ and $x=h_2$ where $h_1=7.5$ mm and $h_2=29.5$ mm. The area A on the sphere of radius r, between the cones $\theta=\theta_1$, θ_2 and the planes $x=0$, h is given by

$$\frac{A}{r^2}=\int_{\theta_1}^{\theta_2}\sin\theta\,d\theta\int_{\pi/2}^{\cos^{-1}(h/r\sin\theta)}d\varphi$$

$$=\frac{\pi}{2}(\cos\theta_1-\cos\theta_2)-\int_{\theta_1}^{\theta_2}\sin\theta\cos^{-1}\frac{h}{r\sin\theta}d\theta.$$

The last integral may be evaluated by expanding the arc cosine in a power series and integrating term by term. We find finally that only the first two terms of the series are of any consequence so that the area is given by

$$\frac{A}{r^2}=\frac{h}{r}(\theta_2-\theta_1)-B(\cot\theta_2-\cot\theta_1),$$

where B is a power series in h/r which converges very rapidly. The formula just developed is only valid for values of θ given by $h^2/(r^2\sin^2\theta)>1$. The area can be computed by simple geometrical means for values of θ below those for which the formula is applicable. Column 3 of Table I gives the results of the calculation for this case (chamber diameter 16 cm) and column 4 the factor by which the observed scattering must be multiplied to correct for both scattering volume in the paraffin and the solid angle of the chamber.

TABLE I. *Number of protons N_p observed in each angular group and calculated scattering per unit relative solid angle, n_p. Ω is the relative solid angle and f is the correction factor.*

Angular range	N_p	Ω	f	n_p
0°–10°	27.5*	1.00	1.000	27.5
10°–20°	41.5	2.24	0.459	19.0
20°–30°	34	2.37	.464	15.8
30°–40°	19.5	2.18	.560	10.9
40°–50°	20.5	2.14	.658	13.5
50°–60°	14	2.12	.821	11.5
60°–70°	2	2.11	1.113	2.2
70°–80°	1	2.10	1.833	1.8

* When a proton occurs exactly on the dividing line of two groups it counts half in each of the two adjacent groups.

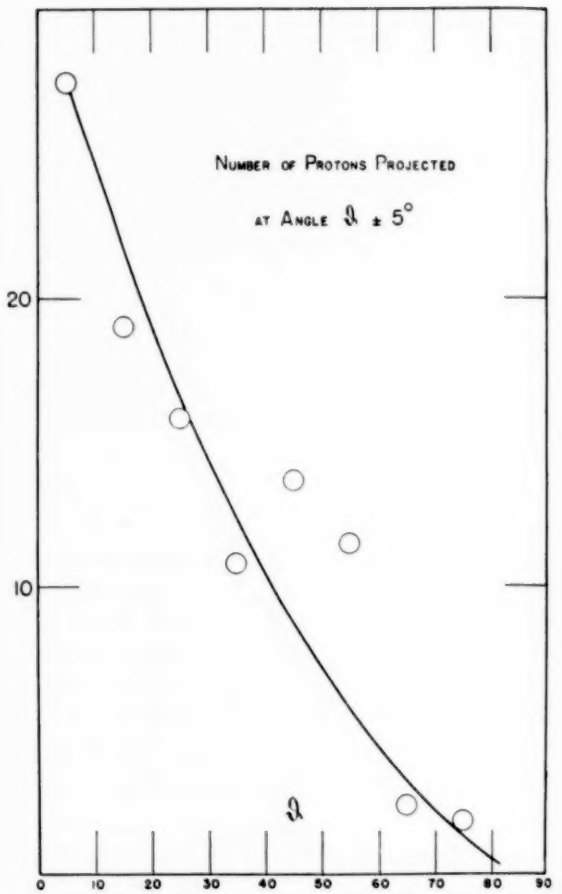

FIG. 6. Distribution-in-angle of protons projected by neutrons, fully corrected for effective scattering volume and for the solid angle subtended by the cloud chamber.

RESULTS AND DISCUSSION

In Table I is given the number of tracks in each of the angular groups and also these numbers multiplied by the proper correction factor. A graph of the corrected numbers is shown in Fig. 6. The curve clearly presents no maximum and is quite unlike any of the distributions predicted theoretically.

It is unfortunate that the neutrons emitted from beryllium are very inhomogeneous in velocity because this factor undoubtedly influences the character of the distribution-in-angle of the projected protons. This fact must be clearly borne in mind in making any deductions from these data. It is also important to recall that the neutrons in this experiment do not proceed from a point source and that the distribution curve is probably slightly exaggerated in the small angles for this reason.

Recently Auger and Monod-Herzen[5] have published measurements similar to those described in the present paper. They observed the number of proton tracks in the same angular domains as here considered, the tracks being excited in a hydrogen-filled cloud chamber by a source of neutrons placed outside the chamber. Dividing the tracks into "long" and "short" tracks they find the 84 long tracks to fit the distribution curve expected for elastic spheres. It is hard to judge the significance of the distribution curve for the long tracks (which are the only ones which may be compared with the present data) since the solid angle subtended by the chamber, an extremely important factor, is difficult to take into account when the tracks are distributed at random through the chamber.

Neither the distribution of Auger and Monod-Herzen nor the one presented in this paper can be considered as being entirely free from criticism. The author believes that in the curve shown in Fig. 6 the fact that it is concave upwards is real, but whether it is a property of the neutron-proton interaction, or of the distribution-in-velocity of the neutrons, or to some other cause cannot be said at this time.

However since the present distribution presents an appearance quite different from that demanded by the theories of a composite neutron built up of an electron and a proton the urge has been strong to suggest that this is an argument in favor of the neutron being an elementary particle. In view of the absence of a relativity quantum mechanics a close combination of electron and proton has not been properly examined. Until that is done such an argument would be of no value.

The view that a neutron is an elementary particle has however been gaining favor in some quarters. The most cogent evidence at present is perhaps the recent demonstration by Parker[6] that the spin of beryllium is one-half. This of course would make the spin of the neutron one-half and point directly to its being an elementary particle.

I wish to thank Professor Alois F. Kovarik for many valuable discussions of this work. To both Professor Kovarik and Professor John Zeleny I am grateful for generous gifts of radon tubes.

[5] P. Auger and G. Monod-Herzen, Comptes Rendus **196**, 1102 (1933).

[6] A. E. Parker, Phys. Rev. **43**, 1035 (1933).

Fluorescence of Diatomic Molecules of Antimony

J. GENARD, *Department of Astrophysics, University, Liége*

(Received June 6, 1933)

The phenomenon of fluorescence has been found for diatomic molecules of antimony excited by the lines 2967, 3022, 3126 and 3132 of a mercury arc. The formulas for these resonance series give for the equilibrium interatomic separation 2.21A and for the moment of inertia 489×10^{-40} g·cm².

THE phenomenon of molecular fluorescence excited by monochromatic light has formerly been studied for relatively few homopolar molecules. In particular, for the elements of the fifth column of the periodic table, only the fluorescence of phosphorus[1] and of bismuth[2] are known. The first has its maximum intensity near λ2050A, while for the second it occurs in the visible.

From the position of antimony in the periodic table, one would expect, if fluorescence of the molecule Sb_2 exists, to observe it in the ultraviolet between λ3000 and λ3500. Unfortunately, the absorption spectrum of antimony has not yet been studied and it has been impossible until the present time to know experimentally (1) if it has absorption bands and (2) if so, where they are to be found.

I have indirectly solved this problem by studying the fluorescence of Sb_2 excited by the ultraviolet radiation from a Hg arc.

Apparatus

The preparation of the antimony vessel is classical. The vessel of fused quartz consisted of two tubes of different diameter in which pressure and temperature could be independently varied by two electric furnaces.

The quartz vessel was cleaned by prolonged heating to eliminate gas occluded in the walls. The antimony was introduced by successive distillations; liquid air was used to prevent impurities from entering the fluorescence vessel.

A very intense Hg arc in a quartz tube shaped so as to surround almost completely the antimony vessel was used.

The quartz spectrograph gave a dispersion of 20A/mm in the region in which fluorescence occurs.

Conditions of Excitation

At 700°C and a pressure corresponding to 550°C weak fluorescence began to appear in the neighborhood of the lines 3126 and 3132. The maximum intensity was always found at a temperature of 950°C and a pressure equivalent to 650°C. The emission was then in the region between λ2900 and λ3400A. In spite of the great intensity of the exciting light, exposures of four hours were necessary to obtain good plates.

Results

It is easy to identify on the plates four resonance series excited respectively by the lines: λλ2967.6, 3021.7, 3125.8, 3132 of Hg I. The lines of each are generally quite distinct and without mutual superposition. In addition to these four lines, it is probable that the lines λλ2925 and 3342 also give rise to resonance. Unfortunately, the small intensity did not permit me to arrange them in series.

In Table I are given the numerical values of the resonance series. The first column contains the values of the "order number"; the second, those of the measured wave-lengths; the third, the measured frequencies corrected to vacuum from Kayser's tables; the fourth, the frequency intervals.

A resonance series may be empirically represented by the formula

$$\nu=\nu^*-a(N+\tfrac{1}{2})+b(N+\tfrac{1}{2})^2,$$

[1] Jakowlewa, Zeits. f. Physik **69**, 548 (1931).
[2] Parys, Zeits. f. Physik **71**, 807 (1931).

TABLE I. *Fluorescence lines excited by λλ2967.6, 3021.7, 3125.8, 3132 of Hg. I.*

N	λ	ν (vac.)	$\Delta\nu$	ν (calc.)	N	λ	ν (vac.)	$\Delta\nu$	ν (calc.)
		Series 2967.6					*Series 3125.8*		
−1	2944.5	33952		33959	−2	3074.5	32516		32521
0	2967.6	33687	265	33687	−1	3100	32249	267	32252
1	2991.5	33418	269	33417	0	3125.8	31983	266	31983
2	3016	33147	271	33148	1	3153	31707	276	31715
3	3040.5	32880	267	32880	2	3179.5	31442	265	31448
4	3065.5	32612	268	32614	3	3206	31183	259	31183
5	3090.5	32348	264	32349	4	3233.5	30917	266	30918
6	3116	32083	265	32086	5	3261	30656	261	30655
7	——	——	——	——	6	3289	30395	261	30393
8	3167	31567	——	31564					
9	3193	31309	258	31305			*Series 3132*		
10	3220	31047	262	31048	−3	3055	32724		32726
11	3247	30789	258	30791	−2	3080.5	32453	271	32456
					−1	3106	32186	267	32187
		Series 3021.7			0	3132	31919	267	31919
−2	2973.5	33621		33627	1	3159	31646	273	31652
−1	2997.5	33351	270	33355	2	3186	31378	268	31385
0	3021.7	33084	267	33084	3	3213	31115	263	31120
1	3047	32810	274	32814	4	3240	30855	260	30855
2	3072.5	32537	273	32546	5	3267.5	30596	259	30592
3	3098	32270	267	32279	6	3296	30331	265	30329
					7	3325	30067	264	30067

where N is the "order number," a and b are two coefficients, and the frequency of the exciting radiation corresponds to $N=0$.

The method of least squares gives the following expressions

Series 2967.6: $\nu = 33822 - 271.7(N+\frac{1}{2}) + 0.70(N+\frac{1}{2})^2$

Series 3021.7: $\nu = 33219 - 271.1(N+\frac{1}{2}) + 0.68(N+\frac{1}{2})^2$

Series 3125.8: $\nu = 32117 - 268.7(N+\frac{1}{2}) + 0.53(N+\frac{1}{2})^2$

Series 3132: $\nu = 32053 - 268.2(N+\frac{1}{2}) + 0.46(N+\frac{1}{2})^2$.

The values of the frequencies calculated from these formulae are given in the fifth column of Table I. Further, the theoretical formula for resonance series derived by wave mechanics may be written in the form

$$\nu = \nu_e - \omega_e''(v''+\tfrac{1}{2}) + \omega_e'' x_e''(v''+\tfrac{1}{2})^2,$$

in which ν_e represents the "system origin"; ω_e'' the fundamental frequency of vibration; x_e'' the correction for anharmonicity and v'' the quantum number of the vibration in the normal state.

It is easily seen that the numerical value of ω_e'' is, in general, much the same as the different coefficients a. If we take as an approximate value of ω_e'' the quantity $\omega_e'' = 277$, the formula of Morse

$$\omega_e'' \cdot r_e''^3 = 3000$$

gives the value of the interatomic equilibrium distance in the normal state, i.e.,

$$r_e'' = 2.21\text{A}.$$

It is easy to deduce from this the moment of inertia in the normal state

$$I'' = 489 \times 10^{-40}\ \text{gc}\cdot\text{m}.^2$$

A variation of some units in the value of ω_e'' changes the value of the moment of inertia by only a few percent.

Hyperfine Structure in Intermediate Coupling*

G. BREIT AND LAWRENCE A. WILLS, *New York University, University Heights*

(Received June 19, 1933)

The theory is extended to intermediate coupling and to cosine laws of force between nucleus and electron varying with different powers of their distance apart. In addition to Goudsmit's constants a', a'', there appears a third coupling constant a''' for each electron, which gives energy matrix elements for the same l and different j. The theory is in approximate agreement with observation. The gross structure is used to determine the parameters of the theory of intermediate coupling and hence $\overline{(1/r^3)}$. This together with a'' gives nuclear magnetic moments having roughly the same value for different configurations and stages of ionization. The variation of $1/r^3$ as determined from gross structure shows changes in screening agreeing with those supposed to exist for $(6s)^2$ of Pb I, Tl I in order to explain the isotope shift as due to differences in nuclear radii. The discrepancies between gross structure and theory are shown to be connected with similar discrepancies in hfs and the discrepancies of the ratios a''/a' are reasonably explained by perturbations due to other configurations.

1. INTRODUCTION

GOUDSMIT[1] had some success in explaining the magnitude of the observed hyperfine structure separations by considering the coupling of an electronic configuration to the nucleus as the resultant effect of the coupling of the individual electrons. At the same time he also found discrepancies of observations with the theory. These have to do with relative amounts of coupling of individual electrons in $np_{1/2}$ $np_{3/2}$ states, i.e., electrons having the same principal and azimuthal but different inner quantum numbers. The above divergences between theory and experiment have nothing to do with the validity of the hypothesis of nuclear spin and of the cosine law of interaction. They may be traced to the way in which the interaction energy between the electron and the nucleus depends on their distance apart.

These discrepancies, if real, indicate that the nucleus does not behave as a little magnet in its action on the extranuclear electrons. Instead, it would be necessary to suppose the existence of some other type of interaction satisfying the cosine law but depending on the distance between the electron and the nucleus in some other and as yet unknown way. The existence of such a force would be of great interest. The present paper contains a critical examination of the meaning of the apparent discrepancies between experiment and the picture of the nucleus as a little magnet. The conclusion is that most of the experimental material is in as good agreement with this picture as may be expected when one considers the approximate nature of calculations with many electrons. It will be recalled that Goudsmit's formulas involve sums of hyperfine splittings for levels having the same j (inner quantum number). By applying his sum relations to experimental data, one obtains a formal answer for the magnitude of coupling of individual electrons to the nucleus. The main advance of the present paper consists in dealing with the levels individually, rather than with all levels of the same j at once. It then becomes apparent that Goudsmit's "coupling constants" for individual electrons are really coupling variables; that their values, as derived from sum relations, may therefore be incorrect by considerable amounts and that the gross multiplet structure disagrees with the usual theory of intermediate coupling by amounts sufficient to account for the apparent variability of the hyperfine structure coupling constants. In order to explain the work we first discuss briefly Goudsmit's theory from a point of view which allows of further extension.

It is well known that if the nuclear spin operator is $\mathbf{I}$ and if $\mathbf{B}$ is any matrix vector involving

* Reported as paper 21, Wash. Meeting Phys. Soc. Apr. 27 (1933).

[1] S. Goudsmit, Phys. Rev. **37**, 663 (1931).

only electron variables, then an interaction energy of the type

$$H' = (\mathbf{BI}) \tag{1}$$

gives rise to energy differences given by

$$\Delta w = (A/2)[f(f+1) - j(j+1) - i(i+1)], \tag{2}$$

where f, j, i are the fine structure, inner and nuclear spin quantum numbers, respectively. Here

$$A = (\mathbf{BJ})_j/j(j+1) \tag{3}$$

and $\mathbf{J}$ is the operator representing the total electronic angular momentum, while the suffix j indicates that one takes the diagonal matrix element of the matrix product of $\mathbf{B}$ and $\mathbf{J}$ in that part of it which corresponds to $\mathbf{J}^2 = j(j+1)$ when $\mathbf{J}^2$ is made diagonal. It is well known that if J_z is also made diagonal and if its matrix elements are m, then the matrix elements of B_z are given by

$$(j, m|B_z|j, m) = mA. \tag{3'}$$

So far use has been made only of the supposition that the law of interaction is a cosine law in the sense of Eq. (1) and of the smallness of the perturbation as expressed by the use of Eq. (2). It is next supposed that the spectroscopic term dealt with can be assigned to a definite electronic configuration and, in order to justify Goudsmit's procedure, it is necessary to suppose that the eigenfunctions representing all the terms of the configuration may be approximated sufficiently well by linear combinations of products of the same single electron eigenfunctions. The validity of this supposition will be examined in more detail later. For the present it will be assumed to hold. The operator B_z is a sum of parts belonging to individual electrons

$$B_z = \sum_i B_z(i). \tag{4}$$

Goudsmit's relations between the values of the interval factors A of the configurations and the single electron coupling constants may be understood in the following way.

According to Eq. (3') it is sufficient to know the diagonal matrix elements of B_z referred to eigenfunctions describing states of definite total angular momentum and of definite projection of this momentum along z. It should be remembered however that a given electronic configuration gives, in general, several ways of obtaining the same total angular momentum. Thus, for example, the configuration sp in Russell-Saunders coupling gives the states $^3P_1$ and $^1P_1$ each of which has the angular momentum 1.

Let us start with three electrons and neglect, for the present, the symmetry due to their identity. The wave function for any spectral term of the configuration is then some linear combination of products of single electron functions and each of these functions is supposed to be the solution of a single electron problem in a proper self-consistent central field. These single electron functions are further supposed to be characterized by values of the principal and azimuthal quantum numbers which are used to designate the configuration. Each electron has $2(2l+1)$ linearly independent eigenfunctions. It is most convenient in the discussion of hyperfine structure to use the functions which correspond to definite total angular momenta of individual electrons. Thus, for each electron we have two sets of functions $u_m^{n,\ j}(j = l \pm \frac{1}{2})$. We consider the matrix for (4) with respect to products

$$u_{m_1}^{n_1,\ l_1 \pm \frac{1}{2}}(1)\ u_{m_2}^{n_2,\ l_2 \pm \frac{1}{2}}(2)\ u_{m_3}^{n_3,\ l_3 \pm \frac{1}{2}}(3).$$

Each of the operators $B_z(i)$ operates on the i^{th} factor in the above product. We consider some value of the resultant angular momentum j and a special value of the projection of this angular momentum on the z axis. The eigenfunction for such a state is a linear combination of the above products. If there are several possible states with the same j there are several linearly independent linear combinations of these products which may be chosen so as to be orthogonal to each other and so as to correspond to the observed states. These states may be denoted by j to indicate the total angular momentum, by $m(j)$ to indicate its z component and by $n(j)$ to distinguish between different coupling possibilities in obtaining the same j. Thus, for example, $n(j)$ should have different values for the $^3P_1$, $^1P_1$ states of the sp configuration. The coupled state is described by the wave function

$$v^{n(j)j}_{m(j)}(1,2,3)=\sum c^{n(j),\,m(j)}_{j_1 m(j_1);\ j_2 m(j_2);\ j_3 m(j_3)}$$

$$\times u^{n_1 j_1}_{m(j_1)}(1)\ u^{n_2 j_2}_{m(j_2)}(2)\ u^{n_3 j_3}_{m(j_3)}(3)\cdots \quad (5)$$

where j may take either of the values $l\pm\frac{1}{2}$ and

$$m(j_1)+m(j_2)+m(j_3)=m(j). \quad (5')$$

It is usually convenient to choose some simple set of functions (5) such as, for example, the functions corresponding to (jj) or to Russell-Saunders coupling. The energy matrix is not necessarily diagonal when referred to these functions. Nevertheless, conservation of angular momentum causes it to be diagonal in j, $m(j)$ and the secular equation for the energy breaks up into sets of equations, each set containing coefficients distinguished only by different values of $n(j)$. The matrix for B_z behaves similarly. No matter what set of functions v is used the sum of the diagonal elements of B_z is therefore the same for fixed j, $m(j)$, because the submatrices of B_z transform themselves canonically as one set of v's is transformed into another. This establishes sum relations between the interval factors A in different types of coupling.

Consider, in particular, the functions v for jj coupling. The summation in Eq. (5) is performed with fixed j_1, j_2, j_3 and the only quantities varied are the $m(j_i)$. Since, according to Eq. (4), B_z is a sum of terms referring to each electron separately, the terms in the summation (5) contribute to the diagonal elements separately.

$$(v^{n(j)j}_{m(j)}\,|\,B_z\,|\,v^{n(j)j}_{m(j)})$$

has the form of a sum of terms, each term being the product of the square of the absolute value of one of the c's in Eq. (5) by the matrix element of some $B_z(i)$ of the type

$$(u^{n_i j_i}_{m(j_i)}(i)\,|\,B_z(i)\,|\,u^{n_i j_i}_{m(j_i)}(i))=m(j_i)a(n_i j_i). \quad (6)$$

These matrix elements are diagonal elements for the single electron i and according to Eqs. (1), (2), (3′) they determine the interval factor A for a single electron in the state n_i, l_i, j_i by

$$A=a(n_i j_i).$$

In order to derive the interval factor A, Goudsmit considers a fixed set j_1, j_2, j_3. The complete set of Eqs. (5) for fixed j_1, j_2, j_3 may be regarded as a unitary transformation between the products of single electron functions

$$u^{n_1 j_1}_{m(j_1)}(1)\ u^{n_2 j_2}_{m(j_2)}(2)\ u^{n_3 j_3}_{m(j_3)}(3) \quad (7)$$

and the functions v. By Eq. (5′) the transformation equations connect only such products for which the sum of m's is equal to the m of v. A canonical transformation connects the matrices for B_z referred to (7) and to v and the sum of their diagonal elements is therefore the same. For each m, linear relations between single electron interval factors and the many electron interval factors are thus established by means of Eqs. (6) and (3′) and the use of the coefficients c of Eq. (5) is avoided.

The representation of the coupled states v by a simple sum of products as written in (5) is not valid on account of the *exclusion principle*. Instead of (7) one should use determinants

$$(3!)^{-\frac{1}{2}}\left|\,u^{n_1 j_1}_{m(j_1)},\ u^{n_2 j_2}_{m(j_2)},\ u^{n_3 j_3}_{m(j_3)}\,\right|. \quad (7')$$

This change affects the discussion only inasmuch as some of the determinants (7′) vanish and some values of j are impossible. The diagonal matrix elements of B_z with respect to (7′) are still given by the same expressions as if (7) were used provided (7′) does not vanish. It is thus only necessary to drop, in discussing sum relations, those combinations of $n_1 j_1 m(j_1)$, $n_2 j_2 m(j_2)$, $n_3 j_3 m(j_3)$ in which two or more sets of quantum numbers are equal.

Comparison of the theoretical formulas obtained in this manner with the experimental material leads to the conclusion that the coupling constants a for a single electron are not in agreement with expectation. Relativity was not taken into account in these considerations and corrections for its influence showed that part of the discrepancy could be explained. These corrections were made[2, 3, 4] by means of Dirac's equation for a single electron. It will be remembered that, according to this equation, there are two radial functions for an electron in a central field and that, for the same l and different j, these func-

[2] G. Breit, Phys. Rev. **35**, 1447 (1930); **38**, 463 (1931)
[3] G. Racah, Il Nuovo Cimento **8**, 178 (1931).
[4] G. Racah, Zeits. f. Physik **71**, 431 (1931).

tions satisfy different equations. Their behavior at the origin is also different, the value of j having more to do with the nature of the singularity at the origin than the value of l. It is thus clear that any attempt at treating the hyperfine structure in intermediate coupling with due regard for relativity must be made *via jj* coupling.

In the calculations given below we suppose that many electron states may be represented by Eq. (5) but we modify the functions to mean the single electron functions of Dirac. The arguments of any u are now the three cartesian coordinates and the four-valued spin variable. The result of this change is to give a function which corresponds to nearly the same state of coupling as before the change was made because the difference between the Dirac and the Schroedinger equation with spin (Pauli's equation) is appreciable only in the small region close to the nucleus. By Dirac's equation, the interaction energy between two particles can be represented with sufficient accuracy as an electrostatic interaction e^2/r as long as one neglects the spin-spin interactions and the interactions between the spin of one electron with the orbit of another. This may be seen by inspecting the derivation[5] of the magnetic interactions in Pauli's equation from Dirac's equation. The electrostatic energy integrals, Slater's F and G integrals, will not be materially affected because contributions to them are made by regions not in the immediate vicinity of the nucleus. The magnetic terms usually attributed to the interaction of the electron spin with its own orbit will not be given quite correctly by $[\varepsilon_1 \times \mathbf{p}_1]\boldsymbol{\sigma}_1$ for heavy nuclei. This is not important however for the applications which we shall make. For, in discussing the state of coupling, we shall not try to calculate the absolute values of the coupling parameters but will determine them from experiment.

In order to calculate the interval factors for states in intermediate coupling, we need to know the matrix elements of the type (6) and, in addition, also matrix elements of the nondiagonal type corresponding to transitions between states having the same l but different j. The possible matrix elements between such states are considered in the next section.

[5] G. Breit, Phys. Rev. **34**, 553 (1929); **39**, 616 (1932).

2. Relativistic Matrix Elements for a Single Electron

The interaction energy (1) consists according to (4) of a sum of parts, each part being due to a single electron. We shall suppose that the nucleus produces a magnetic field and that this magnetic field acts on the electrons. If the nucleus is very small and if it produces the magnetic field as though it were a little magnet,

$$\mathbf{B}(i) = eg\mu_0 r_i^{-3}[\boldsymbol{\alpha}_i \times \mathbf{r}_i] \tag{8}$$

where e is the absolute value of the electronic charge, $\mu_0 = eh/4\pi mc$ is the Bohr magneton, r is the distance of the electron from the nucleus and α_i is the vector having for components the first three of Dirac's α's. Since we are interested, in this section, in a single electron, we need not use the letter i to distinguish between different electrons. We also find it easy to make calculations for a generalization of (8)

$$\mathbf{B} = eg\mu_0 r^{-n}[\boldsymbol{\alpha} \times \mathbf{r}]. \tag{9}$$

For $n=3$ we have the interaction energy corresponding to a little magnet. For other values of n we obtain the interaction energy due to a nucleus having finite dimensions. The nucleus is thought of as being spherical; the intensity of magnetization is supposed to be parallel to $\mathbf{I}$ and uniform in concentric spherical shells. Thus, if the intensity of magnetization at a point R is $\mathbf{I}f(R)$, the interaction energy is

$$eg\mu_0 \boldsymbol{\alpha}[\mathbf{X} \times \mathbf{I}] \tag{10}$$

with

$$\mathbf{X} = \int_0^\infty (\mathbf{r} - \mathbf{R}) \, |\mathbf{r} - \mathbf{R}|^{-3} f(R) 4\pi R^2 dR. \tag{11}$$

Here $\mathbf{X}$ may be interpreted as the electric intensity at $\mathbf{r}$ due to a charge distribution uniform in concentric layers and having the value $f(R)$ and it may thus be taken to be $(\mathbf{r}/r^3)\int_0^r 4\pi f(R) R^2 dR$. The spherical shell model gives, thus, instead of $1/r^3$ in (8), simply some function of r. By means of sums of expressions (9) multiplied by proper coefficients we can represent such a function.

We use the form of solution of Dirac's equation in a central field due to Darwin[6] in the notation of Roess.[7] We have then certain expressions for

[6] C. G. Darwin, Proc. Roy. Soc. **A118**, 654 (1928).

[7] L. C. Roess, Phys. Rev. **37**, 532 (1931).

Dirac's wave function in terms of two radial functions which are denoted by F_l and G_l if $j=l+\frac{1}{2}$ and by F_{-l-1}, G_{-l-1} if $j=l-\frac{1}{2}$. We recall that the matrix elements of a matrix vector are given by formulas of the type

$$(j+1, m\pm1|X+iY|j, m) = \mp\rho(j\pm m+2)^{\frac{1}{2}}(j\pm m+1)^{\frac{1}{2}} \quad (12.1)$$

$$(j, m\pm1|X+iY|j, m) = \sigma(j\pm m+1)^{\frac{1}{2}}(j\mp m)^{\frac{1}{2}} \quad (12.2)$$

$$(j-1, m\pm1|X+iY|j, m) = \pm\tau(j\mp m)^{\frac{1}{2}}(j\mp m-1)^{\frac{1}{2}} \quad (12.3)$$

if a suitable canonical transformation is performed on these matrices.[8] The Roess functions[7] are not necessarily such as to give matrix elements just in this form. They make, however, the Z components diagonal and thus they differ from the functions which one must use in order to obtain Eqs. (12) only by constant phase factors which are not necessarily the same for different j, l, m. Their relative values for the same j and l do not interest us because they can be properly adjusted so as to correspond to (12.2). The value of σ is then independent of the common phase factor, as is seen from the Eq. (12.2). The values of ρ, τ will be affected, however, by the choice of common phase factors for each j. This circumstance will have to be considered in applying the formulas. By means of Eqs. (12) the calculation reduces itself to the calculation of $(J, m|B_z|j, m)$ where $J=j\pm1$, j. We are, therefore, concerned with

$$[\mathfrak{a}\times\mathfrak{r}]_z = ir\sin\theta \begin{Bmatrix} 0 & 0 & 0 & e^{-i\phi} \\ 0 & 0 & -e^{i\phi} & 0 \\ 0 & e^{-i\phi} & 0 & 0 \\ -e^{i\phi} & 0 & 0 & 0 \end{Bmatrix}. \quad (13)$$

The dependence of Ψ on the azimuthal angle ϕ and on the colatitude angle θ restricts the possibilities for nonvanishing matrix elements. Performing summations over the four-valued spin variable and using Eq. (13) we obtain

$$(\Psi'^*[\mathfrak{a}\times\mathfrak{r}]\Psi).$$

[8] B. L. van der Waerden, *Die gruppentheoretische Methode in der Quantenmechanik*, p. 78, Berlin, Julius Springer (1932).

TABLE I. *Nonvanishing matrix elements for* B_z.

l'	j'	m'	l''	j''	m''	$(l', j', m'\|B_z\|l'', j'', m'')$
$l-1$	$l-\frac{1}{2}$	$l-\frac{1}{2}$	$l+1$	$l+\frac{1}{2}$	$l-\frac{1}{2}$	$\tau(2l)^{\frac{1}{2}}$
l	$l+\frac{1}{2}$	$l-\frac{1}{2}$	l	$l-\frac{1}{2}$	$l-\frac{1}{2}$	$\rho(2l)^{\frac{1}{2}}$
l	$l+\frac{1}{2}$	$l+\frac{1}{2}$	l	$l+\frac{1}{2}$	$l+\frac{1}{2}$	$(l+\frac{1}{2})\sigma_1$
l	$l-\frac{1}{2}$	$l-\frac{1}{2}$	l	$l-\frac{1}{2}$	$l-\frac{1}{2}$	$(l-\frac{1}{2})\sigma_2$

For the Roess form of the Dirac wave functions and (13) we find for B_z as given by Eq. (9) only the nonvanishing matrix elements shown in Table I where

$$\tau = -I/(2l+1), \quad (14.1)$$

$$\rho = I/(2l+1), \quad (14.2)$$

$$\sigma_1 = (l+1)I/j(j+1), \quad (14.3)$$

$$\sigma_2 = -lI/j(j+1) \quad (14.4)$$

and

$$I = eg\mu_0\int_0^\infty (F'^*G''+G'^*F'')r^{3-n}dr.$$

Here F', G' are radial factors in the Roess form[7] corresponding to j', l' and F'', G'' are similarly solutions corresponding to j'', l''. Eqs. (14.3), (14.4) will be applied in most cases to the calculation of diagonal elements, i.e., to the condition in which F', $G'=F''$, G''. In such cases σ is determined by the above formulas quite independently of common phase factors in F, G. The connection with $\overline{r^{-3}}$ is as in reference 2. We introduce the functions used by Gordon[9] which are related to Darwin's functions by

$$rG=\phi_2, \quad rF=-\phi_1 \quad (15)$$

and Dirac's quantum number k which has been denoted by $-j'$ in reference 2. We note that

$$k(k-1)=l(l+1) \quad (16)$$

and we may thus summarize (14.3) and (14.4) by the single formula

$$\sigma = -\frac{2keg\mu_0}{j(j+1)}\int_0^\infty \phi_1\phi_2 r^{1-n}dr = -\frac{2eg\mu_0}{k-1}\frac{l(l+1)}{j(j+1)}\int_0^\infty \phi_1\phi_2 r^{1-n}dr \quad (17)$$

[9] W. Gordon, Zeits. f. Physik **48**, 11 (1928).

when the principal quantum numbers are the same and the functions ϕ_1, ϕ_2 are real. This formula is equivalent to Eq. (10) of reference 2. From the nonrelativistic[10] $1/r^3$ it may be expressed as

$$l(l+1)\overline{(r^{-3})}\rightarrow-(ek/\mu_0)\int_0^\infty \phi_1\phi_2/r^2dr. \quad (17')$$

This gives Eq. (17) when $n=3$.

We now consider ρ as given by (14.2) for the case of the same principal quantum number in the $'$ and $''$ states. The function G is closely related to the radial factor in the solution of Schroedinger's nonrelativistic equation and is approximately equal to it except in the neighborhood of the nucleus. We standardize the choice of phase factors by requiring G to be approximately the same in two functions corresponding to $j=l\pm\frac{1}{2}$. For large r the function F is not important. The two functions of the Roess type which enter the matrix element (14.2) are:

$$\begin{aligned} &j=l+\tfrac{1}{2},\quad m=l-\tfrac{1}{2},\\ &\qquad \Psi=M_\theta'(\quad,\quad,2lG'P_l{}^{l-1},-G'P_l{}^l)\\ &j=l-\tfrac{1}{2},\quad m=l-\tfrac{1}{2},\\ &\qquad \Psi=M_\theta''(\quad,\quad,G''P_l{}^{l-1},G''P_l{}^l). \end{aligned} \quad (18)$$

These wave functions should be compared with wave functions for Pauli's equation. The third place in Ψ refers to the spin being parallel and the fourth place to the spin being antiparallel to z. The function $GP_l{}^l$ is an orbital function corresponding to $m_l=l$ while $GP_l{}^{l-1}$ similarly corresponds to $m_l=l-1$. The relative signs of these functions are not correct, however, if one wishes to obtain matrices of the form of Eqs. (12). To obtain this form for $\mathbf{L}$ and other orbital matrix vectors[11] one must use $(-)^nP_l{}^n$ as the angular factor. We see therefore that the Pauli approximation to the functions (18) may be taken to be

$$\begin{aligned} &j=l+\tfrac{1}{2},\quad m=l-\tfrac{1}{2},\\ &\qquad \psi=(2l+1)^{-\frac{1}{2}}[(2l)^{\frac{1}{2}}u_{l-1}s_+ + u_ls_-]\\ &j=l-\tfrac{1}{2},\quad m=l-\tfrac{1}{2},\\ &\qquad \psi=(2l+1)^{-\frac{1}{2}}[u_{l-1}s_+ - (2l)^{\frac{1}{2}}u_ls_-] \end{aligned} \quad (18')$$

where u_l, u_{l-1}, are normalized orbital functions which correspond to the form of Eq. (12) and s_+, s_- are similarly chosen spin functions referring to the electron spin being parallel and antiparallel to the z axis. A common phase factor or sign in the two functions (18′) is still immaterial because it does not affect the value of ρ. Having fixed the relative phase factors of the two functions (18′) we have automatically fixed the relative phase factors between all functions corresponding to $j=l\pm\frac{1}{2}$ because the form Eq. (12) determines all functions[12] of one j when one of them is given. Such phase relations between functions of the same j we will call standard phase relations and the phase relations between all functions of the same principal and azimuthal quantum numbers which are determined by (18′) we will also call standard. The matrix elements $(j'=l+\frac{1}{2},\ l'=l,\ m'|\mathbf{s}|j''=l-\frac{1}{2},\ l''=l,\ m'')$ are given by (12.1) where the constant of proportionality ρ is

$$s_{l+\frac{1}{2},\,l-\frac{1}{2}}=1/(2l+1), \quad (19)$$

while the orbital angular momentum matrix elements are similarly given by (12.1), the constant of proportionality ρ having the value

$$l_{l+\frac{1}{2},\,l-\frac{1}{2}}=-1/(2l+1). \quad (19')$$

The correctness of Eqs. (19), (19′) is readily verified by computing the z components of $\mathbf{s}$, $\boldsymbol{l}$ by using Eqs. (12), (18′).

Approximate expressions for the constants ρ, σ in Eqs. (14) may be obtained by using Darwin's approximations to F and G by means of Bessel functions in the neighborhood of $r=0$, similarly to the way in which Racah[3, 4] has given approximations to σ for the case $n=3$. We use the symmetrical form[2] of the Bessel function approximations

$$\begin{aligned} &j=l+\tfrac{1}{2},\quad k'=l+1;\quad \phi_1=C'Z\alpha J_{2\rho'};\\ &\qquad \phi_2=C'[y^{\frac{1}{2}}J_{2\rho'+1}-(k'+\rho')J_{2\rho'}] \end{aligned} \quad (20.1)$$

$$\begin{aligned} &j=l-\tfrac{1}{2},\quad k''=-l;\quad \phi_1=C''Z\alpha J_{2\rho''};\\ &\qquad \phi_2=C''[y^{\frac{1}{2}}J_{2\rho''+1}-(k''+\rho'')J_{2\rho''}] \end{aligned} \quad (20.2)$$

where

$$y=2Zr/a_H;\quad \rho=(k^2-Z^2\alpha^2)^{\frac{1}{2}},\quad \alpha=2\pi e^2/hc. \quad (20')$$

Here the Bohr radius $h^2/4\pi^2me^2$ is denoted by a_H, Z is the atomic number and the Bessel functions have the argument $2y^{\frac{1}{2}}$. For sufficiently large r, the Bessel functions can be approximated

[10] G. Breit, Phys. Rev. **37**, 51 (1931).

[11] H. C. Brinkman, Dissertation, Utrecht, 1932.

[12] Gray and Wills, Phys. Rev. **38**, 248 (1931)

by their asymptotic expansions.[13] The important function is ϕ_2 because for large r it becomes approximately the Schroedinger radial function multiplied by r. We select values of r sufficiently small to have Eqs. (20) valid and sufficiently large to make it possible to approximate Eqs. (20) by asymptotic expansions of the Bessel functions. For such r both (20.1) and (20.2) are approximately

$$\phi_2 \cong C\pi^{-\frac{1}{2}}y^{-\frac{1}{4}}[y^{\frac{1}{2}}\sin(2y^{\frac{1}{2}}-\pi\rho-\tfrac{1}{4}\pi) - (\rho^2-k+3/16)\cos(2y^{\frac{1}{2}}-\pi\rho-\tfrac{1}{4}\pi)] \quad (21)$$

and here

$$\rho^2-k+3/16=l(l+1)+3/16-Z^2\alpha^2$$

is the same for $j=l+\frac{1}{2}$ and $j=l-\frac{1}{2}$. According to (21) the two states with the same l and different j can be described as slowly oscillating functions having the same amplitude factor and phases differing by a constant amount $(\rho'-\rho'')\pi$. This may be taken to indicate that C' and C'' are approximately equal to each other essentially because the values of r for which Eq. (21) applies are sufficiently large to make the differential equations, satisfied by ϕ_2 for $j=l+\frac{1}{2}$ and ϕ_2 for $j=l-\frac{1}{2}$, differ very little from each other. Thus, under these conditions, the Schroedinger radial functions for the two states $j=l\pm\frac{1}{2}$ are obtained from the Schroedinger radial equation by continuing the two solutions (21) towards larger r. The process of continuation may be thought of as being approximated by the method of Wentzel-Kramers-Brillouin. As r increases the two solutions for $j=l\pm\frac{1}{2}$ will approach each other also in their phase because the initial phase difference $(\rho'-\rho'')\pi$ will be gradually compensated by the phase difference in the usual $\int f dx$ arising from the energy difference of the two states. The energy difference makes itself felt only for values of r comparable with a_H while the values of r dealt with in Eq. (21) are of the order of a_H/Z. As long as the above assumptions can be made consistently the W.K.B. approximation to the radial functions will approach each other in the oscillating region for large r. The normalization integral is approximately determined by this region and the region beyond the turning point of classical motion which is represented by the exponential branch of the W.K.B. solution. The absolute values of C', C'' are expected therefore to be approximately equal, provided there exists a region for r which satisfies all the above requirements, provided the W.K.B. approximation is good enough and provided the turning points which correspond to the largest possible classical distances of the electron from the nucleus are approximately in the same region. Under these conditions we may connect the constants C', C'' with the corresponding constant for the nonrelativistic approximations to (20.1), (20.2):

$$j=l+\tfrac{1}{2}, \quad \phi_2=-C'y^{\frac{1}{2}}J_{2l+1}; \quad (21.1)$$

$$j=l-\tfrac{1}{2}, \quad \phi_2=C''y^{\frac{1}{2}}J_{2l+1} \quad (21.2)$$

which is obtained from the above equations by letting $\rho=|k|$. For $j=l+\frac{1}{2}$ the difference between ρ and $|k|$ is relatively insignificant because $|k|\geqq 2$ as long as we do not deal with s states for which these considerations are not necessary. The solutions (20.1) and (21.1) thus approach each other as they are continued towards large r on account of the gradual compensation of their phase difference and similarly for (21.1) (21.2). Thus if we wish to start with radial eigenfunctions for $j=l\pm\frac{1}{2}$ which are approximately equal to each other for large r we must make

$$C'=-C''. \quad (22)$$

This relation is essential for the identification of the two functions G', G'' in Eq. (18). The additional corrections to C', C'' can be found by considering the solutions for ϕ_2 more accurately and will be called normalization corrections. They may be ascertained by numerical solutions as has been done for instance in reference 2.

We now calculate (14.2), (14.3), (14.4). We have[14]

$$(p,q,s)=\int_0^\infty J_p(t)J_q(t)t^{-s}dt=\frac{\Gamma(s)\Gamma[(p+q-s+1)/2]}{2^s\Gamma[(1+p-q+s)/2]\Gamma[(1+q-p+s)/2]\Gamma[(1+q+p+s)/2]}. \quad (s>0) \quad (23)$$

[13] This argument is essentially Racah's.[2] We discuss the degree of approximation somewhat differently and in more detail.

[14] Whittaker and Watson, *Modern Analysis*, p. 385, Problem 50, Cambridge University Press, 1920. We let $z\to 1$ in this formula.

Hence for $s=3$

$$(p, q, 3)=\frac{4\sin\frac{1}{2}\pi(p-q)}{\pi(p^2-q^2)[(p+q)^2-4][4-(p-q)^2]}, \tag{23.1}$$

and as special cases of this

$$(2\rho+1, 2\rho+1, 3)=1/[16\rho(\rho+1)(2\rho+1)], \tag{23.2}$$

$$(2\rho, 2\rho+2, 3)=1/[32\rho(\rho+1)(2\rho+1)], \tag{23.3}$$

$$(2\rho-1, 2\rho, 2)=1/[8\rho(2\rho-1)], \tag{23.4}$$

$$(2\rho', 2\rho'', 3)=\sin\pi(\rho'-\rho'')/[16\pi Z^2\alpha^2(2l+1)], \tag{23.5}$$

$$\lim_{\alpha\to 0}(2\rho', 2\rho'', 3)=1/[32l(l+1)(2l+1)]. \tag{23.6}$$

For $n=3$ we perform in Eq. (17) the integration over r with the aid of (23.4), (23.2). We have

$$\int_0^\infty \phi_1\phi_2 r^{-2}dr=-(2k+1)C^2Z^2\alpha/\rho(4\rho^2-1)a_H \tag{24}$$

and hence

$$\sigma=[2g\mu_0^2 l(l+1)/j(j+1)]\overline{(r^{-3})}F, \tag{25}$$

where

$$F=\frac{k(2k+1)(2l+1)}{\rho(2\rho-1)(2\rho+1)} \tag{25'}$$

and

$$\overline{(r^{-3})}=\left(\int_0^\infty \phi_2{}^2 r^{-3}dr\right)_{\alpha\to 0}=2C^2Z^2/a_H{}^2 l(l+1)(2l+1) \tag{26}$$

is the nonrelativistic average of $1/r^3$. The factor F represents the relativistic correction to Eq. (17′) essentially in Racah's form. It is equivalent to (17″) as long as Eq. (20) applies and as long as the conditions necessary for the validity of Eq. (22) are fulfilled.

The constant ρ of Eq. (14.2) is obtained by substituting Eq. (20) by making use of Eq. (21) and the first Eq. (20′). We have then

$$\rho=-\frac{(-C'C'')}{C^2}\frac{g\mu_0{}^2}{2l+1}\overline{\left(\frac{1}{r^3}\right)}G, \tag{27.1}$$

where

$$G=[2l(l+1)/\pi Z^2\alpha^2]\sin\pi(\rho''-\rho') \tag{27.2}$$

is the relativity correction factor to the approximate form

$$\rho\cong -g\mu_0{}^2\overline{(r^{-3})}/(2l+1). \tag{27.3}$$

By Eq. (22) the factor $(-C'C''/C^2)$ in Eq. (27.1) is approximately $=1$. More accurately, we should apply it as a normalization correction. Its form shows that it is approximately equal to the geometric mean of the normalization corrections which must be applied to Eq. (25).

We need also the connection of $\overline{(1/r^3)}$ or C^2 with the magnitude of the doublet splitting for a single electron. According to Racah[3] this is given approximately by

$$\delta=(2l+1)HZ\mu_0{}^2\overline{(r^{-3})}, \tag{28}$$

where

$$H=2(\rho'-1-\rho'')l(l+1)/Z^2\alpha^2 \tag{28.1}$$

represents the relativity correction factor obtained formula. If by means of Sommerfeld's doublet the spin orbit interaction is represented by $\bar{a}(\mathbf{ls})$ then $\delta=(l+\frac{1}{2})\bar{a}$ so that

$$\bar{a}=2HZ\mu_0{}^2\overline{(r^{-3})}. \tag{28.2}$$

It should be noted that the use of Eqs. (28) implies, in addition to the simplifying assumptions made in discussing ρ, σ, also the supposition that the region responsible for the magnetic interaction is so close to the nucleus that the screening of the nucleus by closed shells may be neglected. The assumption is satisfied for heavy elements if l is not too great. Under all conditions, however, we expect that instead of Z one should use in (28.2) some number smaller than Z.

We have given the matrix elements ρ, σ only for $n=3$, i.e., for a nucleus forming a magnetic doublet. Eq. (23) enables one to compute these matrix elements by direct substitution for any n as long as the integrals converge. The two values of σ which correspond to $j=l+\frac{1}{2}$ and $j=l-\frac{1}{2}$

will be written a', a'' respectively, this notation being in agreement with Goudsmit's. We thus have

$$\frac{2g\mu_0^2 l(l+1)}{j(j+1)}\overline{\left(\frac{1}{r^3}\right)}F \leqq \begin{cases} a'(j=l+\frac{1}{2}), \\ a''(j=l-\frac{1}{2}, \end{cases} \tag{29.1}$$

$$-[g\mu_0^2\overline{(r^{-3})}/(2l+1)]G \leqq a''', \tag{29.2}$$

and these coefficients give matrix elements of single electron states for the vector **B** by means of Eqs. (12.2), (12.1), respectively; to obtain these matrix elements we substitute a' or a'' for σ and a''' for ρ.

3. Two Electron Configurations

According to the view of Section 1 we represent the wave functions of a two electron configuration as a linear antisymmetric combination of products of wave functions describing the two single electron states. If the two electrons are not equivalent, we need not consider the antisymmetric property of the wave functions. How this comes about for the magnetic interaction has been shown by Johnson[15] by means of quantized amplitudes.

According to Güttinger and Pauli[16] the matrix elements of (**BJ**) are given by

$$\begin{aligned} (j_1, j_2|\mathbf{BJ}|j_1 j_2) &= Q_{12}a_1 + Q_{21}a_2, \\ (j_1, j_2|\mathbf{BJ}|j_1-1, j_2) &= P_{12}a_{j_1, j_1-1}, \end{aligned} \tag{30}$$

where

$$Q_{12} = (1/2)[j(j+1)+j_1(j_1+1)-j_2(j_2+1)],$$

$$P_{12} = (1/2)[(j+j_1-j_2)(j-j_1+j_2+1) \times (j+j_1+j_2+1)(j_1+j_2-j)]^{\frac{1}{2}}.$$

Here a_1, a_2 are the constants of proportionality, denoted by σ in Eq. (12.2), which are supposed to be used for the calculation of the single electron operator **B**. The constant a_{j_1, j_1-1} is similarly the constant of proportionality ρ of Eq. (12.1). The discussion of Güttinger and Pauli does not determine the sign of the second Eq. (30). It may be shown [for example by the symbolic method[17]] that the signs of the eigenfunctions may be consistently chosen so that

$$a_{j_1, j_1-1} = a'''(n_1, l_1), \tag{31}$$

where a''' is given by (29.2). This applies not only to **B** but to any other vector. In particular

$$(j_1, j_2|\mathbf{JS}|j_1, j_2) = (g_{j_1}-1)Q_{12} + (g_{j_2}-1)Q_{21}, \tag{32.1}$$

$$(j_1, j_2|\mathbf{JS}|j_1-1, j_2) = S_{j_1, j_1-1}P_{12}, \tag{32.2}$$

$$(j_1, j_2|\mathbf{JS}|j_1, j_2-1) = S_{j_2, j_2-1}P_{21}, \tag{32.3}$$

where

$$g_{j_1} = 1 + \frac{j_1(j+1)+s_1(s_1+1)-l_1(l_1+1)}{2j_1(j_1+1)} \tag{32.4}$$

is the Landé g factor and $S_{j, j-1}$ is given by Eq. (19). By means of Eqs. (32) we can find simultaneously the secular equations for the coefficients of eigenfunctions and formulas for the hfs coupling constants A by means of Eq. (2). The care which must be exercised as to signs of the functions makes it dangerous to use the existing discussions of intermediate coupling without some additional considerations. We use these discussions to check our calculations.

Configurations p·p and p²

The $p \cdot p$ configuration will be taken as a good example of the general procedure. Since the electrons are not equivalent we need not consider the exclusion principle. We denote the states by such symbols as (3/2, 1/2) meaning that the first electron state is $np_{3/2}$ and the second is $mp_{1/2}$ where $n \neq m$. This symbol in this section stands not for a product of two single electron functions but for a combination of products. The two electrons are supposed to be in states having different principal quantum numbers and the order in which the values of j are put into the symbol (j_1, j_2) is always the same with respect to the two electrons. A resultant $j=3$ can be obtained in only one way *viz.*, by vector composition of 3/2 and 3/2. The

---

[15] M. H. Johnson, Jr., Phys. Rev. **43**, 627 (1933).

[16] Güttinger and Pauli, Zeits. f. Physik **37**, 743 (1931).

[17] H. A. Kramers, Proc. Amst. Academy **33**, 953 (1930); 965 (1931); H. C. Brinkman, Dissertation, Utrecht 1932; The operator which gives these matrix elements is $\left(\xi_2\frac{\partial}{\partial\xi_1}+\eta_2\frac{\partial}{\partial\eta_1}\right)\left(\frac{\partial^2}{\partial\xi_2\partial\eta_1}-\frac{\partial^2}{\partial\xi_1\partial\eta_2}\right)=\Omega$. In the notation of Kramers $\Omega(\alpha, \beta, \gamma)=\alpha\beta(\alpha+\beta+\gamma+1)(\alpha-1, \beta-1, \gamma+1)$ and $\int N(\alpha-1, \beta-1, \gamma+1)\cdot(\alpha-1, \beta-1, \gamma+1)^*\Omega N(\alpha, \beta, \gamma)\cdot(\alpha, \beta, \gamma)=[2l(2l+1)]^{\frac{1}{2}}[(l+s-j)(j+l+s+1)(j-l+s+1)(j+l-s)]^{\frac{1}{2}}$ where $N(\alpha, \beta, \gamma)$ is the normalization integral given in Brinkman's Appendix as Eq. (11).

eigenfunction is simply (3/2, 3/2) and we thus obtain $j(j+1)A=12A$ by substituting $j=3$, $j_1=j_2=3/2$ into Eq. (31). The coefficients a_1, a_2 are in this case a_1', a_2' since $j=l+1/2$ for both single electron states. Thus $A=(1/2)(a_1'+a_2')$.

The value $j=2$ can be obtained in three ways and the general eigenfunction can be written as

$$c_1(3/2, 3/2)+c_2(3/2, 1/2)+c_3(1/2, 3/2).$$

Hence we obtain $j(j+1)A=6A$ and find

$$A=\tfrac{1}{2}c_1^2(a_1'+a_2')+\tfrac{1}{4}c_2^2(3a_1'+a_2'')+\tfrac{1}{4}c_3^2(a_1''+3a_2')+c_1c_2a_2'''+c_1c_3a_1'''. \quad (33)$$

Here we must still determine c_1, c_2, c_3. It is convenient to work out the transformation from Russell-Saunders to jj coupling. This can be done easily by means of Eqs. (32.1) in which the same convention as to signs of eigenfunctions has been used as in Eqs. (30). Thus

$$\sum(\mathbf{JS})_{ik}c_k^\lambda=j(j+1)(g^\lambda-1)c_i^\lambda, \quad (34)$$

where g^λ is the g value of the particular state in Russell-Saunders coupling. The g values are easily computed, Table II. $(\mathbf{JS})_{ik}$ involves the

TABLE II. *g values.*

	(3/2, 3/2)	(3/2, 1/2)	(1/2, 3/2)
$^3D_2$	0	$2^{-\frac{1}{2}}$	$-2^{-\frac{1}{2}}$
$^3P_2$	$2/6^{\frac{1}{2}}$	$1/6^{\frac{1}{2}}$	$1/6^{\frac{1}{2}}$
$^1D_2$	$1/3^{\frac{1}{2}}$	$-1/3^{\frac{1}{2}}$	$-1/3^{\frac{1}{2}}$

same quantities Q_{12}, Q_{21}, P_{12} as were used in Eq. (33). The orthogonality serves as a check. We work out the matrix for the magnetic energy $\tilde{a}_1(\mathbf{l}_1\mathbf{s}_1)+\tilde{a}_2(\mathbf{l}_2\mathbf{s}_2)$ by the formula

$$(j_1', j_2'; j|\boldsymbol{l}_1\mathbf{s}_1|j_1'', j_2''; j)=\delta_{j_1'j_1''}\delta_{j_2'j_2''}(1/2)\times[j_1'(j_1'+1)-s_1'(s_1'+1)-l_1'(l_1'+1)] \quad (35)$$

and obtain thus only diagonal elements. In the present case they are $(1/2)(\tilde{a}_1+\tilde{a}_2)$ for (3/2, 3/2), $(1/2)\tilde{a}_1-\tilde{a}_2$ for (3/2, 1/2), $(1/2)\tilde{a}_2-\tilde{a}_1$ for (1/2, 3/2), $-\tilde{a}_1-\tilde{a}_2$ for (1/2, 1/2) and a simple calculation shows that the magnetic energy matrix is the same as that of Johnson.[18] Similarly for $j=1$ we have the transformation matrix given in Table III and if the function is

[18] M. H. Johnson, Jr., Phys. Rev. **38**, 1628 (1931).

$$c_1(3/2, 3/2)+c_2(3/2, 1/2)+c_3(1/2, 3/2)+c_4(1/2, 1/2)$$

then

$$A=\tfrac{1}{2}c_1^2(a_1'+a_2')+\tfrac{1}{4}c_2^2(5a_1'-a_2'')+\tfrac{1}{4}c_3^2(-a_1''+5a_2')+\tfrac{1}{2}c_4^2(a_1''+a_2'')+5^{\frac{1}{2}}c_1c_2a_1'''+5^{\frac{1}{2}}c_1c_3a_2'''+2^{\frac{1}{2}}c_2c_4a_1'''+2^{\frac{1}{2}}c_3c_4a_2'''. \quad (36)$$

From the results for two nonequivalent electrons we can obtain the formulas for two equivalent electrons without further calculation. We note that the only possible states for two equivalent p electrons are ^1S, ^3P, ^1D. Thus only $^3P_2$, $^1D_2$ of Table II survive because the functions (3/2, 3/2) and (3/2, 1/2)+(1/2, 3/2) are already antisymmetric. The function (3/2, 1/2)+(1/2, 3/2) must be multiplied by $1/2^{\frac{1}{2}}$ in order to make it noralized. Thus for equivalent p electrons the states with $j=2$ are represented by

$$c_1(3/2, 3/2)+2^{-\frac{1}{2}}c_2[(3/2, 1/2)+(1/2, 3/2)]$$

and A is obtained by substituting in Eq. (33) $2^{-\frac{1}{2}}c_2$ for both c_2 and c_3 and letting $a_1'=a_2'=a'$, $a_1''=a_2''=a''$. Thus

$$A=c_1^2a'+\tfrac{1}{4}c_2^2(3a'+a'')+2^{\frac{1}{2}}c_1c_2a'''. \quad (37)$$

For $j=1$ only the $^3P_1$ state survives. In this case (3/2, 1/2)−(1/2, 3/2) is antisymmetric while (3/2, 3/2) and (1/2, 1/2) are symmetric as is obvious from Table III. For this state A is obtained by setting $c_1=c_4=0$, $c_2=c_3=2^{-\frac{1}{2}}$ and thus $A=\frac{1}{4}(5a'-a'')$ in agreement with the formula for jj coupling as should be the case since there is only one state with $j=1$. Similarly the matrices for the electrostatic and magnetic energies for equivalent electrons can be obtained from the corresponding matrices for nonequivalent electrons. We see that by means of Eqs. (30), (32) the calculations can be made quite mechanically.

The same results can be obtained also by using antisymmetric eigenfunctions for definite j, m.

TABLE III. *Configuration pp.*

	(3/2, 3/2)	(3/2, 1/2)	(1/2, 3/2)	(1/2, 1/2)
$^3D_1$	$-2/3(6)^{\frac{1}{2}}$	$5^{\frac{1}{2}}/3(6)^{\frac{1}{2}}$	$5^{\frac{1}{2}}/3(6)^{\frac{1}{2}}$	$-2(10)^{\frac{1}{2}}/3(6)^{\frac{1}{2}}$
$^3P_1$	0	$1/2^{\frac{1}{2}}$	$-1/2^{\frac{1}{2}}$	0
$^1P_1$	$5^{\frac{1}{2}}/3$	$-1/3$	$-1/3$	$-2^{\frac{1}{2}}/3$
$^3S_1$	$2(5)^{\frac{1}{2}}/3(6)^{\frac{1}{2}}$	$4/3(6)^{\frac{1}{2}}$	$4/3(6)^{\frac{1}{2}}$	$2^{\frac{1}{2}}/3(6)^{\frac{1}{2}}$

One must then also work out the transformation from jj to Russell-Saunders coupling in order to be able to determine the coefficients c from the empirical energy values. We have used both methods and also checked the results against nonrelativistic formulas for A in Russell-Saunders coupling derived by a third method. These formulas are

$$\frac{j(j+1)A}{2g\mu_0^2}=\overline{(r_1^{-3})}\left\{\tfrac{1}{2}[l(l+1)+l_1(l_1+1)-l_2(l_2+1)]+\frac{3Q_2(l,s,j)}{2l(l+1)(2l-1)(2l+3)}\left[\tfrac{1}{2}l_2(l_2+1)-\tfrac{1}{2}l(l+1)\right.\right.$$
$$\left.-\frac{3Q_2(l_1l_2l)}{4(2l_1-1)(2l_1+3)}\right]+\frac{j(j+1)-l(l+1)-s(s+1)}{2l(l+1)}\left[\tfrac{1}{2}l_1(l_1+1)-\frac{3Q_2(l_1l_2l)}{4(2l_1-1)(2l_1+3)}\right]\Bigg\}$$
$$+\overline{(r_2^{-3})}\{\text{symmetric term}\},\quad (38)$$

where

$$Q_2(l,s,j)=[j(j+1)-l(l+1)-s(s+1)]^2+[j(j+1)-l(l+1)-s(s+1)]-4l(l+1)s(s+1)/3$$
$$j=l+1,\quad s=1,$$

$$\frac{j(j+1)A}{2g\mu_0^2}=\overline{\left(\frac{1}{r_1^3}\right)}\left[\alpha+\frac{\beta}{(l+1)(2l+3)}+\frac{\alpha+\beta}{l+1}\right]+\overline{\left(\frac{1}{r_2^3}\right)}[\text{symmetric term}],\quad (39.1)$$

where

$$\alpha=\tfrac{1}{2}[l(l+1)+l_1(l_1+1)-l_2(l_2+1)],$$
$$\beta=\tfrac{1}{2}[l_2(l_2+1)-l(l+1)]-\tfrac{3}{4}Q_2(l_1,l_2,l)/(2l_1-1)(2l_1+3),$$

$$\begin{cases} j=l,\quad s=1,\\ j(j+1)A=2g\mu_0^2\overline{(r_1^{-3})}\left[\alpha-\dfrac{\alpha+2\beta}{l(l+1)}\right]+2g\mu_0^2\overline{(r_2^{-3})}[\text{symmetric term}],\end{cases}\quad (39.2)$$

$$\begin{cases} j=l-1,\quad s=1,\\ j(j+1)A=2g\mu_0^2\overline{(r_1^{-3})}\left[\alpha+\dfrac{\beta}{l(2l-1)}-\dfrac{\alpha+\beta}{l}\right]+2g\mu_0^2\overline{(r_2^{-3})}\ [\text{symmetric term}],\end{cases}\quad (39.3)$$

$$\begin{cases} j=l,\quad s=0,\\ l(l+1)A=2g\mu_0^2\overline{(r_1^{-3})}\alpha+2g\mu_0^2\overline{(r_2^{-3})}[\text{symmetric term}].\end{cases}\quad (39.4)$$

We give the results for the simpler configurations.

Configurations *sp*, *sd*, *sf*

These have been already discussed by Racah.[4] Since the contributions due to p, d, f, $\cdots$ electrons are not taken into account relativistically in his work we treat this case again. The difference between his results and ours is important only for sp and perhaps sd because the coupling of f, g, $\cdots$ electrons to the nucleus is usually small. The triplet states with inner quantum numbers $l+1$, l, $l-1$ are denoted by ${}^3L_{l+1}$, ${}^3L_l$, ${}^3L_{l-1}$, respectively, and the singlet state is denoted by ${}^1L_l$. We use these symbols both in designating atomic states and as an abbreviation for the eigenfunctions. We represent the eigenfunction for a state with $j=l$ as

$$\psi=c_1(1/2,l+1/2)+c_2(1/2,l-1/2),\quad (j=l),$$

where (j_1,j_2) refers to the angular momenta of the s and l electrons, respectively. The states ${}^3L_l$, ${}^1L_l$ in Russell-Saunders coupling are special cases of the above state and correspond to certain values of c_1, c_2. As the coupling changes, the values of c_1, c_2 change also. The states obtained in this manner from ${}^3L_l$, ${}^1L_l$ will be denoted by ${}^3L_l'$, ${}^1L_l'$.

For either of these states

$$l(l+1)A=(1/2)[(l+1)c_2^2-lc_1^2]a(s)$$
$$+(1/2)l(2l+3)c_1^2a'+(1/2)(l+1)(2l-1)c_2^2a''$$
$$+2[l(l+1)]^{\frac{1}{2}}c_1c_2a''' \quad (j=l),$$

where a', a'', a''' are the coupling constants of the l electron. Also

$$A(^3L_{l+1})=\frac{a(s)}{2(l+1)}+\frac{2l+1}{2(l+1)}a';$$

$$A(^3L_{l-1})=-\frac{a(s)}{2l}+\frac{2l+1}{2l}a''.$$

The parameters c_1, c_2 can be represented in terms of a single parameter θ which increases from zero in Russell-Saunders to $\theta_0=\tan^{-1}(l/l+1)^{\frac{1}{2}}$ in jj coupling.

$$^1L_l' : c_1=\cos(\theta_0-\theta), \quad c_2=-\sin(\theta_0-\theta);$$

$$^3L_l' : c_1=\sin(\theta_0-\theta), \quad c_2=\cos(\theta_0-\theta).$$

The connection with the Landé g values is given by

$$l(l+1)[g(^1L_l')-1]=\sin^2\theta;$$

$$l(l+1)[g(^3L_l')-1]=\cos^2\theta.$$

The energy matrix with respect to states in Russel-Saunders coupling is given in Table IV. Here

TABLE IV. *Energy matrix in Russell-Saunders coupling.* $W_0=2G^1/3$.

	$^3L_{l+1}$	^1L_l	^3L_l	$^3L_{l-1}$
$^3L_{l+1}$	$\frac{1}{2}\bar{a}l$	0	0	0
^1L_l	0	W_0	$\frac{1}{2}\bar{a}[l(l+1)]^{\frac{1}{2}}$	0
^3L_l	0	$\frac{1}{2}\bar{a}[l(l+1)]^{\frac{1}{2}}$	$-\frac{1}{2}\bar{a}$	0
$^3L_{l-1}$	0	0	0	$-\frac{1}{2}(l+1)\bar{a}$

W_0 is expressed in terms of Slater's integral G^1 and is the energy difference between the singlet and triplet systems due to electrostatic forces. We denote the energy of a state with $j=l$ by W and let

$$2W/\bar{a}=w; \quad 2W_0/\bar{a}=w_0.$$

The secular equation is

$$w^2+(1-w_0)w-w_0-l(l+1)=0;$$

$$w(^3L_{l+1})=l; \quad w(^3L_{l-1})=-l-1.$$

Letting $w(^3L_l')=w_3$, $w(^1L_l')=w_1$ we have

$$\tan\theta=\frac{[l(l+1)]^{\frac{1}{2}}}{w_1+1}=\frac{w_1-w_0}{[l(l+1)]^{\frac{1}{2}}}$$
$$=-\frac{(1+w_3)}{[l(l+1)]^{\frac{1}{2}}}=\frac{[l(l+1)]^{\frac{1}{2}}}{w_0-w_3}$$

which may be used for the calculation of θ. For the discussion of experimental material, graphs are more convenient than equations. These are computed easily by means of

$$w_1=-1-l(l+1)/(w_3+1)$$

together with $w_0=1+w_1+w_3$ giving the usual relations between energy intervals in intermediate coupling. At the same time we easily get θ, the g values and the coefficients c_1, c_2. The sp configuration is the most important one of this kind and we give a short table (Table V) of the necessary values.

TABLE V. *Numerical values for sp configuration.*

w_3	w_1	w_0	$(g-1)(^3P_1)$	$(g-1)(^1P_1)$	$\cos(\theta_0-\theta)$	$\sin(\theta_0-\theta)$
−2	1	0	0.334	0.167	1	0
−1.80	1.50	0.70	.378	.121	0.995	0.101
−1.666	2	1.333	.409	.088	.984	.175
−1.50	3	2.50	.445	.056	.962	.272
−1.40	4	3.60	.462	.037	.943	.334
−1.25	7	6.75	.485	.015	.904	.427

For this case $\theta_0=35.3°$ and

$$A=\tfrac{1}{4}(2c_2^2-c_1^2)a(s)+5c_1^2a'/4+\tfrac{1}{2}c_2^2a''+2^{\frac{1}{2}}c_1c_2a'''.$$

The values of Table V are shown graphically in Fig. 1.

Configuration p^2

We denote again by ′ states in intermediate coupling. We obtain

$$A(^3P_1)=\tfrac{1}{4}(5a'-a''),$$

$$A(^1D_2')=c_1^2a'+\tfrac{1}{4}c_2^2(3a'+a'')-2^{\frac{1}{2}}c_1c_2a''',$$

$$A(^3P_2')=c_2^2a'+\tfrac{1}{4}c_1^2(3a'+a'')+2^{\frac{1}{2}}c_1c_2a''',$$

where in terms of antisymmetric wave functions denoted by [ ]

$$^1D_2'=c_1[3/2, 3/2]-c_2[3/2, 1/2);$$

$$^3P_2'=c_2[3/2, 3/2]+c_1[3/2, 1/2];$$

$$[3/2, 3/2]=(3/2, 3/2);$$

$$[3/2, 1/2]=2^{-\frac{1}{2}}[(3/2, 1/2)+(1/2, 3/2)],$$

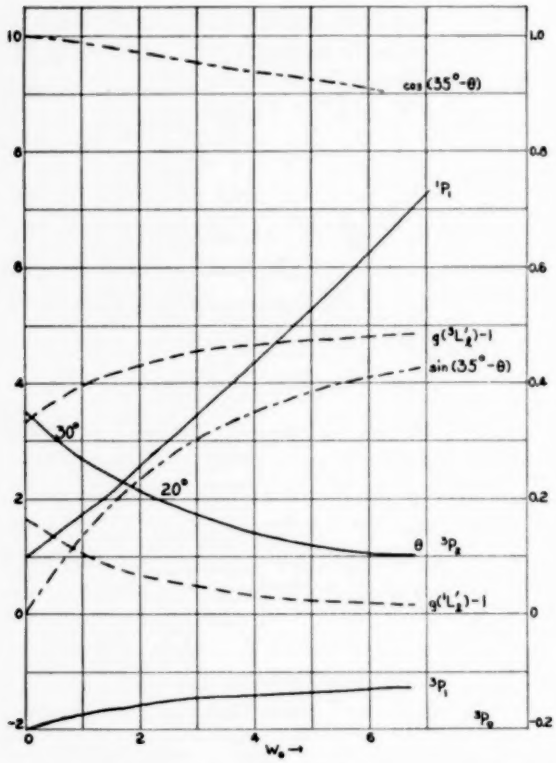

FIG. 1. Configuration sp in intermediate coupling. Extreme jj coupling is represented on the left and Russell-Saunders coupling on the right. The scale of ordinates for the broken curves is on the right; for the solid curves, with the exception of the angle θ, on the left. The scale for θ is inserted on the graph itself.

as has been shown in the explanation of the method of calculation.[19]

The numbers c_1, c_2 are obtainable from the empirical energies and g values of the configuration. The connection with the usual theory[20] of intermediate coupling is given by

$$c_1=\cos(\phi_0-\phi),\quad c_2=\sin(\phi_0-\phi),\quad \tan\phi_0=2^{\frac{1}{2}},\quad \phi_0=54.7^\circ,$$

where ϕ is connected with Landé g values by

$$g(^1D_2')=\tfrac{1}{4}(5-\cos 2\phi),\quad g(^3P_2')=\tfrac{1}{4}(5+\cos 2\phi),$$

and with the energy values through the secular equations

$$W(^3P_1)=0;\quad X=3F^2/25;$$

$$[W=W(^1S_0'),\ W(^3P_0')],\qquad W^2-5XW-5\tilde{a}X/2+9(\tilde{a}/2)^2=0;$$

$$[W=W(^1D_2'),\ W(^3P_2')],\qquad W^2-(3\tilde{a}/2+2X)W+2\tilde{a}X=0,$$

which give in terms of

$$w_1=2W(^1D_2')/\tilde{a},\ w_3=2W(^3P_2')/\tilde{a},\qquad w_2=2W(^1S_0')/\tilde{a};\ w_4=2W(^3P_0')/\tilde{a},$$

the angle ϕ by

$$\tan\phi=2^{\frac{1}{2}}/(w_1-2)=(w_1-2x-1)/2^{\frac{1}{2}}=2^{\frac{1}{2}}/(2x+1-w_3)=(2-w_3)/2^{\frac{1}{2}}$$

in terms of $x=2X/\tilde{a}$. The relations for intermediate coupling as well as ϕ are easily computed by varying w_3, w_4 in

$$w_1=(6-2w_3)/(2-w_3),\qquad x=\tfrac{1}{4}w_1w_3=(1/2)(w_1+w_3-3),$$

$$w_2=(9+w_4)(-1-w_4),\quad x=(w_2+w_4)/5.$$

Simultaneously one computes ϕ, the g values and, from ϕ, one obtains c_1, c_2. The angle $\phi=0$ for Russell-Saunders and $\phi=\phi_0$ for jj coupling. The results are shown in Fig. 2.

Configuration $p.p.$

This has been discussed in connection with Eqs. (34), (37). The determination of coupling parameters is more difficult in this case on account of the larger number of coupling parameters involved. Johnson[18] worked out the secular equations. (There are some misprints in these.) Using his notation we obtain from the empirical energies the quantities

$$X_1=\beta+\delta-(3/2)(\tilde{a}_1+\tilde{a}_2),$$

$$X_2=\beta\delta-\tfrac{1}{2}(\tilde{a}_1+\tilde{a}_2)(\beta+2\delta),$$

$$X_3=\alpha+\beta-(3/2)(\tilde{a}_1+\tilde{a}_2),$$

$$X_4=\beta-\gamma/2-3(\tilde{a}_1+\tilde{a}_2)$$

as sums and products of energies.

Eliminating α, β, γ one obtains

$$\delta^2-[19X_1/9-20(X_3+X_4)/27]\delta+(5/18)[4X_1-5(X_3+X_4)/3][X_1-(X_3+X_4)/3]+X_2/6=0.$$

[19] For $m=2$ these functions are
$[3/2,\ 3/2]=2^{-\frac{1}{2}}[(p_{3/2}{}^1)_{3/2}(p_{3/2}{}^2)_{1/2}-(p_{3/2}{}^2)_{3/2}(p_{3/2}{}^1)_{1/2}]$;
$[3/2,\ 1/2]=2^{-\frac{1}{2}}[(p_{3/2}{}^1)_{3/2}(p_{1/2}{}^2)_{1/2}-(p_{3/2}{}^2)_{3/2}(p_{1/2}{}^1)_{1/2}]$
where the superscripts refer to electrons and the subscripts inside parentheses to j and outside parentheses to m.

[20] S. Goudsmit, Phys. Rev. **35**, 1325 (1930).

Solving this for δ one obtains also α, β, γ, $\tilde{a}_1+\tilde{a}_2$. From the equations in W for $J=1$, 2, one also obtains $\tilde{a}_1-\tilde{a}_2$. From the energy matrices given in Johnson's paper[18] on p. 1636, one obtains the coefficients of the Russell-Saunders functions and, by means of Tables II, III given here, one converts these coefficients into our coefficients c. In the applications which we have tried, this way of determining the state of coupling led to poor results because we are interested in cases approximating jj coupling. It is probable that the smaller of the two $\tilde{a}$ and α, β, γ have different values in the lower and upper groups of levels. Under these conditions it is better to write out the energy matrices in terms of states in jj coupling[21] and if the energy difference between the $(1/2, j)$ $(3/2, j)$ groups of levels is great in comparison with other energy differences the matrix elements between these groups of levels may be neglected. We obtain then the following energy matrices as well as the energy matrix shown in Table VI.

TABLE VI. *Energy matrix for $j=2$.*

	$(3/2, 3/2)$	$(3/2, 1/2)$
$(3/2, 3/2)$	$(\alpha+2\beta)/3$	$(\beta-\alpha)/3$
$(3/2, 1/2)$	$(\beta-\alpha)/3$	$\alpha/3+\beta/6$ $-3\tilde{a}_2/2$

Upper group

$$j=3,\ W=0;\quad j=0,\ W=(\beta+2\delta)/3$$

Lower group

$$j=0,\ W=-(3/2)(\tilde{a}_1+\tilde{a}_2)+(1/3)(2\beta+\delta),$$

$$j=2,\ W=-3\tilde{a}_1/2+\alpha/3+\beta/6,$$

$$j=1,\ W((1/2, 3/2))=-3\tilde{a}_1/2-\gamma/3+\tfrac{1}{2}\beta;$$
$$W((1/2, 1/2))=-3(\tilde{a}_1+\tilde{a}_2)/2+\gamma/6.$$

It will be noted that for the lower group the energy matrix is diagonal. This shows that we may treat the states of the lower group as in jj coupling even if the two states in $j=1$ are close enough to expect a perturbation between them.

[21] G. H. Shortley, Proc. Am. Phys. Soc. Washington Meeting, April 28, 1933, treats in a similar way the p^5p configurations of the rare gases. The transformations from jj to Russell-Saunders coupling have been treated by Shortley similarly to the way done here in Phys. Rev. **43**, 451 (1933).

4. MANY ELECTRON CONFIGURATIONS

These are usually calculated expediently by using eigenfunctions for a given magnetic quantum number.

Configuration p^3

In Russell-Saunders coupling we have the ^4S, ^2P, ^2D terms. There are three terms with $j=3/2$ and one each with $j=1/2$, $5/2$. The terms with $j=3/2$ can be also obtained in three ways in jj coupling, *viz.*, as $(3/2, 3/2, 3/2)$, $(3/2, 3/2, 1/2)$, $(3/2, 1/2, 1/2)$ where each number gives a j for an individual electron state. In intermediate coupling the wave function is a linear combination of these three functions. In terms of their coefficients

$$A=(c_1^2+6c_2^2/5+c_3^2)a'-c_2^2a''/5$$
$$-4(2/5)^{\frac{1}{2}}c_2(c_1-c_3)a'''\quad (j=3/2).$$

Also, we add the previously derived results of Goudsmit

$$A=(4a'+a'')/5,\quad (j=5/2);\qquad A=a''(j=1/2).$$

We use the results of Inglis and of Inglis and Johnson[22] and obtain the following relations between c_1, c_2, c_3 and the energy w of the terms with $j=3/2$.

$$c_1=\frac{w+3}{3(2)^{\frac{1}{2}}\beta^2}[3\beta+2(w-2)]c_4,\quad c_2=(5^{\frac{1}{2}}/w)c_4,$$

$$c_3=\frac{w+3}{3(2)^{\frac{1}{2}}\beta^2}[3\beta-2(w-2)]c_4,$$

$$c_4=[1+(1+5\beta^2/4w^2)(3+w)^2\beta^{-2}]^{-\frac{1}{2}}$$

and

$$w=W/X,\quad \beta=\tilde{a}/X,\quad X=3F^2/25,\quad w(^3P_{1/2})=2,$$
$$w(^2D_{5/2})=0.$$

The parameter β is expressed in terms of w by $\beta^2=(4/9)w(w+3)(w-2)/(w+5/3)$. By means of this equation the graph for w against β is easily plotted. The energy reference point was chosen here so that for $^2P_{1/2}$, $^2D_{5/2}$, w has the values 2 and 0, respectively. One thus obtains X as $\frac{1}{2}[W(^3P_{1/2})-W(^2D_{5/2})]$. Knowing X one calculates w from the experimental W and sees at

[22] D. R. Inglis, Phys. Rev. **38**, 862 (1931); D. R. Inglis and M. H. Johnson, Phys. Rev. **38**, 1642 (1931).

what part of the graph the empirical values fit, as has been done by Inglis. If the agreement is satisfactory the point at which the fit is obtained determines β and hence $\bar{a}$.

Configuration p^2s

The functions in jj coupling are conveniently thought of as arising from the coupling of the states of p^2 with an s electron. The states of p^2 are given in Table VII. The coupling of the s electron to these states can be taken into account without paying attention to symmetry. The state $j=5/2$, $m=5/2$ can be obtained as

$$(5/2)_{5/2}=c_1 s_{1/2}\phi_2{}^2+c_2 s_{1/2}\psi_2{}^2.$$

Hence, by Eq. (3′)

$$A(5/2)=(4c_1{}^2+3c_2{}^2)a'/5+c_2{}^2a''/5 +4(2)^{\frac{1}{2}}c_1c_2a'''/5+a(s)/5.$$

The state $j=3/2$, $m=3/2$ may be obtained in three ways in jj coupling. The resultant states are

$$\mathrm{I}=5^{-\frac{1}{2}}(2s_{-\frac{1}{2}}\psi_2{}^2-s_{\frac{1}{2}}\psi_1{}^2);\quad \mathrm{II}=5^{-\frac{1}{2}}(2s_{-\frac{1}{2}}\phi_2{}^2-s_{\frac{1}{2}}\phi_1{}^2);\quad \mathrm{III}=s_{\frac{1}{2}}\psi_1{}^1,$$

and hence for

$$\psi=c_1\mathrm{II}+c_2\mathrm{I}+c_3\mathrm{III},$$

$$A=\{(6/5)c_1{}^2+(9/10)c_2{}^2+(5/6)c_3{}^2+c_2c_3/(15)^{\frac{1}{2}}\}a' +\{(3/10)c_2{}^2-(1/6)c_3{}^2-c_2c_3/(15)^{\frac{1}{2}}\}a''' +\{(6/5)c_1c_2+2/(15)^{\frac{1}{2}}c_1c_3\}(2)^{\frac{1}{2}}a +\{-(1/5)c_1{}^2-(1/5)c_2{}^2+(1/3)c_3{}^2\}a(s).$$

The state $j=1/2$, $m=1/2$ can be obtained in three ways and in intermediate coupling may be represented by

$$\psi=c_1\mathrm{IV}+c_2s_{\frac{1}{2}}\phi_0{}^0+c_3s_{\frac{1}{2}}\psi_0{}^0;\quad \mathrm{IV}=3^{-\frac{1}{2}}(2^{\frac{1}{2}}s_{-\frac{1}{2}}\psi_1{}^1-s_{\frac{1}{2}}\psi_0{}^1).$$

We find

$$A(1/2)=(5/3)c_1{}^2a'-\tfrac{1}{3}c_1{}^2a''+[-4(2/3)^{\frac{1}{2}}c_1c_2 +8(1/3)^{\frac{1}{2}}c_1c_3]a'''+(-c_1{}^2/3+c_2{}^2+c_3{}^2)a(s).$$

Table VII. *States of p^2.*

$(j_1, j_2)=$	(1/2, 1/2)	(3/2, 1/2)		(3/2, 3/2)	
Resultant $j=$	0	1	2	0	2
Symbol	ψ^0	ψ^1	ψ^2	ϕ_0	ϕ_2

We obtain the following connections with the functions in Russell-Saunders coupling used by Johnson.[23] The coefficients c in intermediate coupling can be obtained by using the matrices given on p. 207 in Johnson's paper to obtain the coefficients of the Russell-Saunders functions and by using the transformation matrices to jj coupling shown in Table VIII. If the coupling is nearly jj it is advisable to have the energy matrices referred to the jj functions. These may be worked out by using Table VIII. We refer the energies to the midpoint between $^4P_{5/2}$ and $^2D_{5/2}$ and obtain for the energy matrix the results shown in Table IX. Here $X=3F^2/25$ as in p^3 and G^1 is Slater's integral already used in sp. This case is somewhat too complicated for ex-

Table VIII.

	$s_{1/2}\phi_2{}^2$	$s_{1/2}\psi_2{}^2$	
$(^4P_{5/2})_{5/2}$	$2^{\frac{1}{2}}$	1	$3^{-\frac{1}{2}}$
$(^2D_{5/2})_{5/2}$	-1	$2^{\frac{1}{2}}$	

	II	I	III
$(^2D_{3/2})_{3/2}$	$(1/3)^{\frac{1}{2}}$	$-(2/3)^{\frac{1}{2}}$	0
$(^4P_{3/2})_{3/2}$	$1/3$	$1/3(2)^{\frac{1}{2}}$	$(5/6)^{\frac{1}{2}}$
$(^2P_{3/2})_{3/2}$	$5^{\frac{1}{2}}/3$	$(5/2)^{\frac{1}{2}}/3$	$-1/(6)^{\frac{1}{2}}$

	IV	$(s_{1/2}\phi_0{}^0)$	$(s_{1/2}\psi_0{}^0)$
$^4P_{1/2}$	$(3^{\frac{1}{2}}$	$-2^{\frac{1}{2}}$	$2)\times 3^{-1}$
$^2P_{1/2}$	$(6^{\frac{1}{2}}$	1	$-2^{\frac{1}{2}})\times 3^{-1}$
$^2S_{1/2}$	$(0$	$2^{\frac{1}{2}}$	$1)\times 3^{-\frac{1}{2}}$

Table IX. *Energy matrices.*

$j=5/2$

	$s_{\frac{1}{2}}\phi_2{}^2$	$s_{\frac{1}{2}}\psi_2{}^2$
$s_{\frac{1}{2}}\phi_2{}^2$	$3a/4-X/3-G^1/18$	$-2/3(2)^{\frac{1}{2}}(X+G^1/6)$
$s_{\frac{1}{2}}\psi_2{}^2$	$-(2/3)(2)^{\frac{1}{2}}(X+G^1/6)$	$-3a/4+X/3+G^1/18$

$j=3/2$

	II	I	III
II	$3a/4-X/3+G^1/2$	$-(4X-G^1)/3(2)^{\frac{1}{2}}$	$-(1/3)(5/6)^{\frac{1}{2}}G^1$
I	$-(4X-G^1)/3(2)^{\frac{1}{2}}$	$-3a/4+X/3+G^1/3$	$-(1/6)(5/3)^{\frac{1}{2}}G^1$
III	$-(1/3)(5/6)^{\frac{1}{2}}G^1$	$-(1/6)(5/3)^{\frac{1}{2}}G^1$	$-3a/4-X$

$j=1/2$

	IV	$s_{\frac{1}{2}}\phi_0{}^0$	$s_{\frac{1}{2}}\psi_0{}^0$
IV	$-3a/4-X+G^1/2$	$(6)^{\frac{1}{2}}G^1/9$	$-2(3)^{\frac{1}{2}}G^1/9$
$s_{\frac{1}{2}}\phi_0{}^0$	$6^{\frac{1}{2}}G^1/9$	$3a/4+X/3+G^1/6$	$5(2)^{\frac{1}{2}}X/3$
$s_{\frac{1}{2}}\psi_0{}^0$	$-2(3)^{\frac{1}{2}}G^1/9$	$5(2)^{\frac{1}{2}}X/3$	$-9a/4+2X/3+G^1/6$

[23] M. H. Johnson, Jr., Phys. Rev. **39**, 197 (1932). The functions used in this paper refer to states of lowest m while ours refer to highest m. We have adjusted the signs of our functions so as to give the same magnetic interaction energy matrices as Johnson's.

plicit formulas for the determination of the c's. They are obtained more easily from the above matrices by successive approximations to the secular equations.

5. Applications

$(6p)^2$ of Pb I

The experimental positions of the terms give for the energies referred to the $^3P_1$ level $W(^3P_2) = W_3 = 2830$ cm^{-1}, $W(^1D_2) = W_2 = 13{,}600$ cm^{-1}. Hence $w_3/w_1 = W_3/W_1 = 0.208$. Also $W(^3P_0) = -7820$, $W(^1S_0) = 21{,}640$ and $w_2/w_4 = -2.77$. According to Fig. 2 these values correspond to $0.60 < x < 0.80$, corresponding to $43° > \phi > 39°$. From sum relations and the experimental hfs material it appears probable that $a'' = 0.372$, $a' = 0.012$. The value of a''' may be obtained approximately from a' [see Eqs. (29.1), (29.2)] using the theoretical result that $a''' = [-j(j+1)/2(2l+1)l(l+1)]a' = -5a'/16$. This neglects the difference in the relativity as well as the normalization corrections to a' and a'''. The ratio of the relativity corrections to a' and a''' is very nearly 1 and the normalization correction can be estimated as the square root of that for a'' as compared with a' or ~ 1.7. In this case it does not matter much whether we use this correction to a''' or not. In Table X we use the data of

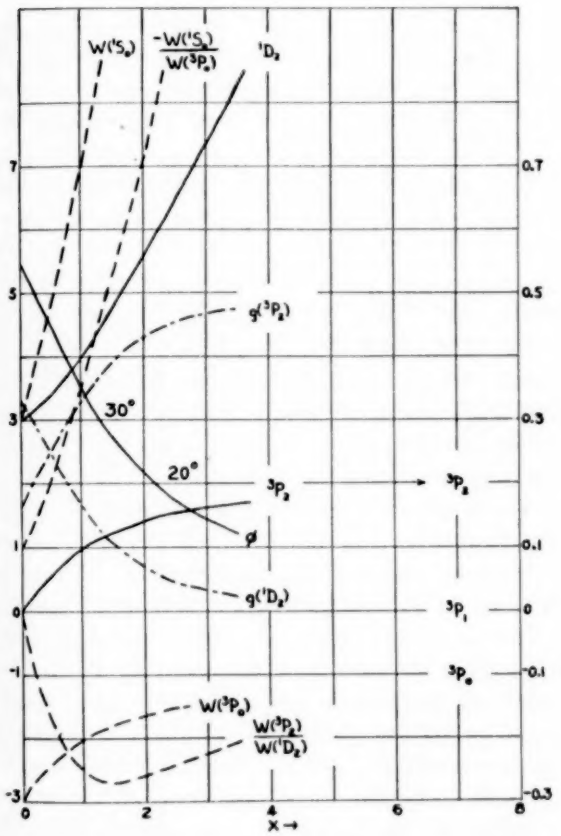

FIG. 2. Configuration p^2 in intermediate coupling. The scale of ordinates is the same as in Fig. 1.

$x = 2X/\tilde{a} = 0.68$ and 0.78, respectively. The empirical g values give $x \cong 0.60$. One can also get x as $3(w_2+w_4)/[5(w_1+w_3)-2(w_2+w_4)] = 0.76$. The state of coupling is thus not determinable with complete certainty and we may determine the parameter x only within certain limits, say

TABLE X. *Constants for* $(6p)^2$ *of Pb I.*

x	ϕ	c_1	c_2	$A(^1D_2)$	$A(^3P_2)$
0.60	43.0	0.979	0.203	0.0167	0.097
0.80	39.0	0.963	0.271	0.0200	0.094
			Observed:	0.026	0.088
			Pure *jj*	0.012	

Kopfermann[24] for $^3P_1$, $^3P_2$ and that of Schüler and Jones[25] for $^1D_2$. The theoretical values are close to the experimental values and the change in the theoretical values in the range of ϕ from 39° to 43° is 0.003 cm^{-1} while the difference between the theoretical and experimental values is 0.006 cm^{-1} for $\phi = 39°$. The fact that these differences are of the same order of magnitude indicates that they may be due to imperfections in the theory of intermediate coupling. This point will be discussed more fully later. The data of Rose and Granath[26] combined with that of Schüler and Jones[25] do not agree as well with the theory. We obtain, using these, $a'' = 0.381$ and $a' = 0.0096$ and for $\phi = 43°$ the formulas give $A(^1D_2) = 0.014$, $A(^3P_2) = 0.098$, while for $\phi = 39°$, $A(^1D_2) = 0.017$, $A(^3P_2) = 0.095$ against the experimental values $A(^1D_2) = 0.026$, $A(^3P_2) = 0.086$. Neither the ratio a''/a' nor the comparison of sum relations with the state of intermediate coupling is as good. The main difference between the observations of Rose and Granath and of Kopfermann is in the value of

[24] Kopfermann, Zeits. f. Physik **75**, 363 (1932).

[25] Schüler and Jones, Zeits. f. Physik **75**, 563 (1932).

[26] J. L. Rose and L. P. Granath, Phys. Rev. **40**, 760 (1932).

$A(^3P_1)$ which has, according to them, the values -0.083 and -0.078, respectively.

$(6p)^3$ of Bi I

The energies referred to $^2D_{5/2}$ and expressed in cm^{-1} are, for this configuration, $-15{,}437$, -4019, $0, 6223, 17{,}728$ for $^4S_{3/2}$, $^2D_{3/2}$, $^2D_{5/2}$, $^2P_{1/2}$, $^2P_{3/2}$ since $w=W/X$ is theoretically 2 for $^2P_{1/2}$ the values of w are empirically -4.97, -1.29, 0, 2, 5.70 and $X=3111$. From a graph such as that given by Inglis,[22] one finds that the values of w for $^4S_{3/2}$, $^2D_{3/2}$, $^2P_{3/2}$ correspond respectively to different values of $\beta(=\bar{a}/X)$ which are approximately 3.05, 2.95, 3.30 and we may take $\beta=3.10$ as a reasonable average. The approximate values of w which correspond to the levels with $j=3/2$ are then -5.05, -1.33, 5.40 and we compute from these the constants c_1, c_2, c_3 by the formulas already given (Table XI). From the sum relations

TABLE XI. *Constants for $(6p)^3$ of Bi I.*

	c_1	c_2	c_3
$^4S_{3/2}$	-0.188	$+0.345$	$+0.918$
$^2D_{3/2}$	$+0.0592$	-0.929	$+0.364$
$^2P_{3/2}$	$+0.980$	$+0.122$	$+0.152$

applied to $^2D_{5/2}$, $^2P_{1/2}$, Goudsmit[1] derived the values $a''=0.375$, $a'=0.007\pm0.003$. Hence we estimate $a'''=-0.00219=-0.0022$. Substituting into the formula derived for p^3, we obtain for the interval factor A of $^4S_{3/2}$, $^2D_{3/2}$, $^2P_{3/2}$ the values -0.0039, -0.055, $+0.0065$, respectively.

These results are affected by the contribution due to a''' and it appears that the uncertainty in a''' is of the same order as the uncertainty in the experimental values. Thus, according to Zeeman, Back and Goudsmit,[27] the total splitting of $^4S_{3/2}$ is -0.08 cm^{-1} which corresponds to $A=-0.0054$, while the tables of Bacher and Goudsmit[28] commit themselves only to the extent of giving $\Delta\nu=-0.1$ or $A=-0.0067$. The value of a''' is uncertain on account of the inaccuracy in a'. A different estimate can be made from the more accurately known a'' as $-0.375/(2\times16)$ where 2 takes care of the relativity correction. This value is -0.011 and is much larger than that obtained from a'. The discrepancy may be due to the inaccuracy of a' or else to the normalization correction. The normalization correction necessary to reconcile Goudsmit's values of a'' and a' is 5.7 which is unreasonably large. Nevertheless we correct $a'''=-0.0022$ by $(5.7)^4$ which gives $A(^4S_{3/2})=-0.009$. This is larger in absolute value than the possible empirical values, while without the normalization correction the theoretical value was smaller in absolute value than the experimental results. We thus see that the uncertainty in a' is quite sufficient to explain the lack of agreement between theory and experiment on account of the uncertainty which is caused in a'''. Besides a' affects $A(^4S_{3/2})$ directly and an increase in a' causes a decrease in the absolute value of $A(^4S_{3/2})$. The approximate experimental value of $A(^4S_{3/2})$ thus indicates that a' is larger than 0.007.

The theoretical value $A(^2D_{3/2})=-0.055$ is in approximate agreement with the experimental values -0.038, -0.039, -0.043 which correspond to the $f=3\to f=4$, $f=4\to f=5$, $f=5\to f=6$ intervals. The value -0.043 is presumably the better value since it is obtained from the larger interval in which the proximity effect of neighboring lines is least. An increase of a' from 0.007 to 0.018 $(=0.375/5\times2\times2)$ is just about sufficient to bring about agreement between the theoretical and experimental values.

We thus see that the hyperfine structure of the $j=3/2$ terms of the $(6p)^3$ configuration of Bi is in fair agreement with the theoretically expected interval factors. The disagreement of the values $a''=0.375$, $a'=0.007\pm0.003$ derived by Goudsmit from the $j=1/2$, $5/2$ terms may be due to experimental inaccuracies because a' is obtained from $j=5/2$ for which $A=(4a'+a'')/5$ and thus the approximately equal numbers A and $a''/5$ are subtracted from each other to obtain a'. In addition to the possible experimental errors it should be remembered that perturbations with other configurations may, in effect, change a' and a''. Thus, if a'' for $^2D_{5/2}$ is smaller than for $^2P_{3/2}$ on account of such perturbations, a' may very well be larger than 0.007. In order to discuss this more fully one will need a more complete theory of perturbations by other configurations. In addition, it must be remembered that the empirical positions of the energy levels are only in approx-

[27] P. Zeeman, E. Back and S. Goudsmit, Zeits. f. Physik **66**, 1 (1930).

[28] Bacher and Goudsmit, *Atomic Energy States*, McGraw Hill (1932).

imate agreement with the theory of intermediate coupling. This indicates directly the presence of other perturbing configurations and makes one expect a certain amount of disagreement between the theoretical and experimental values.

$6p^2\ 7s$ of Bi I

The experimental values are due to Fisher and Goudsmit and they also discussed their results theoretically.[29] They treat the levels $1_{1/2}$, $5_{1/2}$, $7_{5/2}$ by formulas derived for jj coupling. The levels $8_{3/2}$, $4_{3/2}$ are left unused. By means of the energy matrices we have given above for this configuration, it is possible to work out the state of coupling more accurately. It is difficult to use the configuration itself to determine the parameters $\bar{a}$, X, G^1. From $6p\ 7s$ of Bi II we obtain $G^1=2.6\times10^3$ and also from $6p\ 7s$ of Pb I $G^1=2.6\times10^3$. From $6p\ 7s$ itself and this G^1 we estimate approximate values $\bar{a}=1.1\times10^4$, $X=3.0\times10^3$, $G^1=2.4\times10^3$. These values do not pretend to be accurate. Only the order of magnitude is of interest in this case. (See Table XII.) The level $1_{1/2}$ is not very closely in jj coupling. This happens

TABLE XII. *Constants for $6p^27s$ of Bi I.*

Term symbol	W*	(c_1, c_2, c_3)	hfs A	Obs. A
$8_{3/2}$	$-\frac{3}{4}\bar{a}+\frac{1}{3}X+\frac{1}{3}G^1$	(.15, .98(5), −.11)	$.87a'+.32a''+$ $.24a'''-.194a(s)$	.094
$4_{3/2}$	$-\frac{3}{4}\bar{a}-X$	(.037, .11, .995)	$.85a'-.157a''+$ $.034a'''+.328a(s)$	0
$5_{1/2}$	$-\frac{3}{4}\bar{a}-X+\frac{1}{2}G^1$	(1, −.03, −.07)	$(5/3)a'-\frac{1}{3}a''-\frac{1}{3}a(s)$ $-.23a'''$	−.142
$1_{1/2}$	$-(9/4)\bar{a}+\frac{2}{3}X+G^1/6$	(.07, −.27, .98)	$a(s)$	.166
$7_{5/2}$	$-\frac{3}{4}\bar{a}+\frac{1}{3}X+G^1/18$	(.22, .98)	$.61a'+.192a''+$ $.24a'''+(1/5)a(s)$	.127

* Diagonal matrix element of energy for nearest state in jj coupling.

not to make much difference because c_1 is small and a'' occurs in the theoretical formula multiplied by $-c_1^2/3$ and a', a''' also occur multiplied by the small c_1. Thus $a(s)$ may be taken to be 0.166. Using the levels $5_{1/2}$, $7_{5/2}$ and supposing that $a'''=-5a'/16$ we obtain $a''=0.409=0.41$, $a'=0.028$ which is in approximate agreement with the values of Fisher and Goudsmit, 0.39, 0.026. Using these values we substitute into the formulas for $8_{3/2}$, $4_{3/2}$ and obtain 0.12(1), 0.01. These values are in approximate agreement with experiment.

$6p\ 7p$ of Bi II

This configuration has also been discussed by Fisher and Goudsmit.[29] The upper group of levels is perturbed by $6p8p$. For the lower group we saw that the perturbation between the two levels with $j=1$ is very small even though the levels may be close together. For this reason we may use formulas for jj coupling, as has been done, apparently without justification by Fisher and Goudsmit. The values obtained by them are $a''(6p)=0.464$, $a'(7p)=0.012$. Here a'' compares well with other values but $a'(7p)$ seems relatively large. This may be due to perturbations by the $j=2$ levels of the upper group which is in turn perturbed by $6p\ 8p$.

$6p\ 7s$ of Pb I and of Bi II

The parameter $w_0=2W_0/\bar{a}$ may be estimated for Pb I from the value of $w_1-1=3[W(^1P_1)-W(^3P_2)]/[W(^3P_2)-W(^3P_0)]=0.284$. According to Fig. 1 this corresponds to $w_0\leqq0.4$ or $\theta=33°$. From the Landé g value $g(^1P_1)=1.131$ we obtain $w_0=.5$, $\theta=31°$ and from $g(^3P_1)=1.349$ $w_0=0.25$, $\theta=33°$. The value of $\bar{a}$ which follows from $W(^3P_2)-W(^3P_0)$ is 8.8×10^3 and the value of G^1 which corresponds to this $\bar{a}$ and $w_0=0.40$ is 2.6×10^3. The values of c_1, c_2 are for $^1P_1$ $(c_1, c_2)=(0.998, -0.060)$ and for $^3P_1$, $(c_1, c_2)=(0.060, 0.998)$. From the sum of $A(^1P_1)$ and

[29] R. A. Fisher and S. Goudsmit, Phys. Rev. **37**, 1057 (1931).

$A(^3P_1)$ we obtain $a(7s)=0.220$ using $a''=0.372$ $a'=0.012$ and $A(^1P_1)=-0.040$, $A(^3P_1)=0.296$. With these values of the coupling constants we find that the coupling is sufficiently close to jj to make the difference between this and the actual condition negligible and the data are in perfect agreement with jj coupling.

For Bi II we similarly obtain $w_0\sim 0.25$ and this is even a more extreme case of jj coupling than that of Pb I. The results of Goudsmit and Fisher can thus be used with complete accuracy in this case so far as corrections for intermediate coupling are concerned. Their values are $a'=0.028$, $a''=0.430$, $a(7s)=0.352$ and the position of the levels gives $\tilde{a}=1.31\times 10^4$, $G^1=(3/4)w_0\tilde{a}=2.5\times 10^3$.

Hg^{199} I $6s\ 6p$

This configuration is more closely in Russell-Saunders coupling than those just discussed. The ratio $[W(^1P_1)-W(^3P_2)]/[W(^3P_2)-W(^3P_0)]$ gives $w_0\cong 5.4$ while $[W(^3P_1)-W(^3P_0)]/[W(^3P_2)-W(^3P_0)]$ gives $w_0>10$. The ordinary intermediate coupling theory thus applies only poorly. The discrepancy between the values of w_0 may be qualitatively described by saying that the interval rule in the ^3P is obeyed better than one would expect from the proximity of ^1P. We do not expect therefore to be able to obtain exact results. Approximately, using $w_0=5.38$ and the separation between $^3P_2$ and $^3P_0$ the intermediate coupling theory parameters are $\tilde{a}=4.26\times 10^3$, $G^1=1.72\times 10^4$. An approximate estimate of $a(6s)$, a'', a' may be made by using sum relations only. The overall hfs splittings of $^3P_2$, $^3P_1$, $^1P_1$ are 0.758, 0.727, -0.181 and the corresponding values of A are 0.303, 0.485, -0.121. From the sum relations we obtain $a''+a'=0.122$ and, supposing that $a'=a''/15$, the approximate value $a''=0.114$ follows. This value may be compared with a more exact estimate by means of formulas for hfs in intermediate coupling. This gives us in addition to the sum relations an additional condition

$$A(^3P_1)-A(^1P_1)=[(3/4)a(s)-(5/4)a'+(1/2)a'']\cos 2(\theta_0-\theta)+2^{\frac{1}{2}}a'''\sin 2(\theta_0-\theta)$$

and $w_0=5.38$ corresponds to $\theta=11.5°$. Supposing that the approximate theoretical relation $a'''\cong 5a'/16$ is satisfied, we obtain $a'=0.016$, $a''=0.10(6)$, $a(6s)=1.16(5)$, which is in fair agreement with our first estimate. We do not examine the data for Hg^{201} separately since this obviously will give no new result.

6. Conclusions

It is seen from the above comparison between theory and experiment that the predictions of the theory of hfs for intermediate coupling are in approximate agreement with the observed patterns. The agreement is best when the electronic configuration approaches pure jj coupling. For coupling conditions intermediate between this and that of Russell-Saunders, neither the theoretical predictions for the positions of electronic energy levels and Landé g values, nor the theoretical predictions for the interval factors of hfs are accurately verified by experiment. Thus for the $6p\ 7s$ configurations of Pb I and Bi II the coupling is very nearly pure jj and the values of $a(7s)$, $a''(6p)$, $a'(6p)$ derived from sum relations of $6p^2$ Pb I fit perfectly the observed splittings of $^3P_1$, $^1P_1$ while in $6s\ 6p$ of Hg I $(6p)^3$ of Bi I, $(6p)^2$ of Pb I, the agreement is only approximate. Also, in the case of $(6p)^2$ of Pb I different ways of determining the state of coupling lead to different results and the uncertainty introduced by this is of the right order of magnitude to account for the differences between theory and experiment. The same is true qualitatively for the other intermediate coupling configurations. On the other hand, in nearly pure jj coupling, the exact state of coupling is immaterial for the comparison between the observed splittings for levels of the same j and the theoretical expressions using a', a'' as derived from sum relations. This is due to the fact that close to jj coupling, the difference between A for the actual condition and for the pure jj condition is represented by terms involving squares of small quantities multiplied by a'', a' and first order small quantities multiplied by a'''. The small numerical value of a''' makes the formulas insensitive to deviations from the pure jj condition and we have thus no decisive evidence that the theory is better when the condition of pure jj coupling is approached. It is simply more difficult to test the theory for internal consistency under these coupling conditions.

On the other hand, we regard it as significant that when the values of a'', a' are tested against experimental data in more detail than the sum

relations permit, disagreements between theory and experiment are found and that these disagreements are connected with imperfections in the theory of intermediate coupling. This fact indicates the necessity of caution in the description of an electronic state by means of wave functions of a single electronic configuration and suggests that in all cases the values of a', a'' may be wrong. This applies, particularly, to the smaller numbers a'.

We have explained above the apparent agreement of theory and experiment in jj coupling by the lack of sensitivity of our formulas to deviations from theory and at the same time we have pointed to evidence of the importance of possible perturbations by other electronic configurations. Now, in general, a perturbation will make our formulas inapplicable and we must conclude that whatever perturbations exist in $6p\,7s$ of Pb I, Bi II they are of such a nature as to leave our equations formally correct. There is an obvious reason for such a formal correctness of the equations. The usual theory of intermediate coupling presupposes that the electronic states of all terms of a given configuration (say $6s\,7p$) can be represented sufficiently well by antisymmetric combinations of products of the $6s$ and $7p$ functions in some suitable central field. The radial parts of both the $6s$ and the $7p$ functions are supposed to be strictly the same for all the four terms of this configuration. A more exact type of consideration is that of Fock.[30] According to this, one looks for solutions of the variational problem by means of trial wave functions having the correct rotational and exchange symmetry types but having arbitrary radial factors for the $6s$, $7p$ wave functions. For the present purpose one must make a slight extension of Fock's scheme by allowing all linear combinations, rather than those belonging definitely to the singlet or triplet systems. Let us suppose, then, for simplicity, that the central field due to the inner closed shells is approximately the same for all four terms. Even so, the self-consistent fields for $6s$ and $7p$ will be different for $^1P_1$, $^3P_0$, $^3P_1$, $^3P_2$ and it is thus clear that with this refinement of the intermediate coupling theory we will obtain also a variation in the hfs coupling "constants" $a(s)$, a'', a', a''' from term to term in the same configuration. Another way of discussing the same solution is to keep the central field for each electron fixed and to allow, then, linear combinations of all antisymmetric products between functions of the type ns, mp. Perturbations between the states $nsmp$ and $6s\,7p$ are then taken into account. We expect that the perturbations which take place between all the successions of $^1P_1$, $^3P_2$ are of the same order, because close to jj coupling, the distance between $^1P_1$, $^3P_2$ is small compared to the distance apart of such successive pairs of levels; similarly for $^3P_0$ and $^3P_1$. There is, on the other hand, no general reason why the perturbations of the $^1P_1$ and $^3P_2$ should be equal to those of $^3P_0$ and $^3P_1$. Thus, for the upper group $[^1P_1, {}^3P_2]$ we may expect one set of coupling constants $a(s)$, a' and for the lower, another set $a(s)$, a''. The empirical comparison in jj coupling is made by using

$$A(^1P_1) = (1/4)a(s) + (5/4)a',$$
$$A(^3P_1) = (1/2)a(s) + (1/2)a'',$$
$$A(^3P_2) = (1/4)a(s) + (3/4)a'.$$

The equations for $^1P_1$, $^3P_2$ just suffice for the determination of $a(s)$, a'. Using the $a(s)$ so found in the equation for $^3P_1$, one determines a''. By this procedure one thus does not even determine a'' correctly for $^3P_1$ because one supposes that $a(s)$ did not change from the upper to the lower group and the ratio of a''/a' does not necessarily have its theoretical value for a single electron in a fixed central field of force. The check between theory and experiment is made for Pb I by comparison with $6p^2$ and for this the agreement between $^1D_2$ and $^3P_2$ was not nearly as good as the one for $6p\,7s$. For $6p\,7s$ of Bi II we can make approximate comparisons with $6p^3$, $6p^2\,7s$ of Bi I, $6p\,7p$, $6p\,6d$ of Bi II. But in no case do we have exact agreement nor evidence of the exact validity of the formulas in jj coupling.

On account of the expected variation of the constants a', a'' within a configuration, we expect the values of a' to be quite inaccurate because a small fractional change in a'' may be responsible for an apparent change in a', as well as on account of the sensitivity of a' to experimental errors. We thus regard the conclusions from sum relations about the ratio a''/a' as questionable and we saw in the case of $6p^3$ of Bi I that there is some evi-

[30] V. Fock, Zeits. f. Physik **81**, 195 (1933); **61**, 126 (1930).

dence in the splitting of $^4S_{3/2}$ for $a'>0.007$. The objections to the little magnet theory of the nucleus on the score of a''/a' being too large are thus not very strong. The only clear case seems to be that of $6p$ of Tl I and here the analysis of the experimental pattern into lines is complicated by the presence of the two isotopes. Just as from $6p^3$ of Bi I, sum relations give an anomalously high value of a''/a', the $^2D_{5/2}$, $^2P_{1/2}$ terms of Sb^{121} I give $a''=0.158$, $a'=0.035$ which corresponds to $a''/a'=4.5$ and is too low in comparison with the theoretical $5\times1.24=6.2$. The agreement between theory and experiment for the relative positions of the levels for this configuration is not very good and we are tempted to ascribe it to the same cause as the discrepancy between the theoretical and experimental values of a''/a'.

TABLE XIII. *Typical results for p electrons.*

		$\bar{a}$	a''	g
Tl	$7p$	3.79×10^3	0.375	2.8
	I $6p$	5.25×10^3	.73	3.9 2.9*
Bi	I $6p^3$	9.6×10^3	.375	1.2
	II $6p\,7s$	1.31×10^4	.430	1.0
Pb^{207}	I $6p^2$	7.4×10^3	.372	1.5
	I $6p\,7s$	8.8×10^3	.372	1.2(5)
Hg^{199}	I $6s\,6p$	4.26×10^3	.106	0.71
Sb^{121}	I $5p^3$	3.50×10^3	.158	1.3
	I $5p\,6s$	4.0×10^3	.191	1.3

* From numerical calculations of eigenfunctions.[2]

Magnetic moments

Even though the determination of either a'' or a' is subject to doubt we expect that a'', which is the larger of these, may be determined approximately by present data. Typical results for p electrons are given in Table XIII.

In Bi, Pb, and Sb we see that there is approximate agreement for the $6p$, $5p$ electron under different conditions. The values of g are not constant, however, but show variations of the order of 20 percent. This again supports our opinion that the numbers a', a'' are only approximately constants. The magnetic moments derivable at present we must thus also regard as only approximately correct. By averaging a large number of magnetic moment determinations for the same element, as has been done in some cases by Goudsmit,[31] the errors may cancel statistically.

Our main conclusions are thus: (1) The experimental data on hfs in intermediate coupling is in as good agreement with the little-magnet picture of the nucleus as may be expected. (2) The discrepancies in the ratio a''/a' are reasonably explained by the sensitivity of the apparent value of a' to the variations in a'', $a(s)$, etc., due to perturbations by other configurations as well as its sensitivity to experimental errors.[32]

[31] S. Goudsmit, Phys. Rev. **43**, 636 (1933).

[32] On completing this manuscript we received a paper by Fermi and Segrè, Zeits. f. Physik **82**, 729 (1933), in which the same conclusion is reached by different methods involving explicit and accurate calculations of $\overline{(1/r^3)}$ and the calculation of the effect of perturbations by high energy levels with large hfs.

A New Analysis of Slater's Compressibility Data

H. M. EVJEN,* *California Institute of Technology*
(Received November 29, 1932)

The variation of interatomic forces with interatomic distances in crystals may be determined empirically from compressibility data. The experimentally possible range of variation in interatomic distance is, however, so small that the form of the force function valid for extrapolation to much greater distances cannot be adequately determined. From an analysis of Slater's compressibility data for the alkali halides it appears that for them the interionic forces of repulsion may be derived from a common force function. Because of the relatively large variation of lattice constant between the different alkali halides it is possible to determine a form for this common force function which is valid for relatively large variations in interatomic separation. The force function so found differs but little from the inverse power or from the exponential forms for small displacements from the equilibrium position. It drops off more rapidly, however, for increasing distances and increases more rapidly for decreasing distances. The solution given has the interesting property that of all possible force functions compatible with Slater's compressibility data it is the least favorable for the formation of a secondary structure.

I. INTRODUCTION

THE interionic forces in heteropolar crystals may be either derived quantum-theoretically, or established empirically, mainly from compressibility data. By the former process an exceedingly complicated problem is involved, and it is not strange that although a gratifying agreement as to order of magnitude has been obtained (for instance, in regard to the lattice constant)[1] the results have not been sufficiently precise to be of any great value for practical purposes.

For most purposes it is necessary to employ an empirical method[2] to calculate the interionic forces. By this method the lattice constant, the compressibility, and certain other quantities which can be determined experimentally are taken for granted, and a number of parameters in a more or less arbitrarily assumed force function are adjusted to give an exact agreement with the real force at least over the small region covered by the measurements. In many cases this method is satisfactory, since usually we are interested in the value of the force only over a small region. When extrapolations beyond this region do become necessary, however, the method is open to legitimate objections, because of the arbitrary manner in which the functional form of the force has been chosen. Since such extrapolations are sometimes of theoretical importance, it is a matter of interest that in the present paper some of the arbitrariness of the empirical method of determining the force has been eliminated.

On account of certain relations between the compressibility data for the alkali halides it is possible to relegate a common force function to all the members of this family. The great diversity in lattice constant among these members thus greatly extends the region of validity of the results. Although no attempt is made to justify theoretically the relationship between the alkali halides, the supposition is reasonable that the forces for the different ions have a similar origin. Since the foundations of the present analysis thus are purely empirical, the results are subject to the same limitations and uncertainties as the experimental data on which the analysis is based. Its main advantages over previous analyses are the greater generality in the results as well as in the treatment, and the fact that insofar as assumptions are involved they are physically well defined and reasonable.

* National Research Fellow.

[1] See for instance, E. A. Hylleraas, Zeits. f. Physik **63**, 771 (1930).

[2] In this category must now be placed Born's original theory (M. Born, *Atomtheorie d. festen Zustandes*, Leipzig, Teubner (1923)), as well as recent attempts to make use of an exponential repulsion. (See, for instance, Born and Mayer, Zeits. f. Physik **75**, 1 (1932).)

II. Interionic Forces in Relation to Compressibility

The change in potential energy per pair of ions, when a crystal is uniformly compressed, may be represented in two different ways as follows:

$$\Delta U=\sum_{n=1}^{\infty}(d^nU/da^n)_{a=a_0}(a-a_0)^n, \qquad (1)$$

where a is the central distance between neighboring atoms, a_0 being the value assumed by a in the equilibrium configuration. Or

$$\Delta U=-\int_{V_0}^{V}p(V)dV, \qquad (2)$$

where the volume per pair of ions is $V=ca^3$ where c is a constant which depends on the crystallographic arrangement of the atoms.

By Eq. (2) the coefficients in the Taylor expansion (1) may be expressed in terms of the pressure, p, and its derivatives with respect to a, since $d^nU/da^n=d^n(\Delta U)/da^n$. The derivatives of the pressure with respect to a, in turn, may be represented in terms of the compressibility, κ, and its pressure derivatives by the definition $\kappa=-dV/V_0dp$, where V_0 is the initial volume per pair of ions.

Consequently we obtain, in general,

$$\left(\frac{d^nU}{da^n}\right)_{a=a_0}=f_n\left(\left(\frac{d^{n-2}\kappa}{dp^{n-2}}\right)_{p=0},\left(\frac{d^{n-3}\kappa}{dp^{n-3}}\right)_{p=0},\cdots\kappa_{p=0},a_0\right). \qquad (3)$$

The quantity dU/da, which represents the central interionic force, therefore is defined as a Taylor expansion around the point $a=a_0$ when the compressibility is known as a function of the pressure.

III. Translation of Slater's Experimental Results into Terms of Interionic Forces

By Slater's measurements[3] the compressibility and its first pressure derivative are known at zero pressure for the alkali halides. Of immediate interest are therefore the three first equations of the general set (3). They are:

$$(dU/da)_{a=a_0}=0;\quad (d^2U/da^2)_{a=a_0}=9ca_0/\kappa_0;$$
$$(d^3U/da^3)_{a=a_0}=27c(2\kappa_0^2+(d\kappa/dp)_{p=0})/\kappa_0^3. \qquad (4)$$

Slater's observations, in conjunction with a determination of the lattice constant, therefore enable us to obtain the three first terms in a Taylor expansion of the central interionic force.[4] For many purposes this information is all that is required,[5] and since our results, so far, are purely empirical and involve no hypothesis, a gratifying degree of rigor is imparted to a group of calculations. When a knowledge of the interionic force is required for a greater range in interionic separation than implied by the three first terms in a Taylor expansion, we must resort to extrapolations. It is the purpose of the following analysis to investigate the possibility of reducing to a minimum the arbitrariness involved in such extrapolations.

For this purpose it is convenient to separate the potential energy of the crystal into two terms, a negative energy of attraction, and a positive energy of repulsion. It has been established by Slater's work[3] that the energy of attraction for the alkali halides is primarily a Coulomb term, although higher order terms are not definitely excluded. We shall, for the present, group these higher order terms with the energy of repulsion, Φ, and therefore bear in mind that Φ may contain negative as well as positive terms. Accordingly the energy per pair of ions is $U=\Phi-Me^2/2a$, where M is the Madelung constant. If now, for simplicity, we write, $d\Phi/da=\frac{1}{2}Me^2F(a,a_0)$, where the force of repulsion F, for reasons which will shortly become obvious, is considered as a function of two variables, Eqs. (4) become:

[3] J. C. Slater, Phys. Rev. **23**, 488 (1924).

[4] For a somewhat more laborious method of arriving at this same result, see G. A. Tomlinson, Phil. Mag. **11**, 1009 (1931). There appears to be a slight discrepancy, however, between Tomlinson's third term in the expansion and ours.

[5] An important application hereof is given in the paper immediately following this.

$$F(a_0, a_0) = -1/a_0^2,$$
$$(\partial F/\partial a)_{a=a_0} = 2/a_0^3 + 18c a_0/Me^2\kappa_0, \quad (5)$$
$$(\partial^2 F/\partial a^2)_{a=a_0} = -6/a_0^4 + 54c(2\kappa_0^2 + (d\kappa/dp)_{p=0})/Me^2\kappa_0^3.$$

We define the dimensionless quantities,

$$p = \mu a_0 = a_0^3(\partial F/\partial a)_{a=a_0}$$
$$Q^2 = -a_0^4(\partial^2 F/\partial a^2)_{a=a_0}. \quad (6)$$

Their meaning is as follows. If the law of repulsion were the inverse power postulated by Born,[2]

$$F = -(a_0/a)^p/a_0^2, \quad (7)$$

p would be the value of the exponent in this representation. In that case, moreover, we would have,

$$Q^2 = p(p+1), \quad (8)$$

a relation which cannot be fulfilled, since, as we shall see, Q^2 is as nearly as we can tell a constant for the alkali halide group, and μ, and not p, is also approximately a constant for this group.[6] On the other hand, if the law of repulsion were the simple exponential also suggested in the literature,[7]

$$F = -e^{-\mu(a-a_0)}/a_0^2, \quad (9)$$

μ would be the coefficient in the exponent of the exponential function. In this case, moreover, we would have,

$$Q^2 = p^2 \quad (10)$$

a condition very similar to (8), and, as we shall see, almost equally incompatible with Slater's observations.[8] In general, the distinction between an inverse power and a simple exponential law of repulsion, for practical purposes, is a rather fine one. In other words, calculations based on the one would, in most cases, lead to results not far removed from those obtained from the other. Certainly, Slater's observations off hand do not enable us to draw conclusions in favor of the one or the other. Although the relation (10) is more nearly fulfilled, on the average, than the relation (8), the difference between the two on the average, is only about one-third of the discrepancy between Q^2 and p^2. In this light it would be absurd to draw definite conclusions in favor of the exponential law of repulsion. Rather, the conclusion must be drawn, that if the experimental quantity $d\kappa/dp$ is accurate to within the limits claimed, neither the exponential nor the inverse power law represents correctly the real law of repulsion, and neither can be reliable for extrapolations.

TABLE I. *Compressibility data for the alkali halides at 30°C.*

Salt	a_0	p	Q^2	μ	$(p-3)/a_0$
LiF	$2.07\cdot10^{-8}$	7.43	98.1	$3.59\cdot10^{8}$	$2.14\cdot10^{8}$
LiCl	2.57	7.80	72.2	3.03	1.87
LiBr	2.74	7.89	71.0	2.88	1.79
NaCl	2.815	8.78	71.2	3.12	2.05
NaBr	2.97	8.91	68.6	3.00	1.98
KF	2.665	8.96	91.1	3.36	2.23
KCl	3.13	9.73	68.9	3.11	2.16
KBr	3.29	9.93	71.5	3.02	2.11
KI	3.525	10.23	69.7	2.90	2.05
RbBr	3.42	9.81	62.6	2.87	1.99
RbI	3.66	10.50	69.4	2.87	2.05
Average			74.0	3.06	2.04
r.m.s.d.			10.1	0.216	0.122
Percent r.m.s.d.			13.7	7.1	6.0

TABLE II. *Compressibility data for the alkali halides reduced to absolute zero.*

Salt	a_0	p	Q^2	μ	$(p-1)/a_0$
LiF	$1.97\cdot10^{-8}$	6.9	95.8	$3.50\cdot10^{8}$	$3.00\cdot10^{8}$
LiCl	2.54	9.0	117.2	3.55	3.16
LiBr	2.71	9.7	135.5	3.58	3.22
NaCl	2.76	10.1	117.8	3.66	3.30
NaBr	2.91	10.5	120.8	3.61	3.26
KF	2.63	8.9	95.0	3.38	3.00
KCl	3.08	10.7	97.5	3.47	3.15
KBr	3.23	11.0	105.9	3.41	3.10
KI	3.47	11.5	108.8	3.31	3.03
RbBr	3.36	11.0	97.8	3.27	2.98
RbI	3.58	12.0	114.0	3.35	3.07
Average			110.0	3.46	3.12
r.m.s.d.			12.2	0.123	0.106
Percent r.m.s.d.			11.1	3.56	3.40

The facts to which we have called attention are illustrated in Tables I and II. The former is based on the data as observed at 30°C. The latter is based on these data as reduced by Slater to the absolute zero.[9] The tables illustrate the approx-

[6] This discrepancy has already been pointed out by Slater. See reference 3.

[7] See reference 4, and also Born and Mayer, reference 2.

[8] Whereas a consideration of more than the next neighbors would slightly modify the function (13), this would not materially affect the conclusions here drawn.

[9] It would have been highly desirable if this discussion had been preceded by a revision of Slater's extrapolation to the absolute zero. In the absence of such a revision,

imate constancy of the quantity μ, which we have already mentioned, and to which attention previously has been called by Tomlinson.[7] It is seen, however, that this constancy refers more nearly to the quantity $\eta=(p-k)/a_0$, where k is a small numerical constant in the neighborhood of 3 for the unreduced data, and in the neighborhood of unity for the data reduced to the absolute zero. Table I also shows that Q^2 is a constant to well within the limits of experimental error, with the exception of the fluorides which appear to form a group by themselves. From Table II, however, it is seen that the trend is for this subgrouping to disappear with decrease in temperature. From Table II it also appears that *the constancies here suggested are improved by reducing the data to absolute zero*, as shown by the root-mean-square deviations from the mean values given at the bottom of the tables. In the case of the quantity Q^2 this is mainly due to the disappearance of the subgrouping of the fluorides. This quantity otherwise behaves somewhat erratically after reduction which undoubtedly can be easily ascribed to the uncertainties of Slater's extrapolations. In the case of the quantities μ and η, on the other hand, the improvement is unmistakable. We are therefore justified in claiming at least an approximate constancy for the quantities η and Q^2 for the alkali halides. In the case of the former the approximation is very good.

IV. Analytic Formulation of the Results and a General Solution

Together with the exact equilibrium condition, the definition (6) lead to the following set of equations:

$$F_{a=a_0}=-1/a_0^2, \quad (\partial F/\partial a)_{a=a_0}=(\eta a_0+k)/a_0^3, \quad (\partial^2 F/\partial a^2)_{a=a_0}=-Q^2/a_0^4. \tag{11}$$

Since Slater's observations indicate that η and Q^2 are constant for the alkali halides, it follows that for them the force of repulsion may be derived from a common force function F by assigning the proper value to a certain parameter, the physical significance of which we do not know, but which depends uniquely on the observed constant of the lattice a_0. In other words the difference between the members of the alkali halide group, in regard to the forces of repulsion, is sufficiently described in terms of a single parameter.[10] Thus, by making F a function of two variables, a and a_0, we have relegated all the members of the alkali halide group to the same force function, the force in any particular case being obtained by assigning the proper value to a_0.

The system of Eqs. (11) admits of an infinite number of solutions. A general solution is

$$F=-a_0^{k-2}a^{-k}\exp\left[-\int_{a_0}^{a}\Gamma(\alpha, a_0)d\alpha\right], \tag{12}$$

where

$$\Gamma(\alpha, a_0)=\eta\exp\left[\int_{a_0}^{\alpha}T(\beta, a_0)d\beta\right] \tag{13}$$

and

$$T(\beta, a_0)=L(a_0)\eta^{-1}\exp\left[\int_{a_0}^{\beta}S(\gamma, a_0)d\gamma\right] \tag{14}$$

$S(\gamma, a_0)$ is an arbitrary function, and

$$L(a_0)=(k+\eta a_0)^2/a_0^2-(Q^2-k)/a_0^2. \tag{15}$$

This general solution, involving an arbitrary function of two variables, represents the maximum information which can be derived from Slater's observations without resort to any hypothesis or additional data. Any theoretical representation of the force, must conform with this general solution to within limits set by the accuracy of Slater's observations. We have already seen that this condition is not fulfilled by either the inverse power or the simple exponential law of repulsion. Similarly it may be shown that a generalized inverse power law, containing reasonable higher order terms of the Coulomb force as well as of the repulsive force, does not withstand this test. Since, however, the probability of such a law is remote in view of recent theoretical developments, we shall not enter into this demonstration. Considerably more probable in this light,[11] is the exponential law or a modification thereof. In the following we shall see that we do,

however, the contents of the second table must be taken to indicate only a trend, and too much significance should not be assigned to the absolute numerical values of the quantities tabulated.

[10] Although this applies rigorously only at the points $a=a_0$, it seems fair to assume that it applies generally. However, no advantage is taken of this in the following.

[11] See, for instance, reference 1.

in fact, arrive at a law of this type by a functional analysis, based on an assumption of a reasonable and general nature.

V. Derivation of a First Approximation Solution

Tomlinson,[7] neglecting the discrepancy in Eq. (10), considered the approximate validity of the force function (9) as evidence that the force of repulsion is a result of an interaction at the "boundaries" of the atom, and therefore is essentially a function of the separation of the "atomic boundaries" rather than of the central separation. The validity of this conclusion, based solely on Slater's results, is doubtful. There are, however, other reasons for believing that Tomlinson's conclusion is essentially correct, to some of which we shall return later. For one thing, it is known that the force of repulsion decreases rapidly with increased separation, so that it is reasonable to assume that only proximate parts of the atoms are materially instrumental in the creation and maintenance of this force. In the limit, therefore, *for the most rapidly decreasing force of repulsion*, this force would be a function of the separation of the atomic boundaries only; aside, perhaps, from a "contact area" which might depend on the atomic separation as well as on the atomic dimensions. In mathematical language:

$$F=\Phi(a, a_0)\Psi(a-r), \tag{16}$$

where $(a-r)$ represents the separation of the atomic boundaries. It may be demonstrated, from Eqs. (11), that a "contact area," Φ, is required. If Φ is to be left as an arbitrary function of two variables the problem is no more determinate than the original one. It is reasonable to assume, however, that if Φ depends on the atomic separation (which, as we shall see, it does) the dependency must be slight; i.e., it must be a slowly changing function of a. In other words, it may be expanded into a power series of a where only the first two terms need be retained. That is,

$$\phi(a, a_0)=\Phi_0(a_0)+a\Phi_1(a_0). \tag{17}$$

For self-consistency, moreover, we must impose the condition:

$$|a_0\Phi_1/\Phi(a_0)|\ll 1. \tag{18}$$

We shall later demonstrate that this condition is fulfilled. As we shall see later, moreover, it follows from the assumption (17) that $a_0-r(a_0)$ is also slowly changing, and therefore may be expanded as follows:

$$a_0-r(a_0)=sa_0 \tag{19}$$

where $s\ll 1$. By removing a factor $(a-r)^{-ks}$ from ψ, we may write

$$F=(\Phi_0+a\Phi_1)(a-r)^{-ks}\psi(a-r). \tag{20}$$

Introducing F into Eqs. (9) we obtain

$$\Phi_1(a_0)/\Phi(a_0)=-\psi'(a_0-r)/\psi(a_0-r)-\eta, \tag{21}$$

$$\frac{\psi''(a_0-r)}{\psi(a_0-r)}-2\eta\frac{\psi'(a_0-r)}{\psi(a_0-r)}-2\left(\frac{\psi'(a_0-r)}{\psi(a_0-r)}\right)^2=\frac{H^2}{a_0^2}, \tag{22}$$

where $H^2=Q^2-k(k+1/s)-2k\eta a_0$. We have already noted that Q^2 is a constant. We are equally justified in claiming that H^2 is constant. In fact, the root-mean-square deviation from the average value of H^2 for the alkali halides is somewhat smaller than that for Q^2. With this assumption Eq. (22) may be reduced to the linear form by the substitution:

$$\psi(x)=y^{-1}x^{-\frac{1}{2}}e^{-\eta x}, \tag{23}$$

where, for short, we have written, $a_0-r=sa_0=x$. The differential equation resulting from this substitution is,

$$y''+(1/x)y'-(\eta^2-(s_1^2-\tfrac{1}{4})/x^2)y=0, \tag{24}$$

where $s_1=sH$. This is the differential equation of a Bessel function of imaginary argument. For $s_1>\frac{1}{2}$ the order of the Bessel function is also purely imaginary. The solution is,

$$y=Z_{i\nu}(i\eta x), \tag{25}$$

where $\nu=(s_1^2-\frac{1}{4})^{\frac{1}{2}}$. Replacing x by $(a-r)$, we obtain by Eqs. (23) and (25) the following functional form for the interaction at the boundaries:

$$\psi(a-r)=(a-r)^{-\frac{1}{2}}e^{-\eta(a-r)}/Z_{i\nu}(i\eta(a-r)). \tag{26}$$

From Eq. (21), moreover, we obtain,

$$\frac{\Phi_1(a_0)}{\Phi(a_0)}=\frac{1}{2sa_0}+i\eta\frac{Z_{i\nu}'(i\eta sa_0)}{Z_{i\nu}(i\eta sa_0)}. \tag{27}$$

The problem is now completely solved aside from the constant s, and a constant of integration implicitly involved in the symbol $Z_{i\nu}$.

We shall first consider the constant s. Its value, insofar as it determines the order of the Bessel function, is of great importance for the interpretation of the results. As noted, the order becomes imaginary for $s_1 > \frac{1}{2}$. The Bessel function of imaginary order as well as argument has the property,[12] that for $0 < z < \nu$, $Z_{i\nu}(iz)$ has an infinity of zeros condensing toward the origin, whereas to the right of the point $z = \nu$, it has *at most* one zero. Thus $\psi(z)$ would have an infinite number of poles for $0 < z < \nu$, whereas by a suitable choice of the constant of integration it can be made analytic throughout the domain $z > \nu$. In the region where observations have been made, the function $\psi(z)$ is finite and continuous. Therefore the region $0 < z < \nu$ must be outside the region of observation. This imposes an upper limit to the value of the constant s, which from the observed range of variability of a_0 may be estimated as

$$s_1 \leq 1/2^{\frac{1}{2}} \quad \text{or} \quad \nu \leq 1/2. \tag{28}$$

A lower limit to the value of s_1 can be set by the largest observed lateral contraction by extension of the crystal. Our force function (20) must yield at least as great a lateral contraction as that observed experimentally, say δ. Translated into terms of the separation of the atomic boundaries, this condition becomes, $s \geq \delta$. If we allow[13] a value of about 6 percent for δ the lower limit becomes, $s_1 \geq \frac{1}{2}$ or $\nu \geq 0$ which combined with the inequality (28) gives,

$$0 \leq \nu \leq 1/2. \tag{29}$$

Direct estimates of the value of s can be obtained in three independent ways. First on the basis of the data on hand: In zero approximation the force of repulsion should be a function of the separation of the atomic boundaries only. That is,

$$F = F(a - r). \tag{30}$$

Accordingly we attempt to satisfy the first two of the Eqs. (11) by this force function. That is,

$$F(a_0 - r) = -1/a_0^2, \quad F'(a_0 - r) = (\eta a_0 + k)/a_0^3.$$

After differentiation of the first of these equations with respect to a_0, we obtain by division:

$$1 - dr/da_0 = 2/(\eta a_0 + k).$$

The right-hand side is small of the order $2/Q$ within the domain in which we are interested, thus justifying our assumption that $(a_0 - r)$ is a slowly changing function of a_0. This estimate of s, namely $s = 2/Q$, is still too large by a factor of about $2^{\frac{1}{2}}$ to comply with our requirement (28), thus indicating that it may be necessary to insert a factor a^{-q} in the zero approximation representation (30).

A second estimate may be obtained directly from scattering experiments on liquids such as mercury.[14, 15] It is possible from these measurements to calculate the distribution of atoms around a given atom in the liquid. These calculations give a mean separation corresponding roughly to the lattice constant of crystalline mercury (aside from the difference in density of liquid and solid Hg and certain other small factors). For smaller separations the distribution drops rapidly to practically zero. Although this cut-off point depends to some extent on the temperature it must correspond roughly to the point at which the boundaries are in contact.[16] The difference between the separation of two neighboring atoms in the crystal and the cut-off separation should correspond roughly to the separation of the atomic boundaries in crystalline Hg, and presumably, as to order of magnitude, to that separation in any crystal. The separation thus calculated[17] is something less than 10 percent of the lattice constant, and therefore agrees roughly with our previous estimate.

The value of this agreement lies primarily in the contact it establishes with an independent domain of physical measurements. These estimates otherwise are too inaccurate to delimit satisfactorily the order of the Bessel function in our solution (26). On the other hand, a knowledge

[12] M. Bocher, Annals of Math. **6**, 137 (1892).

[13] In this connection may be mentioned that the inverse power law gives a lateral contraction of about 5 percent. See F. Zwicky, Phys. Zeits. **24**, 131 (1923).

[14] J. A. Prins, Naturwiss. **19**, 435 (1931).

[15] For an account of the theoretical features, see F. Zwicky, Proc. Nat. Acad. Sci. **17**, 524 (1931).

[16] If a physical definition is to be given to the term "atomic boundary" it clearly must be in terms of the gradient of the repulsive potential; that is, where this gradient becomes very large.

[17] Numerical values obtained from P. Debye; Lecture, California Institute of Technology, October, 1932.

of the quantity $a_0^5(\partial^3 F/\partial a^3)_{a=a_0}$, even though it be to a rather rough approximation, enables us to arrive at a closer estimate. From Slater's compressibility data and its temperature dependence this quantity may be judged to have a value nQ^3, where n is in the neighborhood of unity although it may be larger than this by at most a factor 5. It can be shown that if n has a value approximately 5, the order of the Bessel function in the solution (26) becomes zero. On the other hand, if we let s_1 assume its maximum value given by the inequality (28), the order of the Bessel function becomes $i/2$ which would make the factor n approximately 1.8. The compressibility data indicate that the latter value is more nearly correct, since the best estimate of the quantity $a_0^5(\partial^3 F/\partial a^3)_{a=a_0}$ leads to a value of n approximately 2. This is also in accordance with the trend indicated by the other two estimates and is, moreover, within the limits indicated in (29).

The fact that the Bessel function is probably of a purely imaginary order is interesting, since, as we have seen, this means that the force function has an infinity of distributed singularities in the region of the boundary of the atom. This perhaps indicates a certain obscurity in the outline of the atom which would not be averse to present ideas.

Although the value of ν probably is nearer to $\frac{1}{2}$ than to 0, we shall for the purpose of illustration employ the latter value. In this limiting case the Bessel function reduces to one of real order and imaginary argument; its properties are well known, and numerous tabulations are available in the literature facilitating numerical calculations.[18] By this choice the singularities of the function $\psi(z)$ are all displaced to the point $z=0$, so that the boundary of the atom becomes clear cut and well defined. The repulsive interaction in that case becomes,

$$\psi(z)=z^{-\frac{1}{2}}e^{-z}/(J_0(iz)+\tfrac{1}{2}ci\pi H_0^{(1)}(iz)), \quad (31)$$

where J_0 is the ordinary Bessel function of zero order, and $H_0^{(1)}$ is the Hankel function of the first kind of zero order. Only one constant of integration, c, appears in this solution since the other constant may be included in Φ, which as yet remains to be determined. An estimate of c can be obtained as follows. The ratio (27), by the inequality (18), should be small throughout the range of variation of a_0. By suitably disposing of c we can make this constant zero at one point at least. For this point we may somewhat arbitrarily choose the midpoint of the range of variation, which is given approximately by $\eta a_0=H$. To demonstrate that our solution is self-consistent, however, it will be necessary to show that this ratio is small for the extreme range of variation of the variable a_0.

The condition that $\Phi_1(a_0)/\Phi(a_0)$ shall be zero for $\eta a_0=H$ yields by Eqs. (27) and (31) the result $c=1.81$. It turns out, moreover, that this ratio is not only zero, but it also has a minimum at this point, so that its greatest value in the range of variability of a_0 is quite small. Calculation will show that the ratio is less than 0.3. Our assumption that the function $\Phi(a, a_0)$ is a slowly changing function of a is therefore borne out by the results, and our solution insofar as can be seen is free from contradictions.

In another important respect our solution exhibits a gratifying self-consistency. Our assumption, that the repulsive force was essentially an interaction along the boundaries of the atoms, implied, that it dropped off exceedingly rapidly with increasing separation. That this is so can best be seen by a comparison with the force functions which have found a predominant application in the literature;[2] i.e., the inverse power force, F_P, (Eq. (7)), and the exponential force, F_E, (Eq. (9)). In Figs. 1 and 2 we have plotted the ratios F_S/F_P and F_S/F_E where F_S represents the force resulting from the present theory. For convenience the calculations were made for a lattice constant, $a_0=H/\eta$, corresponding roughly to the middle of the scale of the alkali halides.

In Fig. 1 these ratios are plotted up to a separation corresponding to the position of the second next neighbors in the crystal. It is seen that the force F_S drops off much more rapidly than the others. In fact, whereas the exponential force, $e^{-\mu a}$, drops off more rapidly than the inverse power, the function F_S drops off essentially as $e^{-2\eta a}$ for large values of a; such that for a separation corresponding to the second next neighbors in the crystal the ratio F_S/F_E is only about one-tenth. With the type of force F_S, *it is consequently*

[18] See, for instance, E. Jahnke and F. Emde, *Funktionentafeln.*

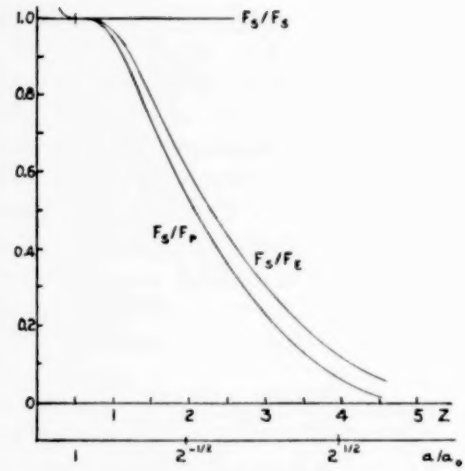

FIG. 1. Comparison of different force functions.

unnecessary to consider more than the next neighbors in calculations involving summations over the infinite lattice of the energy of repulsion or its derivatives. Our solution (20), therefore, refers not only to the crystal as a whole, but in first approximation it also gives the force between two individual ions in the crystal (after division by the number of next neighbors).

From the behavior of the ratio F_S/F_E we can also estimate the integral of the force function F_S, since the integral of F_E is known. In this way we arrive at the result that the energy of repulsion, from the present theory, is something less than 20 percent smaller than the energy of repulsion which would have been obtained from the simple exponential law. The latter, in turn, is smaller numerically than the negative Coulomb energy by a factor $p=\mu a_0$. The total energy in the present case thus would be approximately 2 percent greater than that calculated on the basis of the exponential law of repulsion (which, in turn, is very nearly the same as that obtained from the inverse power law). This difference, however, probably would be too small for experimental verification.

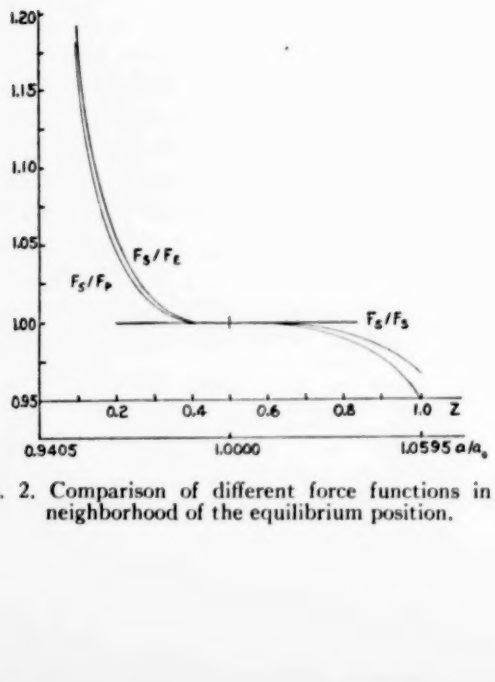

FIG. 2. Comparison of different force functions in the neighborhood of the equilibrium position.

In Fig. 2 the ratios F_S/F_P and F_S/F_E are plotted in the neighborhood of the equilibrium position $a=a_0$. It is seen that, over a region amounting to about 6 percent of the lattice constant around this point, the three functions F_P, F_E, and F_S are within 5 percent of each other, because of course, they have three terms of a Taylor expansion in common. This illustrates our contention that when we are interested primarily in this region it makes very little difference what type of functional form is assumed for the force. The very considerable success of the theory of the solid state, based on the inverse power law of repulsion, might perhaps be explained in this light. Attention is also called to the extremely rapid increase in F_S for separations smaller than the lattice constant, as illustrated by the rapid rise in the ratios F_S/F_P and F_S/F_E in this region. This rapid increase is significant for the remarks which we shall make in the final section, and is moreover in accordance with the assumption on which this analysis was based.

The self-consistency of this first approximation theory is gratifying, as is also the agreement with the independent domains of physical measurement which we have pointed out. The force, F_S, however, remains a first approximation, or perhaps not so much a first approximation as an extreme possibility, in that we have assumed the greatest possible decrease in the force of repulsion with increased separation which is compatible with the compressibility data. No attempt will be made here to improve the order of approximation. In a qualitative way, however, we can off hand point out certain modification possibilities. As to the interaction, $\psi(z)$, the main effect of refinement in the treatment probably would be to replace the distributed singularities in the neighborhood of $z=0$ (that is, near the boundary of the atom), by some array of steep but finite

potential walls. This again would lead to a less steep and more smooth force function, particularly for atomic separations less than the lattice constant. For separations greater than this, the effect of the modification should be less marked. Probably, therefore, our result that only the next neighbors need be taken into account in calculating the energy of repulsion of the crystal, would remain valid. The exponential term in the interaction is present in quantum-theoretical derivations of the force,[1] and its retention is otherwise strongly indicated by the experimental data, so that this term is fairly well established.

The failure of the zero approximation (30) to give correctly, except as to order of magnitude, the numerical value of the constant s, indicated that it might be necessary to insert a factor a^{-q} in the right-hand side of Eq. (30), where q probably would have a value k. This would imply that in our final solution (20), the factor $(a-r)^{-k\cdot}$ would be replaced by a factor a^{-k}. This is also borne out by our interpretation of the function $\Phi(a, a_0)$ as essentially a "contact area," not only dimensionally, but also because, as such, it should increase in a general way with a_0. Our choice of the constant of integration, c, in some measure was arbitrary, and might have to be modified. The solution is not much affected, however, by small changes in the value of this constant.

VI. Relation of the Results to the Stability of Heteropolar Crystals

We have shown in a previous paper[19] that, with the inverse power law of repulsion, all crystals of the NaCl- and particularly the CsCl-type are unstable against the so-called φ-variation. Only in the limit when the exponent of the repulsive force becomes infinite are these types definitely stable against this variation. Now of course, any theory of the solid state must explain the stability of crystals against all variations. The failure of the old theory to explain the stability of such crystals as CsCl therefore is a question of fundamental importance. The failure might be ascribed to one or both of the following sources. The forces which we have postulated may be inadequate. In that case the force of repulsion, which is much less firmly established than the Coulomb force of attraction, would come first in line for suspicion. Secondly, our postulated forces may be adequate, but we may have failed to take account of certain "cooperative phenomena,"[20] which arise as a natural consequence of these forces and do not require any new postulates for their explanation.

Here we shall consider briefly only the first possibility. It is significant that the type of crystals mentioned become stable for an infinite exponent of repulsion. The infinite exponent is characterized by the fact that the repulsive effect of all but the next neighbors disappears. This fact is responsible for the discontinuity in the first derivative of the stability curve at the angle, φ, corresponding to the CsCl-type of crystal where the number of next neighbors changes from six to two. This discontinuity again is responsible for the sharp maximum in the stability curve at this point. The repulsive force (20), in general, would not give rise to quite as abrupt a change as this, but it is clear that it would more nearly correspond to this condition than either the exponential or the inverse power law of repulsion. Therefore we can say that this repulsive force would be more favorable to the removal of the "φ-paradox" than either of the other two, and it might even be possible by the adoption of some such law of force to save the situation without calling into play Zwicky's cooperative actions.

These cooperative forces are necessarily based on and accompanied by certain departures from ideal symmetry in the crystal. This slight asymmetry, manifested as a secondary structure, may in turn be produced from the ideal crystal by imposing upon it certain finite but small variations. A necessary (but not sufficient) condition for the thermodynamic stability of this secondary structure is that the energy change by the variation shall be negative. We have shown, at least in a particular case, that the adoption of a force of repulsion, such as (20), may obviate in some measure the necessity of calling into play the cooperative forces to explain the stability of certain crystals. On the other hand, it is of interest to find out what a repulsive force of the form (20) would do to the energy change for variations leading to a secondary structure. This type of

[19] H. M. Evjen, Phys. Rev. **39**, 675 (1932).

[20] See reference 15, and also a more extensive paper by the same author shortly to be published.

force would make the gain in energy smaller, and therefore would be unfavorable to the formation of a secondary structure, the reason being that almost invariably by any variation leading to a secondary structure, there is an increase in the positive energy of repulsion. It is seen from Fig. 2 that the force of repulsion (20) leads to a greater increase in energy than either the exponential or the inverse power law of repulsion, so that the net gain in energy with a force of this type would be smaller. This is illustrated perhaps most clearly in the case of the variation in which advantage is taken of the gain in energy by the contraction of a single plane from the lattice constant of the crystal to that of the plane.[21] It is obvious from Fig. 2 that such a contraction would be accompanied by a larger increase in positive energy with the force function F_S than with either F_E or F_P. What is more, the amount of contraction would be smaller with the former than with either of the latter, so that not only is there a relative increase in the positive energy, but there is also an absolute decrease in the negative Coulomb energy gained.

[21] F. Zwicky, Helv. Phys. Acta **3**, 269 (1930); H. M. Evjen, Phys. Rev. **34**, 1385 (1929).

It is now pertinent to ask whether from the general solution (12) we could not construct the particular solution which would be *the least favorable to the formation of a secondary structure.* If, with this force function, we should still be able to find variations from the ideal crystal by which the energy would be decreased, the evidence would be more convincing than heretofore that the ideal crystal is not the thermodynamically most stable state. Some of the most legitimate arguments against the theory of the secondary structure would thereby be practically refuted. The evidence is that we have in the force function (20) the solution which is the least favorable to the formation of a secondary structure. This evidence is based on the fact that, of all the solutions which are consistent with the various physical observations to which we have called attention in this paper, the solution (20), by hypothesis, is the steepest in the region $a<a_0$, which is the main criterion as to whether or not the force function is favorable to the formation of a secondary structure. Regardless of whether this solution represents a good approximation to the real force or not, it therefore has considerable theoretical interest on account of its extreme character.

A Contribution to the Theory of Heteropolar Crystals

H. M. EVJEN,* *California Institute of Technology*

(Received April 24, 1933)

It is shown that the failure of theories of the solid state to account for the stability of ideal crystals cannot be due to inadequacy of the force postulate. A number of existing crystals, if ideal, would be dynamically unstable, with respect to certain variations, for any force postulate compatible with the compressibility data. These crystals cannot be ideal. A possible type of departure from the ideal state is suggested which involves a change of energy comparable with the heat of fusion (in agreement with Zwicky's theory). The change in volume at the melting point may be accounted for. Evidence from the photoelectric properties of these crystals indicates that this proposed type of departure may have physical reality although undoubtedly accompanied by asymmetries. A consideration of the changes necessary in the energy function to permit the existence of secondary structure indicate that such secondary may exist even in crystals apparently dynamically stable. It is conjectural whether any crystal is thermodynamically stable in the ideal state. A working hypothesis that all crystals have a secondary structure leads to a rational explanation of the doublet nature of residual rays in cubic crystals and to an improved form of Lindemann's law.

I. INTRODUCTION

ANY theory of the solid state must explain the stability of existing crystals. Zwicky[1] and the writer[2] have shown that variations exist for which the conventional crystalline model[3] is not stable, whereas the real crystal is definitely stable. As we have pointed out,[4] the failure of the theory must be ascribed either to an inadequacy of the force postulate, or to failure to take account of certain "cooperative actions."[5] The latter, arising as a natural consequence of the forces already postulated, would not require any new hypothesis.

In the present paper we shall demonstrate that modifications of the force postulate alone cannot save the situation;[6] and that therefore we have here new evidence that Zwicky's cooperative actions, (and consequently the secondary structure which, however, may be deformed into a mosaic structure),[7] are necessary accompaniments to any theory of the solid state.

In the paper immediately preceding this we examined the experimental background of the force postulate. We saw that extrapolations beyond the immediate neighborhood of the equilibrium configuration are uncertain because the functional form of the force of repulsion is arbitrary. This uncertainty might be responsible for the failure of the ideal model to explain the stability of crystals. We pointed out, however, two different ways in which this uncertainty might be eliminated. By one method we constructed the force of repulsion, compatible with the experimental data, which would be the least favorable to the formation of a secondary structure. By the other, we confined attention to the neighborhood of the equilibrium position of the atoms, where the force is given experimentally, and where thus no hypothesis in regard to the functional form of the force is required. The latter method is more direct and requires less analysis, but the former has a wider field of

* National Research Fellow.

[1] F. Zwicky, Helv. Phys. Acta **3**, 269 (1930); **4**, 49 (1931); Phys. Rev. **38**, 1772 (1931).

[2] H. M. Evjen, Phys. Rev. **34**, 1385 (1929); **39**, 675 (1932).

[3] M. Born, *Atomtheorie d. Festen Zustandes*, Teubner, 1923.

[4] See paper by Evjen immediately preceding this.

[5] F. Zwicky, Proc. Nat. Acad. Sci. **17**, 524 (1931); Phys. Rev. **43**, 270 (1933).

[6] Although it is not immediately apparent, our demonstration will also cover the possibility that the forces have a noncentral component, at least insofar as the next neighbors are concerned. (See particularly Eq. (12a) and its implications.) This possibility has been suggested by L. Brillouin, Scientia, p. 206, March, 1932.

[7] F. Zwicky, Phys. Rev. **40**, 63 (1932).

application, in that it is suitable when extrapolations are involved. Since, however, the former method is available for the purpose of the present paper, it will be employed. The problem which will be considered is that of obtaining the change in energy when a variation of the "residual ray" type[8] is imposed on the crystal.

II. The Residual Ray Variation

By this variation the negative lattice is displaced as a whole, over certain regions, with respect to the positive lattice. For convenience, the energy of the crystal may be divided into a negative energy of attraction and a positive energy of repulsion. Beyond reasonable doubt[9] the energy of attraction for the heteropolar crystals, with which we shall be mainly concerned, is essentially a Coulomb term. The energy remaining after this term has been subtracted will be called the energy of repulsion. It is easily demonstrated that, because of the conditional convergence of the series involved, the change in Coulomb energy for the residual ray variation depends on the macroscopic shape of the region affected. We shall consider only the possibility that the shape of this region is either a needle or a thin slab, the relative displacement of the negative lattice being in the former case along the axis of the needle, in the latter, parallel to the boundary planes of the slab. These shapes can be shown to give rise to the greatest negative change in Coulomb energy. By subdividing the crystal, in a regular manner, into regions of these shapes, such that the displacements in neighboring regions are always in opposite directions, it is of course possible to have all the ions in the crystal take part in the variation. The manner of subdivision, however, is related to the geometry of a possible secondary structure, the discussion of which we shall defer.

The change in Coulomb energy per pair of ions by the relative displacement of the negative lattice against the positive lattice in a needle shaped or slab shaped region may be most easily found by considering the electric field in which the displacement takes place. Since this relative displacement is mathematically equivalent to a superposed dipole lattice, it turns out that the electric field is in a direction to assist in the displacement, and is given by[10]

$$E=2\pi e\Delta/3a_0^3(1-4\pi\alpha/3a_0^3),$$

where e is the individual electric charge of the ions, a_0 is the central separation of two neighboring ions, and Δ is the relative displacement. For generality the possibility also has been considered that the ions are deformable, the average polarizability of the two ions present being α. The change in Coulomb energy[11] consequently is given by:

$$W_c=-\int_0^{\Delta}eEd\Delta=-\pi e^2\Delta^2/3a_0^3(1-4\pi\alpha/3a_0^3). \quad (1)$$

Previous considerations[4] have indicated that in calculating the energy of repulsion the effect of all but the next neighbors may be neglected. If we do consider more than the next neighbors, the gain in energy by the residual ray variation is actually somewhat greater. The error therefore is such as not to invalidate the main conclusion which is to be drawn, namely, that the ideal crystal is not always a dynamically stable state.

The change in energy of repulsion then may be represented in terms of the first nonvanishing term in a Taylor expansion, as follows

$$W_r=\tfrac{1}{2}\sum_{i=1}^{m}\frac{1}{m}\frac{\partial^2\phi}{\partial x_i^2}\Delta^2,$$

where m is the number of next neighbors and x_i is the x-coordinate of the ith next neighbor. In our previous notation,[4] if we limit ourselves to crystals of the NaCl-type, this may be rewritten as

$$W_r=(1/12)Me^2\Delta^2\{(\partial F/\partial a)_{a=a_0}+(2/a_0)F_{a=a_0}\},$$

where

$$(\partial F/\partial a)_{a=a_0}=p/a_0^3, \quad \text{and} \quad F_{a=a_0}=-1/a_0^2.$$

[8] F. Zwicky, Phys. Rev. **38**, 1772 (1931).

[9] J. C. Slater, Phys. Rev. **23**, 488 (1924).

[10] H. F. Herzfeld, Phys. Rev. **29**, 701 (1926); and reference 8.

[11] The force of electric origin exerted during the displacement is actually,

$$f=eE+\alpha E(dE/dx)_{\Delta=\text{const.}}$$

namely, the force on the ion plus the force on the induced dipole. It can be shown, however, that so long as we are interested in infinitesimal displacements only, $(dE/dx)_{\Delta=\text{const.}}$ vanishes, so that the latter term drops out.

Finally,

$$W_r = M(p-2)e^2\Delta^2/12a_0^3, \qquad (2)$$

where p may be determined from the compressibility, κ, of the crystal, as follows $p=2+18ca_0^4/Me^2\kappa$.

The total change in energy, by Eqs. (1) and (2), consequently is,

$$W=(M(p-2)-4\pi/(1-4\pi\alpha/3a_0^3))e^2\Delta^2/12a_0^3. \qquad (3)$$

This change in energy will be negative if,

$$M(p-2)(1-4\pi\alpha/3a_0^3)<4\pi. \qquad (4)$$

The least favorable condition for the fulfillment of this inequality is $\alpha=0$. In this case, the inequality reduces to,

$$p<2+4\pi/M \qquad (5)$$

or, expressed in terms of the compressibility, $\kappa>9Ga_0/2\pi N\rho e^2$, where G is the gram molecular weight, N is the Loschmidt number, $(6.06\cdot 10^{23})$, and ρ is the density of the crystal.

The inequality (5) is not quite fulfilled for any available crystal. There is, however, no known reason why this inequality never should be fulfilled, so that, even in this extreme case, the ideal crystal is not always stable against the residual ray variation.

The more general condition (4), which would have to be used to test the stability of real crystals, can be rewritten in a more convenient form by means of the Lorenz-Lorentz law[12] for a non-absorbing medium. For crystals of the NaCl-type this law may be written,

$$4\pi\alpha/3a_0^3=(n^2-1)/(n^2+2), \qquad (6a)$$

where n is the index of refraction, so that the inequality (4) becomes:

$$n^2>(3M(p-2)/4\pi)-2 \qquad (6)$$

or, expressed in terms of the compressibility,

$$n^2>(27a_0G/2\pi N\rho e^2\kappa)-2.$$

The latter form has the advantage that it contains nothing but well-known constants and directly measurable quantities. In its derivation we have limited ourselves to crystals of the NaCl-type. Before we apply this test to real crystals, however, we shall consider somewhat more in detail the possibilities involved if the inequality (6) should happen to be satisfied.

III. Secondary Structure

It was shown by Zwicky[8] that the instability of an ideal crystal against the residual ray variation would lead to a secondary structure, since the variation, in order to be effective in decreasing the energy of the crystal, must take place over discrete regions of definite geometrical shape. This much is indubitable. Somewhat more doubtful is the question of the dimensions of the secondary structure. Zwicky[8] estimated the dimensions by considering the lateral displacement which accompanies the variation. On account of the resulting strains, stresses are set up along the boundaries of the regions affected by the variation which ultimately may delimit the dimensions of the secondary structure. It can be shown that the lateral as well as the longitudinal change in lattice constant, accompanying the residual ray variation, are of a higher order. That is, if the latter is infinitesimal of the order Δ, the former will be of the order Δ^2. Correspondingly the energy changes will be of the order respectively Δ^2 and Δ^4. If therefore we start with the ideal crystal, there will be no change in lattice constant, either lateral or logitudinal, at the outset of the residual ray variation; and at this stage of the development these secondary effects play no part in the energetic equation. On the other hand, along the boundaries of the regions affected by the variation, the ions will find themselves in different surroundings from those prevailing in the interior of these regions, and the energy change here, whereas in general different from that in the interior, is of the same order of magnitude. If the gain in energy along the boundaries is smaller than that in the interior, we should expect as few boundary planes as possible. In this case the dimensions of the secondary structure evidently would be determined by considerations analogous to those of Zwicky's, or else we would get macroscopic

[12] See, for instance, P. Debye, Handb. d Radiologie, VI, p. 597. If so desired, Eq. (6a) may be considered as a definition of n, and the most reliable determinations of α may be inserted into this equation for the purpose of obtaining n. See Born and Bolinov, Handb. d. Physik **24**, 449.

electric moments such as exhibited by electrets, as also suggested by Zwicky. On the other hand, if the gain in energy should be greater along the boundaries of the polarized regions, other things being equal, we should expect as many boundaries as possible. In the limit, the secondary structure would be reduced to dimensions not far removed from those of the elementary cell of the primary structure.

To settle some of these questions we have in the following calculated the change in energy of ions at the boundaries of various polarized configurations. It should be noticed that the change in energy of these ions depends on the manner in which the adjoining regions are polarized. If the negative lattice in one region is displaced in one direction, that in the adjoining region in the opposite direction, such that the entire positive lattice remains undisplaced, the electric field at the positive boundary ion is different from that at the negative ion. On the other hand, if the negative lattice in one region is displaced in one direction, and the positive lattice in the adjoining region in the same direction, the electric field at the positive boundary ion is the same as that at the negative ion. In general, it appears that the latter "boundary condition," that is, the symmetrical one, gives the more favorable energy change. We therefore give the results only for this condition. Likewise we have omitted the results for slabs of minute thickness which, in general, appear to be energetically less favorable than very thin needles.

The calculation of the change in Coulomb energy, wherever possible, has been carried out by two or more methods, simplest and most direct of which is the method involving the change in energy by the displacement of an ion against a Madelung line.[13] These calculations, although somewhat tedious, are quite straightforward and no further comment is required.

The most important results of the calculations in terms of the index of refraction and the quantity p are summarized in the following four equations, where, for the sake of completeness, we have also repeated a statement of Eq. (3).

Change in energy per pair of ions by the residual ray variation

(1) Interior ions in needles or slabs.

$$W_1=[M(p-2)-4.1888(n^2+2)]e^2\Delta^2/12a_0^3.$$

(2) Boundary ions of these needles or slabs.

$$W_2=\left\{M(p-3/2)-\frac{4.5168\cdot 12.5664(n^2+2)}{(12.8944-0.328n^2)}\right\}e^2\Delta^2/12a_0^3.$$

(3) Needles of four ions cross section.

$$W_3=\left\{M(p-1)-\frac{4.8120\cdot 12.5664(n^2+2)}{(13.1896-0.6232n^2)}\right\}e^2\Delta^2/12a_0^3.$$

(4) Madelung lines polarized alternately in opposite directions.

$$W_4=\left\{Mp-\frac{5.3536\cdot 12.5664(n^2+2)}{(13.7312-1.1648n^2)}\right\}e^2\Delta^2/12a_0^3. \quad (7)$$

From these equations it is seen that when $W_2<W_1$, or $n^2>1.95$, the gain in energy of the boundary ion is greater than that of the interior ion, so that the tendency would be for as many boundary planes as possible. If $W_3<W_2$, or $n^2>2.05$, the tendency would be for the needles to have a cross section of four ions or less. Similarly the tendency would be for a cross section of a single ion if $W_3<W_4$, that is, $n^2>2.10$. Finally, it is seen that for $n^2>11.8$ the

[13] E. Madelung, Phys. Zeits. **19**, 524 (1918).

polarizing force in the Madelung lines becomes infinite so that the atoms would be stripped of an electron. This may be contrasted with Herzfeld's condition,[10] which, based essentially on the first of these equations, gives the same result only for an infinite index of refraction. It should be noticed that the facts to which we have called attention refer only to the tendency at the outset of a variation which starts from the ideal crystal. For reasons which we shall shortly point out, we are not justified in drawing conclusions about the state of affairs which will prevail at the end of the variation.

All that can be said with certainty is that if any one of the energy changes W_1 to W_4 should turn out to be negative, the ideal state would be dynamically unstable. In Fig. 1 we have mapped,

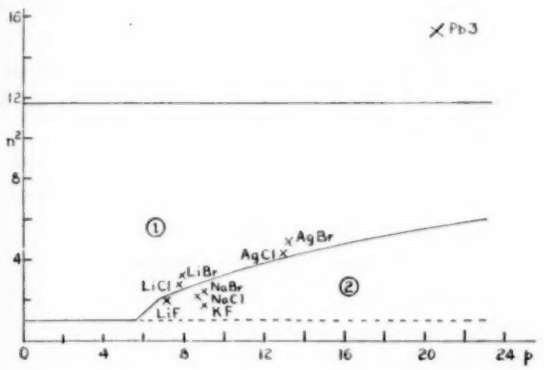

FIG. 1. Regions of dynamic stability and instability of the ideal state. (1) Ideal state dynamically unstable in regard to the residual ray variation. (2) Ideal state dynamically stable but not necessarily thermodynamically stable.

in terms of n^2 and p the region in which this would be true. In the preparation of this map the benefit of any doubt has been given to the ideal crystal. Otherwise it entails no hypothesis of any kind, and only directly measurable quantities are required to give the position of a real crystal in the map. Now, it may be that for reasons unknown to us, all real crystals would fall in the region assigned to the ideal crystal. If, on the other hand, we should find some crystals, having such properties that they would fall in the region where the ideal state is dynamically unstable, the evidence would be overwhelming that non-ideal states have real physical significance.

IV. Introduction of the Real Crystal

In the preparation of the map, Fig. 1, we have limited ourselves to crystals of the NaCl-type. In our search for non-ideal crystals we shall therefore be limited to crystals of this same type. Among the well-known alkali halides we find crystals which are definitely unstable in regard to the residual ray variation. Whereas LiF must be classified as doubtful,[14] LiBr and LiCl fall well outside the region in which the ideal state is stable. For these crystals, therefore, the ideal state is not even pseudostable, and the existence of a secondary structure may be considered as well established. The silver halides likewise appear to be definitely unstable in the ideal state. PbS, on the basis of values obtained from the *Critical Tables*, appears to fall in the region of infinite polarizing fields, and therefore should have the properties of a metal by our modified Herzfeld condition. This result, however, is not conclusive, since the fact that PbS is definitely not ideal ruins the premises of our calculations. For this same reason, and also because higher order terms have not been considered, we can draw no definite conclusions about the ultimate nature and dimensions of the secondary structure which will result when the ideal crystal is dynamically unstable. All that can be said with certainty is that a secondary structure of some kind will come into existence. There are, however, indications that the present variation has a real physical significance with perhaps minor modifications, relating mainly to a redistribution of atoms at the boundaries of the polarized regions.

By Zwicky's general theory of the solid state[5] the secondary structure with its cooperative actions is not only to be considered as a slight modification of the ideal state; it is, in fact, supposed to be responsible for the very existence of the crystal. By this theory the energetic aspects of the ideal state are already roughly realized in a statistical manner in the melt. It follows that the heat of fusion of the crystal should be roughly the same as the gain in energy

[14] In Section V we shall see that there is good reason to believe that LiF is at least *thermodynamically* unstable in regard to the present variation. This is of interest in view of the direct experimental evidence obtained by Johnson for a secondary structure in this salt. See Thomas H. Johnson, J. Frank. Inst. **212**, 507 (1931).

by a variation leading from the ideal state to the secondary structure. We can estimate fairly well the gain in energy by a variation of the present type. A simple calculation, the details of which we shall not include, will show that for such crystals as AgBr and LiCl this gain in energy is in good agreement with the heat of fusion. Likewise, from more general considerations, to which we shall return in the last paragraph of this paper, it appears that the change in volume at the melting point may be accounted for in this same way. From this we can probably conclude that the secondary structure in these crystals depends in some essential manner on a variation of the present type.

Further evidence that the present type of departure from the ideal state has physical reality is furnished from the field of non-metallic electronic conduction. The residual ray variation, in its essence, involves a partial liberation of electrons, implied by the deformation of the ions. On this idea, in its extreme of course, is based Herzfeld's theory of metals,[10] the difference being that in the present case the polarizing fields are not sufficient completely to strip the ion of an electron. If the departure from the ideal state here described has physical reality, the individual ions of the crystal would be in a state of deformation depending on their polarizability as well as on the polarizing fields. It is therefore not unreasonable that a correlation should exist between the liberation of conduction electrons by say photoelectric means and the existence of a secondary structure of the present type. Such a correlation does in fact appear to exist. We are referring to the photoelectric output maxima characterized by their presence at the lower limit of the ultraviolet region of absorption.[15] An examination of the photoelectric data available does indeed indicate that these output maxima can occur only in crystals which, in the ideal state, are definitely unstable in regard to the residual ray variation. Empirically this condition has found expression in the rule that these output maxima can occur only in crystals having an index of refraction greater than 2.[15] It is otherwise not unreasonable that these particular photoelectrons should originate in a secondary structure of the present type. On the one hand, an exhaustive review of the field has led Gudden[15] to believe that nonmetallic conduction electrons, whether liberated photoelectrically or thermally, never originate in the ideal lattice. On the other hand, the strong dependence of these photoelectric and related phenomena on impurities and the past history of the sample brands these as structure-sensitive properties, which by Zwicky's theory[1] are closely related to the existence of a secondary structure. Finally the residual ray type of secondary structure is distinguished from other proposed structures in that it is essentially a volume effect. The presence of impurities therefore should have a smaller effect with this type than with the two-dimensional type[1] where the relative abundance in the secondary network may be quite considerable even though the total amount of impurities is vanishingly small. It is a characteristic of the particular photoelectric output maxima with which we here are concerned that they are less influenced by impurities than other such maxima.[15]

From the preceding calculations and considerations we now summarize: Crystals exist which are definitely unstable in the ideal state. Consequently these crystals cannot be ideal. Although the exact manner in which these crystals will depart from the ideal state is not accessible to calculations there is evidence to the effect that the secondary structure depends in some essential manner on the so-called residual ray variation. In the cases where the ideal state is a real minimum and not a saddle point in regard to this variation the question is still open whether or not the ideal crystal is thermodynamically stable. In the following paragraph we shall attempt to show that the ideal state in these cases should not always be expected to be thermodynamically stable.

V. Energy of Residually Displaced Heteropolar Crystal, and a Derivation of Lindemann's Law

In the preceding pages has been demonstrated the possibility that real crystals have a secondary structure of the residual ray type. In general, therefore, we are not justified in writing the energy of the crystal in the con-

[15] B. Gudden, Phys. Zeits. **21**, 825 (1931).

ventional manner as $U=U_c(a)+U_r(a)$, where the Coulomb energy and the energy of repulsion both are considered as functions of the single variable, a, or the atomic separation. To include the possibility that the crystal may be residually displaced, we must now write the energy of the crystal as follows:

$$U=U_c(a,\Delta)+U_r(a,\Delta). \tag{8}$$

To replace the simple conventional equilibrium condition, $[dU/da]_{a=a_1}=0$, we now obtain the two equations:

$$\begin{aligned}&[\partial U/\partial a]_{(a=a_0)/(\Delta=\Delta_0)}=0;\\ &[\partial U/\partial \Delta]_{(a=a_0)/(\Delta=\Delta_0)}=0,\end{aligned} \tag{9}$$

where, to exclude saddle points and maxima, we must impose the additional restrictions:

$$[\partial^2 U/\partial a^2]_{a_0,\,\Delta_0}>0, \quad [\partial^2 U/\partial \Delta^2]_{a_0,\,\Delta_0}>0. \tag{10}$$

Furthermore, the function U is no longer tied up with the compressibility, κ_0, in the simple manner,[4]

$$d^2U/da^2=9ca_1/\kappa_0. \tag{11}$$

The correlation now becomes:

$$\partial^2U/\partial a^2-\frac{[\partial^2U/\partial a\partial\Delta]^2}{\partial^2U/\partial\Delta^2}=9ca_0/\kappa_0.$$

The phenomenological theory of the interatomic forces in heteropolar crystals thus needs revision. A general quantitative treatment will not be attempted in the present paper. We shall, however, attempt to demonstrate that a revision may be required also in the cases when the ideal state is dynamically stable. For this demonstration certain simplifying assumptions are permissible. In the first place, all terms of order higher than Δ^2 will be neglected in the Coulomb and polarization energies. Since all higher order terms are negative, this neglect favors the ideal crystal. In the second place, only the next neighbors will be considered insofar as the energy of repulsion is concerned. This also favors the ideal crystal. Finally we shall only consider the Madelung line case, which for finite displacements, Δ, is undoubtedly less favorable energetically than Zwicky's secondary structure. *With three perpendicular sets of such lines, intersecting to form a secondary structure of minimal dimensions in the crystal,* Eq. (8) may be written:

$$U=Me^2(-\tfrac{1}{2}a-g\Delta^2/a^3+\phi(a+\Delta)+\phi(a-\Delta))], \tag{12a}$$

where, by Eq. (7),

$$g=\frac{5.3536\cdot 12.5664(n^2+2)}{4M(13.7312-1.1648n^2)}.$$

Eqs. (9) similarly become:

$$\begin{aligned}&\tfrac{1}{2}(\phi'(a+\Delta)+\phi'(a-\Delta))=-1/a^2-6g\Delta^2/a^4,\\ &\tfrac{1}{2}(\phi'(a+\Delta)-\phi'(a-\Delta))=4g\Delta/a^3.\end{aligned} \tag{12}$$

The latter of these equations is satisfied identically for $\Delta=0$. The corresponding solution of the first equation is say, $a=a_1$. This solution does not always represent a real minimum, however; for when $p=a_1^3\phi''(a_1)<4g$, the second one of the inequalities (10) is not satisfied, so that the solution represents a saddle point. This is the case which we have already considered, namely the case when W_4 in Eq. (7) is negative, and the ideal state is dynamically unstable. We are now interested in the case when the ideal state is apparently dynamically stable, that is, $p>4g$. For the sake of argument it is assumed that the real crystal is ideal in this case, so that Eq. (11) is applicable. Calculations demonstrate that Eqs. (12) ordinarily have real solutions other than $\Delta=0$, $a=a_1$, satisfying the inequalities (10). The question whether these other minima represent lower energies than the ideal state, requires knowledge about the functional form of the energy of repulsion. For functions such as the exponential or the inverse power,[4] it appears that when a condition, $(p-4g)/p<s$ is fulfilled, where s is of the order 1/5 to 1/10, energy states exist which are lower than that of the ideal state. In other words, the boundary in Fig. 1, to the left of which the ideal state is dynamically unstable, is more or less parallelled by another boundary, to the left of which the ideal state is thermodynamically unstable. An exact calculation of this second boundary is hardly worth the trouble in view of the uncertain nature of the premises of the calculations. It should be noted, however, that in these premises the benefit of any doubt has been given to the ideal crystal. It is therefore significant that, for any reasonable

functional form of the energy of repulsion, the maximum ratio, s, for which the ideal state is thermodynamically unstable, is definitely positive. We are therefore justified in believing that a number of the real crystals which are dynamically stable in the ideal state will be thermodynamically unstable. The number of such crystals cannot be calculated without hazardous extrapolations. It is as yet conjectural whether any crystal exists that is thermodynamically stable in the ideal state.

From these considerations it is permissible to adopt, as a working hypothesis, the view that the secondary structure here implied is a general phenomenon, since there is no evidence definitely negating its existence even in crystals which are apparently dynamically stable in the ideal state. The existence of such a general type of secondary structure would be highly desirable from the aesthetic point of view, and even may be said to be phenomenologically suggested. The following experimental evidence, supporting this view, is presented:

In the first place, Professor F. Zwicky called the attention of the writer to the doublet nature[16] of the so-called residual rays (Reststrahlen) in cubical crystals which appears to be a quite general phenomenon. Such a doublet nature is apparently inconsistent with the cubical symmetry of the ideal state[17] but, as pointed out by Zwicky, is exactly what we should expect if the crystal is submicroscopically slightly tetragonal as implied by the residual ray secondary structure. In the second place, if we assume that this type of secondary structure is a general phenomenon which, in accordance with Zwicky's theory of the solid state,[5] is responsible for the existence of the solid phase, the so-called Lindemann's law may be satisfactorily accounted for and even improved upon.

Lindemann's law[18] connects the residual ray frequency with the melting point, T_s, of the crystal, and was first derived by Lindemann on the basis of an improbable model. Independently of this derivation dimensional analysis[19] yields,

$$\nu = CR^{\frac{1}{2}}N^{\frac{1}{2}}(T_s/MV^{\frac{1}{3}})^{\frac{1}{2}},$$

where R is the gas constant, $N=6.06\cdot 10^{23}$, M the molecular weight, and $V=M/\rho$ the specific volume per mol. C is dimensionless and was found by Lindemann to be approximately constant for a number of crystals. The law otherwise has found no satisfactory theoretical explanation.

On the basis of the present hypothesis, however, this same law may be easily derived. If we disregard the volume contraction, which, as we have seen, would accompany the residual displacement, the change in energy by the displacement is given by the following expansion:

$$\Delta U = -c_1\Delta^2 + c_2\Delta^4,$$

where terms of the order six and higher in the displacement have been neglected. Equilibrium will be reached when, $\partial\Delta U/\partial\Delta = 0$ or $\Delta_0^2 = c_1/2c_2$ and consequently the maximum gain in energy will be, $\Delta U_0 = -\frac{1}{2}c_1\Delta_0^2$. By carrying out this variation in three mutually perpendicular directions we arrive, as we have previously seen, at a secondary structure; and by the argument previously advanced, the total gain in energy by this variation should form a substantial fraction, say β, of the heat of fusion, h, of the crystal, the remainder being furnished mainly by a contraction corresponding to the change in volume at the melting point. We can therefore write,

$$c_1 = 2\beta h/3\Delta_0^2 = (2^{5/3}/3)(N/V)^{\frac{1}{3}}(a/\Delta_0)^2\beta h,$$

where $\beta<1$ may be expected to be roughly constant for different crystals. For convenience this result may be expressed in terms of the melting point by the following relation: $Nh/RT_s = 4.19\alpha/8.31$, where α has been shown by J. W. Richards[20] to be roughly constant for a number of crystals. For the alkali halides α ranges in the neighborhood of 5.

The residual ray frequency, by a well-known elementary theory,[21] may be expressed as follows:

$$2\pi\nu = (\lambda(m_1+m_2)/m_1m_2)^{\frac{1}{2}},$$

[16] Karl Korth, *Göttinger Nachrichten*, p. 576, 1932.

[17] See, however, attempt by M. Born and M. Blackman, Zeits. f. Physik **82**, 551 (1933), to reconcile this doublet nature with the ideal state (an article which appeared after the preparation of this manuscript).

[18] F. A. Lindemann, Phys. Zeits. **11**, 609 (1910).

[19] A. Einstein, Ann. d. Physik **35**, 689 (1911). E. Grüneisen, Ann. d. Physik **39**, 257 (1912).

[20] A. Eucken, Lehrb. d. Chem. Phys., p. 220, Leipzig, 1930.

[21] See, e.g., reference 3, p. 740.

where m_1 and m_2 are the masses of the two ions of the heteropolar crystal. If we disregard the slight tetragonality, introduced by the secondary structure, which as we have seen would give rise to two characteristic frequencies, the quantity λ is given by,

$$\lambda = (\partial^2 \Delta U/\partial \Delta^2)_{\Delta=\Delta_0} = 4c_1.$$

Consequently the residual ray frequency becomes,

$$\nu = 0.465(\alpha\beta)^{\frac{1}{4}}(a/\Delta_0)R^{\frac{1}{4}}N^{\frac{1}{4}}(T_s/\overline{M}V^{\frac{1}{3}})^{\frac{1}{4}}, \quad (13)$$

where $\overline{M} = 4M_1M_2/(M_1+M_2)$.

This result is essentially Lindemann's law with the exception that $\overline{M}$ has replaced M. In Table I we have tabulated the data employed by Lindemann to test the validity of his formula. It is seen that the substitution of $\overline{M}$ for M, generally speaking, improves the representation. This is particularly noticeable in the case of KI where the discrepancy between $\overline{M}$ and M is particularly great.

TABLE I. *Comparison of Lindemann's formula with ours.*

Crystal	$\lambda_{obs.}$	$\lambda_{Lind.}$	λ_{ours}
KCl	63.4	(63.4)	(63.4)
KBr	82.3	85.6	84.0
KI	96.7	112.2	95.4
NaCl	51.7	49.8	48.8

To see whether our formula (13) gives reasonable values for the ratio Δ_0/a we shall employ more recent and more accurate determinations[16] of the residual wave-lengths. In Table II we have tabulated essentially this ratio, calculated from the shorter of the two characteristic frequencies.

TABLE II. *Residual displacement predicted by the theory.*

Crystal	$\lambda_{1\ obs.}$	$(\Delta_0/a)(\alpha\beta)^{-\frac{1}{4}}$
KCl	45.5	0.061
NaCl	38.0	0.066
NaF	24.0	0.064
LiF	16.8	0.068

The quantity $(\alpha\beta)^{\frac{1}{4}}$ is of the order of unity, so that this result is reasonable, and is consistent with estimates of the residual displacements arrived at in independent ways.[8] The approximate constancy of the ratio $(\Delta_0/a)(\alpha\beta)^{-\frac{1}{4}}$ is interesting, and it can be shown that this is also consistent with the theory. For this demonstration it is necessary to consider the problem thermodynamically, which will not be here attempted. We shall, however, indicate the result of a preliminary statistical treatment. For an exponential law of repulsion the following equation represents a first approximation:

$$(\Delta_0/a)(\alpha\beta)^{-\frac{1}{4}} = 1/(3^{\frac{1}{4}}p).$$

With the values of p, previously tabulated,[4] we obtain for KCl, 0.0595, for NaCl, 0.0656, and for LiF, 0.077. This is in excellent agreement with Table II, and is encouraging evidence for the general occurrence of the residual ray type of secondary structure.

LETTERS TO THE EDITOR

Prompt publication of brief reports of important discoveries in physics may be secured by addressing them to this department. Closing dates for this department are, for the first issue of the month, the twentieth of the preceding month; for the second issue, the fifth of the month. The Board of Editors does not hold itself responsible for the opinions expressed by the correspondents.

The Raman Spectra of Three Amines

During the study of the Raman spectra of a series of chain compounds, the spectra of *n*-butylamine, *n*-heptylamine, and secondary butylamine have been determined. The frequencies and relative intensities are given in Table I.

TABLE I.

n-butylamine	330(0), 338(1), 399(4), 440(1), 472(0), 495(0), 794(1), 813(1), 842(1), 872(1), 896(2), 935(1), 962(1), 1030(2), 1050(3), 1083(3), 1123(1), 1184(0), 1301(4), 1442(7), 1459(4), 1476(0), 2727(0), 2873(10), 2906(7), 2930(7), 2960(2), 3317(1), 3383(0).
n-heptylamine	274(3), 822(0), 838(0), 865(0), 894(1), 1066(3), 1120(1), 1164(0), 1296(5), 1433(7), 1454(3), 2719(0), 2847(10), 2890(5), 2925(3), 2951(0), 3315(0).
secondary butylamine	479(3), 765(5), 805(5), 917(3), 996(3), 1048(3), 1130(1), 1160(1), 1263(0), 1299(0), 1344(1), 1376(1), 1439(7), 2727(0), 2871(10), 2924(7), 2961(5), 3321(1), 3364(0).

It seems strange that *n*-butylamine has not previously been studied but the author has not been able to find any reference to such work. The Raman spectrum of this substance is remarkable for the absence of continuous background and for the large number of frequencies which appear for such a low member of the series. It has been impossible, so far, to obtain the spectrum of *n*-heptylamine as free from background as that of *n*-butylamine. There are dark regions on the heptylamine plates which indicate that if the continuous background could be removed the spectrum would be almost identical with that of *n*-butylamine.

The weak line at about 2725 cm^{-1} seems never to have been reported before for any amine. As was found by Wood and Collins[1] for the alcohols, the 1450 cm^{-1} line seems to have a structure in the case of the amines. A fairly intense exposure with freedom from background seems necessary to show the nature of this line.

A preliminary plate of the spectrum of furane gives the following frequencies: 597, 647, 723, 840, 870, 989, 1034, 1055, 1139, 1380, 1488, 3158. The spectrum of furane is needed to complete the study of the three similar substances, furane, thiophene, and pyrrol.

The Wood-Pfund arrangement of filters was used,—sodium nitrite solution, and praseodymium and ammonium nitrate solution, placed in tubes parallel to the mercury arc. A dispersion of about 20A per mm at 4358A was obtained by the spectrograph. Without the praseodymium filter many lines could not have been distinguished from the background. The sodium nitrate solution was of such a concentration that only the merest trace of the 4046A line was visible on the plates. Thus only those Raman lines due to the 4358A group could possibly be present.

The author is indebted to the Eastman Kodak Company for the privilege of spending a summer in their research laboratories during which time all the preliminary work on these compounds was carried out.

P. L. BAYLEY

Lehigh University,
Bethlehem, Pa.,
August 17, 1933.

[1] Wood and Collins, Phys. Rev. **42**, 386–392 (1932).

On the Recombination of Electrons and Positrons

The discovery of the positron has opened the possibility of a physical interpretation of the negative energy levels in Dirac's relativistic theory of the electron. In particular the formation of a positron-electron pair under a hard γ-radiation, as observed by Anderson, has been interpreted by Oppenheimer and Plesset[1] as a kind of photoelectric effect, whereby the energy of the absorbed γ-quantum raises an electron from a negative energy state to a positive one, forming a hole or positron and an electron. The reverse process, recombination of a positron and an electron under emission of γ-radiation, has been suggested by Blackett and Occhialini[2] as a possible explanation of the radiation observed by Gray and Tarrant[3] in the scattering of hard γ-rays. According to these authors, the scattered radiation contains besides the normal Compton scattering, two fairly monochromatic components with energies of about 0.5 and 1×10^6 volts, i.e., very nearly mc^2 and $2mc^2$. The intensity of the hard component is smaller than that

[1] Oppenheimer and Plesset, Phys. Rev. **44**, 53 (1933). See also Beck, Zeits. f. Physik **83**, 498 (1933).

[2] Blackett and Occhialini, Proc. Roy. Soc. **A139**, 699 (1933).

[3] Gray and Tarrant, Proc. Roy. Soc. **A136**, 662 (1932).

of the soft component, increases somewhat with the atomic number Z, and is for lead 1/3 of the total radiation. The recombination energy of an electron and a positron, both with negligible kinetic energies, is the sum of the rest masses or $2mc^2 \leqq 10^6$ volts. Because of the necessary conservation of energy and momentum this energy, in the case that both particles are free, can only be emitted in the form of two quanta of the same energy ($=0.5\times10^6$ volt). This type of radiation would therefore explain the soft component. For the hard component the energy must be emitted in one quantum, which is only possible for a strongly bound electron, where the nucleus can take up the recoil momentum of the quantum.

According to this explanation the mechanism of the scattering would be as follows. First the primary γ-quantum is absorbed forming a pair. The high velocity positron which is formed loses its kinetic energy by collisions, and at the end of its path there is a chance of its being destroyed by either of the two processes mentioned above. The ratio of the intensities of the two components should be equal to the ratio of the probabilities of the two processes. Now it has been shown by several authors that the rate of destruction of a low velocity positron by the two quanta process is:

$$R_2 = N\pi e^4/m^2c^3 = 7.5\times10^{-15}N, \qquad (1)$$

where N is the electron density. The nuclear repulsion prevents the positron from reaching the inner parts of the atoms. Therefore not all electrons are effective, so that N will lie between n and nZ, n being the number of atoms per unit volume. For lead $n=3.3\times10^{22}$ which gives as lower limit for $R_2=2.5\times10^8$. To explain the intensity of the hard component we must therefore expect for the one quantum process a rate of the order 10^8.

We have calculated the cross section for the destruction of the positron by the one quantum process. Since we are dealing with low velocity positrons one might expect that a nonrelativistic approximation[4] will give at least the right order of magnitude. We find as the contribution to the cross section due to the K-shell of the atom, neglecting the screening by the atomic electrons:

$$\sigma_K = (4/3)\pi^2\alpha^9a^2Z^6(1+Z^2/W)\{\exp(2\pi Z/W^{\frac{1}{2}})-1\}^{-1}, \qquad (2)$$

where α is the fine structure constant, a is Bohr's radius and W is the energy of the positron expressed in Rydbergs. The contribution of the L-shell is considerably smaller; we find:

$$\sigma_L = (1/24)\pi^2\alpha^9a^2Z^6(4+7Z^2/W)\{\exp(2\pi Z/W^{\frac{1}{2}})-1\}^{-1}. \qquad (3)$$

From these cross sections we find the rate of destruction by multiplying with nv. For positrons of low velocity it is not permissible to neglect the screening, because the exponential factor which is the main term in (2) and (3) and is due to the repulsion of the positron by the nuclear charge, is essentially reduced by the screening. Using the statistical model one can show that instead of $\exp(-2\pi Z/W^{\frac{1}{2}})$ one gets:

$$\exp\{-2.66Z^{1/3}\phi(0.442W/Z^{4/3})\}, \qquad (4)$$

where $\phi(\xi)$ has the following values: $\phi(0)=4.18$; $\phi(0.0018)=3.13$; $\phi(0.0158)=2.63$; $\phi(0.122)=1.96$; $\phi(0.425)=1.48$; $\phi(1.31)=1.06$ and $\phi(\xi)=(\pi/2)(\xi+1)^{-\frac{1}{2}}$ for larger values of ξ. For example in lead ($Z=82$) we get for resp. $W=1$, 100, 10,000, and 75,000 ($=10^8$ volts) the following rates for destruction: $R_1=2\times10^{-5}$, 10, 5×10^7, 10^9. The last value is only given as an indication, since the velocity is so high that (2) is no longer applicable.

The first value shows that the original explanation of the hard component as due to positrons which have completely lost their initial velocity cannot be maintained. We get a rate too small by a factor 10^{13}. One might perhaps still expect a very hard component due to the destruction of positrons at the beginning of their path, since the probability for destruction is then much higher. For an estimate, take positrons of 10^8 volts, which have a range in lead of 0.06 cm. The time required is about 3×10^{-12} sec., so that even if we assume during this time the maximum rate of 10^9 we get as total probability of destruction by the one quantum process 0.003. This would give of course radiation of about 2×10^6 volts. The probability is still very small, but one might perhaps hope that the relativistic corrections will increase this result appreciably.

We do not think however that this is very likely, because one needs an increase by a factor 100 to get an observable result. To estimate very roughly what the influence of relativity can be, we have made a numerical calculation of the cross section for destruction of positrons of 10^8 volt in lead. To simplify the calculation we have only considered the contribution due to transitions of s-states of the positron to s-states of the electron. In nonrelativistic approximation the rate is 0.4×10^9. The relativistic calculation gave instead 2.3×10^7. This of course does not necessarily mean that the relativistic result will really be smaller than the one given by the approximate formula (2), because we have many more transitions to take into account. But it makes one doubt if really the exact calculation will considerably increase the nonrelativistic result.

Finally one should of course not forget the probability of destruction by the two quantum process before the positron has lost its kinetic energy. This would give rise to a continuous band above 0.5×10^6 volts. The upper limit for this probability is however for lead and 10^8-volt positrons only 5 percent and the actual value is probably less.

In conclusion our results are that it is difficult to reconcile the explanation of the hard component of Gray and Tarrant as due to the destruction of positrons with the Dirac theory.

ENRICO FERMI
GEORGE E. UHLENBECK

Department of Physics,
University of Michigan,
August 18, 1933.

[4] Nonrelativistic means here that nonrelativistic radial eigenfunctions are used, and that one keeps only the terms with the smallest power of $1/c$. This corresponds to the first formula of Oppenheimer and Plesset, which we have been able to check except that we got a result larger by a factor 2.

The Hyperfine Structure and Nuclear Moment of Gold

The spectra of Au I and Au II were excited in a horizontal water-cooled hollow cathode tube and in a vertical liquid air-cooled tube. The tubes were operated with an applied voltage of 1000 and from 30 to 500 m.a. current. Reversal of the resonance lines of Au I took place down to 75 m.a. of current. The spectra were first examined in the higher orders of the 35 foot 30,000 lines per inch concave grating of the Institute and then examined with Fabry-Perot etalons of 5–25 mm spacing. For the region above 4500A evaporated silver films were employed, below 3000A aluminum-silicon, and aluminum for the intermediate region. Above 3500A the etalon was employed in the parallel beam of a Zeiss three-prism spectrograph and below 3500 the rings were projected on the slit of a Hilger E1 spectrograph with a long focal length achromat.

The splitting of the resonance lines is in good agreement with previous results of Ritschl.[1] The slight difference in splitting in the two lines 0.003 cm^{-1} can be attributed partially to the influence of the p level. A detailed intensity study of the two components in each of the lines using high contrast plates and stepped exposures as well as measurements with calibrated screens[2] permits a determination of $I=3/2$ with greater certainty.

Many of the lines such as 4607, 4488, 4439, 3029, 2883, and 2388, show four components. The levels involved have been investigated in other lines and in most cases can be relegated to a hyperfine structure term system if an I value of 3/2 is assumed which confirms Ritschl's previous assumption. The interval rule is better satisfied in a number of levels for an I value of 5/2 yet one would not expect it to be valid in view of the character of the coupling involved. Those levels of copper which show large isotope shifts have been investigated in gold. The relatively slight abundance of the weaker isotope and the apparent fine splitting involved does not permit any conclusion to be drawn in regard to its nuclear moment.

A detailed report of the above will be published in the near future.

JOHN WULFF

Eastman Research Laboratories,
Massachusetts Institute of Technology,
August 21, 1933.

[1] Ritschl, Naturwiss. p. 690, 1931.
[2] Harrison, J.O.S.A. **19**, 267 (1929).

Stability of Beryllium

The existence of the alpha-radioactivity of beryllium reported by Langer and Raitt[1] having been made questionable by the work of Evans and Henderson[2] with the linear amplifier, a search for particle radiation of any kind, excepting neutrons possibly, with a sensitivity at least equal to those of the above-mentioned measurements for alpha-particles appeared to be of some interest.

This has been done by means of Geiger-Müller tube counters modified by using 40×40 mesh copper screen for the wall. The counter used had a diameter of 3.5 cm, a length of 17.5 cm, and a zero count of about 30 per minute when shielded from visible light, γ-rays, and cosmic rays by tar paper and an iron shield 1 ft. thick in nearly all directions. Air was used in the chamber at about 2 cm pressure and the operating voltages ranged between 1000 and 1300 volts. The amplifying mechanism was essentially that previously described.[3]

Samples were deposited uniformly over an area of 437 cm^2 by moistening soluble salts with alcohol and drying on the inner surface of a glass cylinder just large enough to slide over the screen counter. The effect per mole of KCl was repeatedly found to agree with 2780±200 counts per half minute. Since potassium is known to emit 27,500 per half minute this shows that about 10 percent of the emitted particles are counted in the case of the potassium β-rays.

Beryllium samples from three different commercial sources were used. All gave activities within 30 percent of a mean before purification. Because this mean value agreed with the Langer and Raitt value it was at first assumed that the activity was really due to Be. A screening test on one sample however showed that 16 percent passed through 0.08 mm of aluminum (13 cm air equivalent stopping power for α-particles) eliminating the possibility of the radiation being solely alpha in nature. Subsequent purification of one of the samples ($Be(NO_3)_2$ of Kahlbaum) gave a sample 0.034 mole of which deposited on the 437 cm^2 of glass surface as a mixture of BeO, $BeCl_2$, and $Be(NO_3)_2$ gave the results in Table I.

TABLE I.

Run	*Zero Count* Count	Time ($\frac{1}{2}$ min.)	Rate	*Zero Count Be Effect* Count	Time	Rate
No. 1	1696	101	16.8±0.3	2583	158	16.4±0.2
No. 2	2215	168	13.2±0.2	1468	110	13.3±0.2
	Effect = 0±0.24					
	Effect/mole = 0±7					

The probable errors given were found by the use of the Bateman formula ($r=0.67(\text{average rate})^{\frac{1}{2}}$) which is known to hold for this work as a result of somewhat extensive investigation during the last two years.

If one takes three times the probable error as an upper limit for the possible activity and assumes the $7.8\cdot10^{-5}$

[1] Langer and Raitt, Phys. Rev. **43**, 585 (1933).
[2] R. D. Evans and M. C. Henderson, Phys. Rev. **44**, 59 (1933).
[3] Libby, Phys. Rev. **42**, 440 (1932).

moles of Be salt per cm^2 of deposit to be sufficiently thin to make self-absorption negligible for β-particles certainly, and within a few percent for the weakest α-particles, the minimum possible apparent half-life for Be with respect to emission of single particles is $2 \cdot 10^{15}$ years. If one calculates on the basis of the emission of 2 particles at once as Langer and Raitt have done, the minimum life would be $4 \cdot 10^{15}$ years.

The sensitivity of the instrument for low-energy particles has been established previously by using aluminum screen instead of the copper and investigating the photoelectric effect. By means of a monochromator the photoelectric threshold of aluminum was found to be as low as 5000 Angstroms, the counting of the emitted photoelectrons being used to detect the effect. Also, calculation from the geometry of the counter, screen sample, etc., of the expected β-radiation effect due to potassium has always given the observed result within a few percent. It therefore seems probable that any radiation producing as much ionization as a photoelectron of a few volts energy should have been counted.

The $Be(NO_3)_2$ was purified by dissolving in water with $Pb(NO_3)_2$, saturating with H_2S, filtering, adding $Ba(NO_3)_2$, then $(NH_4)_2C_2O_4$ solution, filtering, titrating roughly with Na_2SO_4 solution to remove residual Ba^{++}, and evaporating to dryness.

The author wishes to thank Professor Latimer and Dr. Evans for assistance in planning this work.

W. F. Libby

Department of Chemistry,
University of California,
Berkeley, California,
August 23, 1933.

On the Nature of Cosmic-Ray Showers

The treatment of positive-negative electron pair formation as arising from the ionization of the completed negative energy electron shell around a positive nucleus, has occurred independently to several investigators.[1] This point of view seems to agree well with the experimental facts of the excess absorption of the 2.6 million volt radiation of Th C″ and the recent measurements of excess absorption by Gentner[2] for energies between 1 and 2.6 million.

However, this theory in its simple form is not in agreement with the state of affairs at very high primary energies, as it affords no explanation of shower formation and it requires the total absorption of the primaries (gamma-radiation or electrons) in pair formation, to vary much faster with the atomic number of the absorber, than the absorption of cosmic rays would seem to indicate. Shower formation cannot be a direct secondary effect of a single pair formation where an extraordinarily high probability of new pair formation by electrons of the original pair exists, for Anderson has obtained photographs of high energy electron tracks passing through thick pieces of Pb without shower formation, and suffering relatively small energy losses.

The results of Rossi[3] indicate that a secondary is produced which within a very short range in Pb, loses its energy principally by shower formation. It is here pointed out that a simple and natural explanation of shower formation follows from the assumption that Rossi's secondaries are very high energy protons or heavier nuclei. For, if a positive nucleus has a sufficiently high relative velocity to electrons at rest, so that this velocity is higher than that which electrons have after falling through 1 million volts, then the electrons at rest will be able to ionize the closed negative energy electron shell of the *oncoming* positive nucleus. In order to obtain this relative velocity for a proton, it is necessary for it to have more than 2000 million volts energy. A proton of less than this energy cannot produce showers. An electron with an energy somewhat over a million volts is assumed to have a high effective cross section of pair formation in collision with a nucleus. This assumption is subject to test in the cloud chamber by determining the frequency of pair formation in a thin metal sheet by electrons with energies between 1 and 2 million volts. The calculations of Furry and Carlson[4] are not applicable to this case. When the nuclei are stationary and the electron is moving, it will only form one pair, as it would lose the largest part of its energy in doing so. When the nucleus has the same velocity relative to electrons at rest, the nucleus loses a relatively small amount of energy in a pair formation, so that many pairs can be produced before the speed of the nucleus becomes too low. The density of electrons in Pb is so large, that these pairs can be formed in a very short length of its path. This would appear as a shower formation apparently originating from a small region.

The formation of very high energy positive nuclei from a penetrating primary could be either due to photoelectric ejection of parts of heavy nuclei by a very high energy gamma-radiation or more probably whole nuclei, or parts of them could be projected with high energy by neutrons of enormous energy constituting part of the primary radiation. Much more experimental evidence is needed to elucidate the exact nature of this primary absorption process. Secondary neutrons causing a tertiary positive nucleus projection would seem to explain the non-ionizing links of Blackett and Occhialini.

Benedict Cassen

Kellogg Radiation Laboratory,
California Institute of Technology,
August 29, 1933.

---

[1] E.g., Beck, Zeits. f. Physik **83**, 498 (1933). Oppenheimer and Plesset, Phys. Rev. **44**, 53 (1933).

[2] Gentner, Comptes Rendus **197**, 403 (1933).

[3] Rossi, Nature **132**, 173 (1933).

[4] Furry and Carlson, Phys. Rev. **44**, 237 (1933).

Artificial Production of Neutrons

It has been shown by Curie and Joliot[1] that α-particles of energy as low as 1,300,000 electron-volts are capable of disintegrating beryllium with the production of neutrons, and that the efficiency of excitation follows roughly that predicted on the basis of the Gamow theory. The present writers have constructed an apparatus for accelerating helium ions up to 1,000,000 volts, with the object in view of obtaining a strong artificial source of neutrons, and of investigating the efficiency of production of neutrons in the region below 1,000,000 volts. This region does not seem to be accessible with the available radioactive sources of α-particles, due to the low efficiency and consequent large number of α-particles which would be required to produce a measurable effect. Theoretically, the probability of a 1,000,000 volt α-particle penetrating the beryllium nucleus is about 10^{-4} times that of a full range polonium α-particle. At 750,000 volts this factor becomes 10^{-5}, and at 500,000 volts it is 10^{-7}. It is therefore necessary in this energy range to have a positive ion current of the order of 10 or 100 microamperes to produce an appreciable effect.

The apparatus used for accelerating the ions consists of two porcelain vacuum tubes, one above the other, with a connecting passage between them for the ions to go through. The 1,000,000 volt cascade transformer set in the High Voltage Laboratory is used as the source of high potential, and the midpoint between the two tubes is connected to the half potential point of the transformer set. The ions, produced in the inner electrode of the upper tube, are accelerated successively in each tube through half the total potential, and are taken out at the bottom of the lower tube, which is at ground potential. A magnetic field is then applied to the ion beam to bend out any electrons which may arrive on the reverse half cycle, and the beam is allowed to strike a 2 inch target. The target is a brass disk, one side of which is covered with beryllium, and which can be rotated by means of a shaft so as to expose either the beryllium or the brass surface to the ion beam without making any other change in the operating conditions.

A quartz fiber electroscope of the cantilever type, having a cylindrical chamber 5 cm in diameter and 8 cm long is employed as a means of detecting the neutrons. The inside wall of the chamber is coated with a layer of paraffin, and the entire electroscope is enclosed in a lead cylinder of 5 cm wall thickness, to shield out x-rays. The center of the chamber is located 13 cm from the center of the target, and in a direction perpendicular to the ion beam. It is supposed that the neutrons will easily penetrate the 5 cm lead wall, and eject recoil hydrogen atoms into the electroscope chamber from its paraffin walls. Any increase in the ionization produced when the beryllium target is bombarded over that produced when the brass target is bombarded, should be just that due to recoil hydrogen atoms ejected by neutrons.

A series of runs of one hour each was made at a number of voltages between 600,000 and 975,000, with a positive ion current of 10 microamperes. The accompanying curves, one for the beryllium target and the other for the brass target, give the deflection of the electroscope during each of these runs as a function of voltage. Exactly the same conditions were maintained while the brass was exposed to the ion beam as when the beryllium was exposed. The brass reading at each voltage is therefore the amount to be subtracted from the beryllium reading due to x-rays plus the natural leak of the electroscope. Below 700,000 volts the deflection

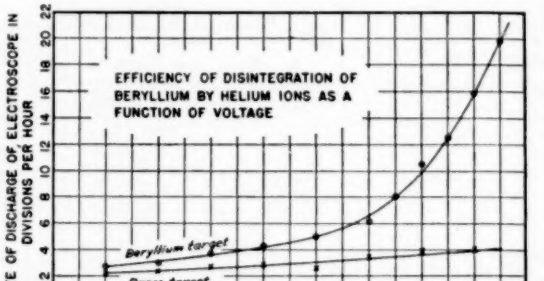

FIG. 1.

during a run with the brass target is not measurably greater than the natural leak of the electroscope when the tube is not running, and at 950,000 volts the deflection is less than twice the natural leak.

The possibility that a part of the effect observed might be due to γ-rays emitted in the disintegration of the beryllium was not overlooked, and a measurement was made at 850,000 volts with the paraffin removed from the electroscope. In this case the deflection with the beryllium target was only 20 percent greater than the deflection with the brass target. With paraffin in the chamber there was a factor of 2 between the beryllium and brass readings at the same voltage. It is therefore concluded that if part of the effect is due to γ-rays, it is small compared to that due to neutrons.

With the apparatus used at the present time, a positive ion current of 30 microamperes can be obtained at 950,000 volts, or 3 times the intensity used in plotting the above curve. This furnishes a source of neutrons which compares favorably in intensity with that obtained by means of the strongest polonium α-particle sources now in use.

H. R. CRANE
C. C. LAURITSEN
A. SOLTAN

Kellogg Radiation Laboratory,
California Institute of Technology,
September 3, 1933.

[1] Curie and Joliot, Comptes Rendus **196**, 397 (1933).

Azimuthal Asymmetry of Cosmic Radiation

Since the curves of latitude against ionization due to cosmic radiation start to dip at geomagnetic latitudes 40 to 45, it is of interest to determine whether the azimuthal asymmetry reported[1] at lower latitudes can be detected in the above region. Observations were made at four elevations: (1) at the Mt. Wilson Observatory Laboratories, Pasadena, elevation 855 ft.; (2) on Mt. Wilson, elevation 5800 ft.; (3) at the Lowell Observatory, Flagstaff, Arizona, elevation 7250 ft.; and (4) on Doyle Saddle, San Francisco peaks, Arizona, elevation 11,280 ft. Stations (1) and (2) are at geomagnetic latitude about 41°; while (3) and (4) are at 43°.

Geiger counters and a circuit, previously described,[2] automatically recording coincidental discharges were employed. The counter cylinders were 9 cm long, 2 cm in diameter, and spaced 11 cm between axes. The individual counting rates varied from 50 to 160 per minute, depending largely on the altitude.

The coincidence counting rates were observed with the axes of the counters determining a plane which could be oriented east or west of the magnetic meridian. The arrangement could be rotated about a vertical axis, and readings were made alternately east and west in order to eliminate effects due to secular changes in sensitivity. The plane determined by the axes of the two counters was set at altitude angles 22, 45, 55 and 67° above the horizontal.

The counting rates east and west at equal angles were found to be equal within the experimental errors of about 3 percent. Since, however, the high altitude observations showed a systematic variation only a little smaller than the probable error, these are tabulated in full in Table I.

TABLE I. *Counting rates and probable errors observed at 11,280 ft. Counters 35° from vertical. Geomagnetic latitude 43°.*

Run	Direction	Rate	W/E	Probable error, percent
1	E	3.32		
1	W	3.36	1.012	3.16
2	E	2.60		
2	W	2.65	1.019	3.50
3	E	3.31		
3	W	3.37	1.018	2.96

The mean rates were 3.001 east and 3.060 west. It will be seen that the systematic variation is in the direction of a west excess of about two percent; but that in view of the probable error this is not to be regarded as conclusive. At the lower elevations the statistical fluctuations gave in general an east excess as often as a west excess. The probable error was computed in the usual manner from the residuals.

This result may be interpreted on the basis of the Epstein-Lemaitre-Vallarta theory as follows: If the magnetically deviable component of the primary radiation lies in the band suggested by Compton, $x=0.45$ to 0.35, (energies 8 to 12×10^9 e.v.) we should expect at geomagnetic latitude 43 an asymmetry not greater than about two percent, as observed If a large fraction of the rays were softer, $x=0.2$ to 0.3, we should expect an effect larger than was observed. Johnson's[3] recent results at Swarthmore indicate that, on the basis of the theory here under consideration, a small fraction of the rays have energies as low as $x=0.2$. This fraction is smaller than the experimental uncertainty of the Arizona observations, and the experiments are consequently in agreement. Moreover it is clear that very few particles of energies less than 4×10^9 volts can reach the surface of the earth after passing obliquely through the atmosphere, even in those latitudes where they would not be swept out by the earth's field. The observations consequently assign a lower limit to the energy of the deviable component of about 8×10^9 volts. If we may trust the theoretical curves, this limit is accurate within 10 percent, since it was observed just on the border of the "equatorial belt." This conclusion is further strengthened by the observations of Stearns and Bennett[4] who find no appreciable west excess at Denver, some three degrees north of Flagstaff.

The above interpretation assumes that there are incoming charged particles which would follow the paths calculated in the theory. It must be remembered that the experiments of Anderson[5] and Kunze[6] have shown only a negligible number of particles in the energy bands postulated above. The possibility of some other explanation of the observations must consequently not be overlooked.

The author wishes to thank Dr. R. A. Millikan for criticism and advice and for permitting this experiment to be conducted through the aid of funds allotted him by the Carnegie Corporation of New York and the Carnegie Institution of Washington for his cosmic-ray program; Drs. Lampland and Slipher for extending the facilities of the Lowell Observatory; and Mr. W. F. Heald for assisting with the observations.

S. A. KORFF

National Research Fellow,
California Institute of Technology,
and Mt. Wilson Observatory,
September 7, 1933.

---

[1] T. H. Johnson, Phys. Rev. **43**, 834 (1933).

[2] S. A. Korff, Phys. Rev. **44**, 130 (1933). (Abs.)

[3] T. H. Johnson and E. C. Stevenson, Phys. Rev. **44**, 125 (1933).

[4] J. C. Stearns and R. D. Bennett, Phys. Rev. **43**, 1038 (1933).

[5] C. D. Anderson, Phys. Rev. **41**, 405 (1932).

[6] P. Kunze, Zeits. f. Physik, **79**, 203 (1932).